2 Translational parallel robots with two degrees of freedom

The translational parallel robots with two degrees of freedom can be actuated by linear and/or rotating actuators. Topologies with coupled, decoupled and uncoupled motions along with maximally regular solutions are presented in this section. They give rise to two independent translations along with a constant orientation of the moving platform.

2.1 *T2*-type translational parallel robots with coupled motions

T2-type translational parallel robots (TPMs) with *coupled motions* and linear or rotating actuators with various degrees of overconstraint can be obtained by using the basic *limb topologies* presented in Figs. 6.1b and 6.2b, c – Part 1. In these solutions the two operational velocities depend on the two actuated joint velocities: $v_1 = v_1(\dot{q}_1, \dot{q}_2)$ and $v_2 = v_2(\dot{q}_1, \dot{q}_2)$. We consider $v_1 = v_x$ and $v_2 = v_y$.

The actuators can be mounted on the fixed base or on a moving link. The first solution has the advantage of reducing the moving masses and large workspace. The second solution is more compact.

2.1.1 Overconstrained solutions

Equation (1.16) indicates that *overconstrained solutions* of *T2*-type translational parallel robots with coupled motions and q independent loops meet the condition $\sum_1^p f_i < 2 + 6q$. Various solutions fulfil this condition along with $M_F = S_F = 2$ and $(R_F) = (\boldsymbol{v}_x, \boldsymbol{v}_y)$. They may have identical limbs or limbs with different structures and may be actuated by linear or rotating motors. The simplest solutions have just two limbs. Solutions with an additional unactuated limb are also presented in this section.

G. Gogu, *Structural Synthesis of Parallel Robots: Part 2: Translational Topologies with Two and Three Degrees of Freedom,* Solid Mechanics and Its Applications 159, 23–106.

Solutions with linear actuators

In the *basic solutions* with linear actuators and coupled motions $F \leftarrow G_1$–G_2, the moving platform $n \equiv n_{Gi}$ ($i = 1$ and 2) is connected to the reference platform $1 \equiv 1_{Gi} \equiv 0$ by two limbs of type $P \perp Pa$ (Fig. 6.1b – Part 1). One prismatic and four revolute joints exist in each limb ($p_{Gi} = 5$). This *topology* is denoted by $2\underline{P}Pa$-type and has the two *linear actuators* situated on the fixed base. They may have any direction parallel to the plane of motion of the moving platform. The axes of the revolute joints in the *parallelogram loop* are perpendicular on the plane of motion of the moving platform.

The example in Fig. 2.1 has the moving platform 5 and the following arrangement of joints: $P_x \perp Pa_z$ in G_1-limb and $P_y \perp Pa_z$ in G_2-limb. Indices x, y and z, associated with the joint symbol denote the direction of the joint axis. Two consecutive joints with the same index have parallel axes. Two consecutive joints with different indices have perpendicular axes. The index of the planar parallelogram closed loop indicates the direction of the axes of revolute pairs. The actuated joint of each limb G_i ($i = 1,2$) is underlined. To simplify link notation e_{Ai} ($e = 1,\ldots,n$ and $i = 1,2$) by avoiding the double index in Fig. 2.1 and the following figures we have denoted by e_A the links of G_1-limb ($e_A \equiv e_{G1}$) and by e_B the links of G_2-limb ($e_B \equiv e_{G2}$).

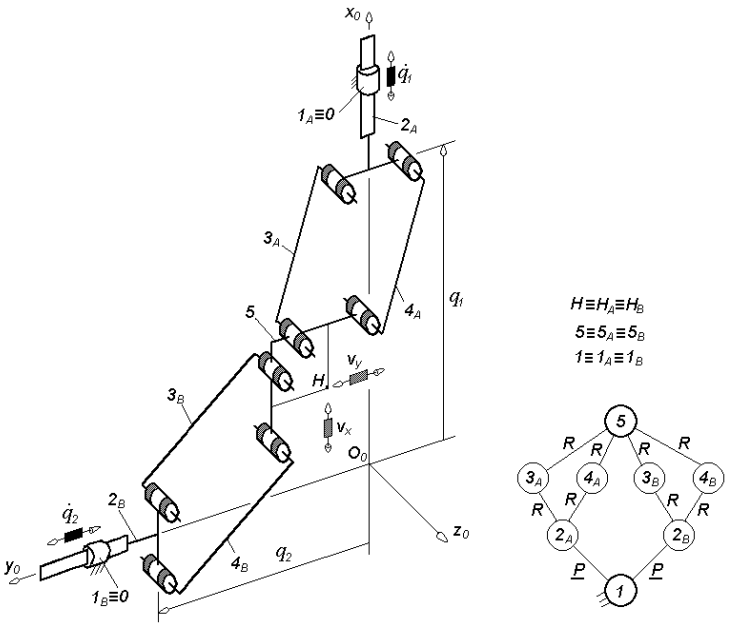

Fig. 2.1. $2\underline{P}Pa$-type translational parallel mechanism with ten overconstraints, limb topology $\underline{P} \perp Pa$

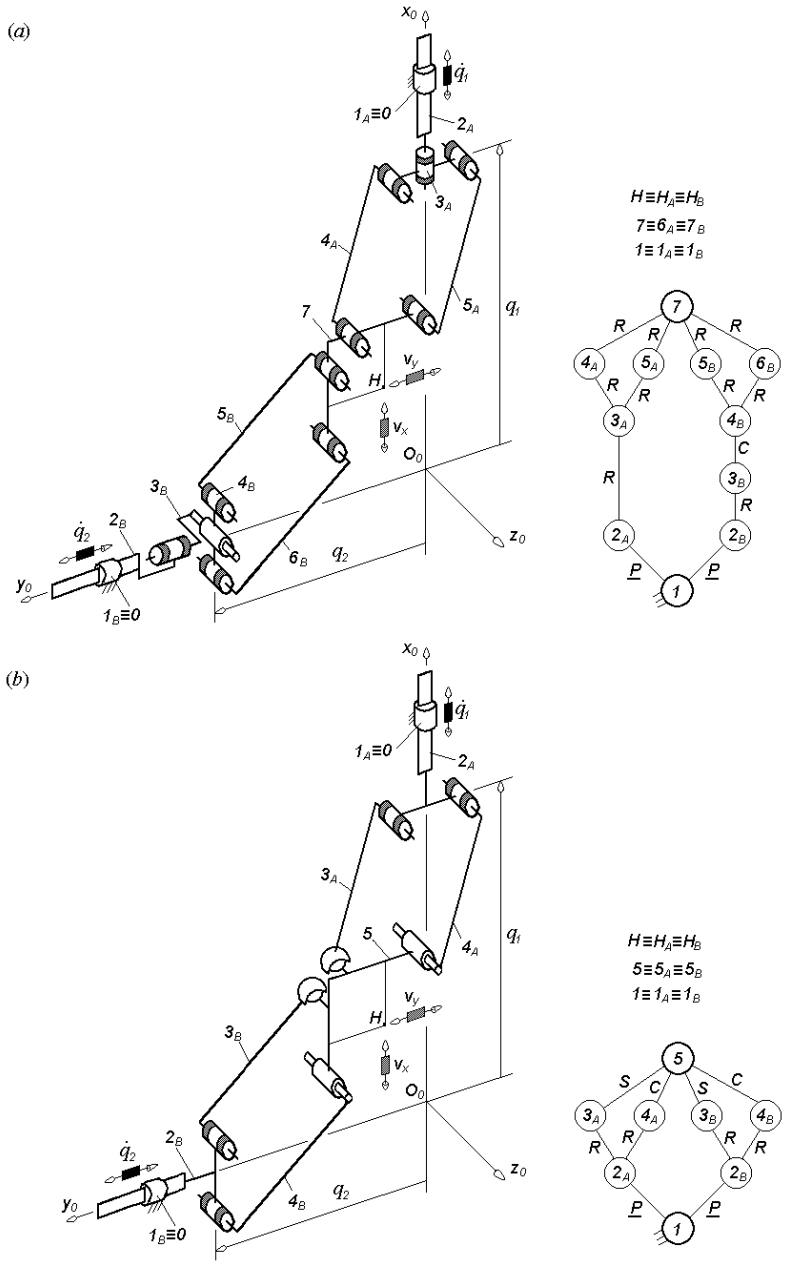

Fig. 2.2. Translational parallel mechanisms of types $\underline{P}R^*Pa$-$\underline{P}R^*C^*Pa$ with six overconstraints (**a**) and $2\underline{P}Pa^*$ with four overconstraints (**b**), limb topologies $\underline{P}||R^* \perp Pa$ and $\underline{P}||R^* \perp C^*||Pa$ (**a**) and $\underline{P} \perp Pa^*$ (**b**)

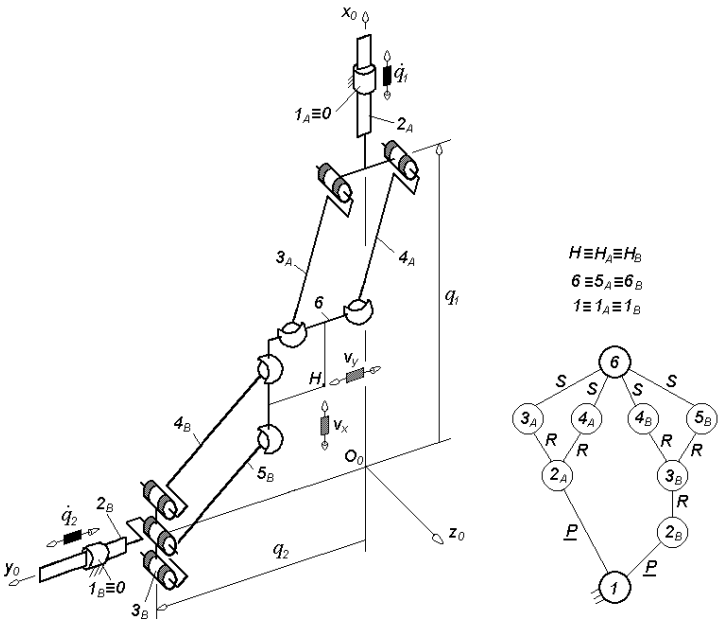

Fig. 2.3. $\underline{P}Pa^{ss}$-$\underline{P}R^{*}Pa^{ss}$-type translational parallel mechanism with one overconstraint, limb topologies $\underline{P} \perp Pa^{ss}$ and $\underline{P} \perp R^{*} || Pa^{ss}$

The vector spaces of relative velocities between the moving and the reference platforms in the kinematic chains G_i ($i = 1$ and 2) disconnected from mechanism F have the same basis $(R_{G1}) = (R_{G2}) = (\boldsymbol{v}_x, \boldsymbol{v}_y)$. This is also the basis of the vector space of relative velocities between the moving and the reference platforms in mechanism F, given by Eq. (1.1), that is $(R_F) = (\boldsymbol{v}_x, \boldsymbol{v}_y)$. This solution with two prismatic and eight revolute joints has $p = 10$ and $\sum_{i=1}^{10} f_i = 10$. The structural diagram in Fig. 2.1b and Eq. (1.9) indicate that the mechanism has three independent closed loops ($q = 3$).

Three joint parameters lost their independence in each closed planar parallelogram loop combined in a complex limb ($r_l^{Gi} = 3$).

For the solution in Fig. 2.1, Eqs. (1.2)–(1.8) and (1.17) give the following structural parameters: $M_{Gi} = S_{Gi} = S_F = 2$, $r_F = 8$, $M_F = 2$, $N_F = 10$ and $T_F = 0$ (see Table 2.1).

A large diversity of overconstrained solutions with coupled motions and linear motors combined in the two complex limbs with parallelogram loops can be derived from the solution in Fig. 2.1. They have $1 \le N_F < 10$

and could integrate up to three *idle mobilities* in each parallelogram loop and up to four idle mobilities outside the parallelogram loops. Structural solutions using parallelogram loops with up to three idle mobilities are presented in Part 1 (Fig. 6.3b–h). The idle mobilities integrated outside the parallelogram loops are three orthogonal rotations and one translation perpendicular to the motion plane of the moving platform. For example, four idle mobilities are introduced outside the parallelogram loop in Fig. 2.2a and six idle mobilities are introduced in the parallelogram loops in Fig. 2.2b.

In the example in Fig. 2.3, three idle mobilities are introduced outside the parallelogram loops and six in the parallelogram loops. The *structural parameters* of the solutions illustrated in Figs. 2.1–2.3 are presented in Table 2.1.

We recall that *C* denotes a cylindrical pair and *S* a spherical pair. The notations Pa^* or Pa^{cs} are associated with a parallelogram loop with three idle mobilities combined in a cylindrical and a spherical pair, and Pa^{ss} with four idle mobilities combined in two spherical joints adjacent to the moving platform. We note that in the parallelogram loop Pa^{ss}-type, three idle mobilities are introduced in the loop and one outside the loop.

The number of overconstraints can be further reduced by replacing one limb by a simple open kinematic chain with $2 < M_{Gi} = S_{Gi} < 6$ that integrates velocities $\boldsymbol{v}_x$ and $\boldsymbol{v}_y$ in the basis of its operational space. In this way, a large diversity of overconstrained translational parallel robots with linear actuators and $0 < N_F \leq 6$ may be set up. They have just two independent loops ($q = 2$). For example, the solution in Fig. 2.4 is obtained by replacing G_2-limb in Fig. 2.1 by a planar kinematic chain $\underline{P}RR$-type ($\underline{P}_y \perp R_z || R_z$). For the solution in Fig. 2.4, Eqs. (1.2)–(1.8) and (1.17) give the following structural parameters: $M_{G1} = S_{G1} = 2$, $M_{G2} = S_{G2} = 3$, $(R_{G1}) = (\boldsymbol{v}_x, \boldsymbol{v}_y)$, $(R_{G2}) = (\boldsymbol{v}_x, \boldsymbol{v}_y, \boldsymbol{\omega}_\delta)$, $(R_F) = (\boldsymbol{v}_x, \boldsymbol{v}_y)$, $S_F = 2$, $r_F = 6$, $M_F = 2$, $N_F = 6$ and $T_F = 0$ (see Table 2.2).

Overconstrained solutions with $0 < N_F < 6$ can be derived from the solution in Fig. 2.4 by introducing up to three idle mobilities in the parallelogram loop and up to three idle mobilities outside the parallelogram loop. The idle mobilities integrated inside and outside the parallelogram loop are two orthogonal rotations and one translation perpendicular to the motion plane of the moving platform.

For example, in Fig. 2.5 two idle mobilities are introduced outside the parallelogram loops and three inside the parallelogram loop. Three idle mobilities are introduced outside the parallelogram loop in Fig. 2.6a and three idle mobilities are introduced in the parallelogram loop in Fig. 2.6b.

The structural parameters of the solutions illustrated in Figs. 2.4–2.6 are presented in Table 2.2.

A solution with linear actuators non adjacent to the fixed base can be derived from the solution in Fig. 2.4 by using, in G_2-limb, a planar kinematic chain $R\underline{P}R$-type (see Fig. 2.7a). This solution also has six overconstraints. Overconstrained solutions with $0 < N_F < 6$ can be derived from the solution in Fig. 2.7a by introducing up to three idle mobilities outside the parallelogram loop (Fig. 2.7b) and up to three idle mobilities inside the parallelogram loop (Fig. 2.8a) The example in Fig. 2.8b has one overconstraint with two idle mobilities outside the parallelogram loop and three idle mobilities in the parallelogram loop. The solutions in Figs. 2.7 and 2.8 have the same structural parameters as their counterparts with linear motors mounted on the fixed base in Figs. 2.4–2.6 (see Table 2.2).

Solutions of type $F \leftarrow G_1$–G_2–G_3 with an additional *unactuated limb* can also be derived by using two *simple actuated limbs* with $2 < M_{Gi} = S_{Gi} < 6$ and an unactuated limb $P \perp P$-type. The directions of the two prismatic joints are parallel to the motion plane x–y of the moving platform. The actuated limbs G_1 and G_2 must integrate velocities $\boldsymbol{v}_x$ and $\boldsymbol{v}_y$ in the basis of their operational space. The three limbs form $q = 2$ independent loops and must meet the conditions: $M_F = S_F = 2$ and $(R_F) = (R_{G1} \cap R_{G2} \cap R_{G2}) = (\boldsymbol{v}_x, \boldsymbol{v}_y)$. Equation (1.16) indicates that the overconstrained solutions of these *T2*-type translational parallel robots with coupled motions and an additional unactuated limb have $\sum_1^p f_i < 14$. Various solutions with identical or different limb architectures exist. The linear actuators can be mounted on the fixed base or on a moving link. For example, the solutions in Fig. 2.9a have two actuated planar limbs of type $\underline{P}RR$ and that in Fig. 2.10a two actuated planar limbs of type $R\underline{P}R$. The axes of the revolute joints are parallel to the z-axis. The solutions in Figs. 2.9a and 2.10a have six overconstraints and that in Figs. 2.9b and 2.10b two overconstraints. The structural parameters of these solutions are presented in Table 2.3.

Table 2.1. Structural parameters of translational parallel mechanisms in Figs. 2.1–2.3

No.	Structural parameter	Solution *2PPa* Fig. 2.1	*PR*Pa-PR*C*Pa* Fig. 2.2a	*2PPa** Fig. 2.2b	PPa^{ss}-*PR*Pa*^{ss} Fig. 2.3
1	m	8	11	8	9
2	p_1	5	6	5	5
3	p_2	5	7	5	6
4	p	10	13	10	11
5	q	3	3	3	3
6	k_1	0	0	0	0
7	k_2	2	2	2	2
8	K	2	2	2	2
9	(R_{G1})	$(\boldsymbol{v}_x, \boldsymbol{v}_y)$	$(\boldsymbol{v}_x, \boldsymbol{v}_y, \boldsymbol{\omega}_\alpha)$	$(\boldsymbol{v}_x, \boldsymbol{v}_y)$	$(\boldsymbol{v}_x, \boldsymbol{v}_y, \boldsymbol{\omega}_\beta)$
10	(R_{G2})	$(\boldsymbol{v}_x, \boldsymbol{v}_y)$	$(\boldsymbol{v}_x, \boldsymbol{v}_y, v_z, \boldsymbol{\omega}_\beta, \boldsymbol{\omega}_\delta)$	$(\boldsymbol{v}_x, \boldsymbol{v}_y)$	$(\boldsymbol{v}_x, \boldsymbol{v}_y, \boldsymbol{\omega}_\alpha, \boldsymbol{\omega}_\delta)$
11	S_{G1}	2	3	2	3
12	S_{G2}	2	5	2	4
13	r_{G1}	3	3	6	6
14	r_{G2}	3	3	6	6
15	M_{G1}	2	3	2	3
16	M_{G2}	2	5	2	4
17	(R_F)	$(\boldsymbol{v}_x, \boldsymbol{v}_y)$	$(\boldsymbol{v}_x, \boldsymbol{v}_y)$	$(\boldsymbol{v}_x, \boldsymbol{v}_y)$	$(\boldsymbol{v}_x, \boldsymbol{v}_y)$
18	S_F	2	2	2	2
19	r_1	6	6	12	12
20	r_F	8	12	14	17
21	M_F	2	2	2	2
22	N_F	10	6	4	1
23	T_F	0	0	0	0
24	$\sum_{j=1}^{p_1} f_j$	5	6	8	9
25	$\sum_{j=1}^{p_2} f_j$	5	8	8	10
26	$\sum_{j=1}^{p} f_j$	10	14	16	19

m number of links including the fixed base, p_{Gi} number of joints in the G_i-limb, p total number of joints in the parallel mechanism[a], q number of independent closed loops in the parallel mechanism[b], k_1 number of simple limbs, k_2 number of complex limbs, k total number of limbs[c], (R_{Gi}) basis of the vector space of relative velocities between the moving and reference platforms in G_i-limb disconnected from the parallel mechanism, S_{Gi} connectivity between the moving and reference platforms in G_i-limb disconnected from the parallel mechanism[d], r_{Gi} number of joint parameters that lost their independence in the closed loops combined in G_i-limb, M_{Gi} mobility of G_i-limb[e], (R_F) basis of the vector space of relative velocities between the moving and reference platforms in the parallel mechanism[f], S_F connectivity between the mobile and reference platforms in the parallel

mechanism[g], r_l total number of joint parameters that lose their independence in the closed loops combined in the k limbs[h], r_F total number of joint parameters that lose their independence in the closed loops combined in the parallel mechanism[i], M_F mobility of the parallel mechanism[j], N_F number of overconstraints in the parallel mechanism[k], T_F degree of structural redundancy of the parallel mechanism[l], f_j mobility of jth joint.

[a] $p = \sum_{i=1}^{k} p_{Gi}$,

[b] $q = p\text{-}m+1$,

[c] $k = k_1+k_2$,

[d] $S_{Gi} = dim(R_{Gi})$, $i = 1,2,...,k$,

[e] $M_{Gi} = \sum_{j=1}^{p_{Gi}} f_j - r_{Gi}$, $i = 1,2,...,k$,

[f] $(R_F) = (R_{G1}) \cap ... \cap (R_{Gk})$,

[g] $S_F = dim(R_F)$,

[h] $r_l = \sum_{i=1}^{k} r_{Gi}$,

[i] $r_F = \sum_{i=1}^{k} S_{Gi} - S_F + r_l$,

[j] $M_F = \sum_{i=1}^{p} f_i - r_F$,

[k] $N_F = 6q - r_F$,

[l] $T_F = M_F - S_F$.

Table 2.2. Structural parameters[a] of translational parallel mechanisms in Figs. 2.4–2.8

No.	Structural parameter	Solution *PPa*-*PRR* (Fig. 2.4), *PPa*-*RPR* (Fig. 2.7a)	*PPa*-*PC***S** (Fig. 2.6a), *PPa*-*C***PS** (Fig. 2.7b)	*PPa**-*PRR* (Fig. 2.6b), *PPa**-*RPR* (Fig. 2.8a),	PPa^{ss}-*PRC** (Fig. 2.5) PPa^{ss}-*RPC** (Fig. 2.8b)
1	m	7	7	7	7
2	p_1	5	5	5	5
3	p_2	3	3	3	3
4	p	8	8	8	8
5	q	2	2	2	2
6	k_1	1	1	1	1
7	k_2	1	1	1	1
8	k	2	2	2	2
9	(R_{G1})	$(\boldsymbol{v}_x, \boldsymbol{v}_y)$	$(\boldsymbol{v}_x, \boldsymbol{v}_y)$	$(\boldsymbol{v}_x, \boldsymbol{v}_y)$	$(\boldsymbol{v}_x, \boldsymbol{v}_y, \boldsymbol{\omega}_\beta)$
10	(R_{G2})	$(\boldsymbol{v}_x, \boldsymbol{v}_y, \boldsymbol{\omega}_\delta)$	$(\boldsymbol{v}_x, \boldsymbol{v}_y, v_z, \boldsymbol{\omega}_\alpha, \boldsymbol{\omega}_\beta, \boldsymbol{\omega}_\delta)$	$(\boldsymbol{v}_x, \boldsymbol{v}_y, \boldsymbol{\omega}_\delta)$	$(\boldsymbol{v}_x, \boldsymbol{v}_y, v_z, \boldsymbol{\omega}_\delta)$
11	S_{G1}	2	2	2	3
12	S_{G2}	3	6	3	4
13	r_{G1}	3	3	6	6
14	r_{G2}	0	0	0	0
15	M_{G1}	2	2	2	3
16	M_{G2}	3	6	3	4
17	(R_F)	$(\boldsymbol{v}_x, \boldsymbol{v}_y)$	$(\boldsymbol{v}_x, \boldsymbol{v}_y)$	$(\boldsymbol{v}_x, \boldsymbol{v}_y)$	$(\boldsymbol{v}_x, \boldsymbol{v}_y)$
18	S_F	2	2	2	2
19	r_1	3	3	6	6
20	r_F	6	9	9	11
21	M_F	2	2	2	2
22	N_F	6	3	3	1
23	T_F	0	0	0	0
24	$\sum_{j=1}^{p_1} f_j$	5	5	8	9
25	$\sum_{j=1}^{p_2} f_j$	3	6	3	4
26	$\sum_{j=1}^{p} f_j$	8	11	11	13

[a]See footnote of Table 2.1 for the nomenclature of structural parameters

Table 2.3. Structural parameters[a] of translational parallel mechanisms in Figs. 2.9–2.10

No.	Structural parameter	Solution *2PRR-PP* (Fig. 2.9a) *2RPR-PP* (Fig. 2.10a)	 *2PRS*-PP* (Fig. 2.9b) *2RPS*-PP* (Fig. 2.10b)
1	m	7	7
2	p_1	3	3
3	p_2	3	3
4	p_3	2	2
5	p	8	8
6	q	2	2
7	k_1	3	3
8	k_2	0	0
9	k	3	3
10	(R_{G1})	$(\boldsymbol{v}_x, \boldsymbol{v}_y, \boldsymbol{\omega}_\delta)$	$(\boldsymbol{v}_x, \boldsymbol{v}_y, \boldsymbol{\omega}_\alpha, \boldsymbol{\omega}_\beta, \boldsymbol{\omega}_\delta)$
11	(R_{G2})	$(\boldsymbol{v}_x, \boldsymbol{v}_y, \boldsymbol{\omega}_\delta)$	$(\boldsymbol{v}_x, \boldsymbol{v}_y, \boldsymbol{\omega}_\alpha, \boldsymbol{\omega}_\beta, \boldsymbol{\omega}_\delta)$
12	(R_{G3})	$(\boldsymbol{v}_x, \boldsymbol{v}_y)$	$(\boldsymbol{v}_x, \boldsymbol{v}_y)$
13	S_{G1}	3	5
14	S_{G2}	3	5
15	S_{G3}	2	2
16	r_{G1}	0	0
17	r_{G2}	0	0
18	r_{G3}	0	0
19	M_{G1}	3	5
20	M_{G2}	3	5
21	M_{G3}	2	2
22	(R_F)	$(\boldsymbol{v}_x, \boldsymbol{v}_y)$	$(\boldsymbol{v}_x, \boldsymbol{v}_y)$
23	S_F	2	2
24	r_1	0	0
25	r_F	6	10
26	M_F	2	2
27	N_F	6	2
28	T_F	0	0
29	$\sum_{j=1}^{p_1} f_j$	3	5
30	$\sum_{j=1}^{p_2} f_j$	3	5
31	$\sum_{j=1}^{p_3} f_j$	2	2
32	$\sum_{j=1}^{p} f_j$	8	12

[a]See footnote of Table 2.1 for the nomenclature of structural parameters

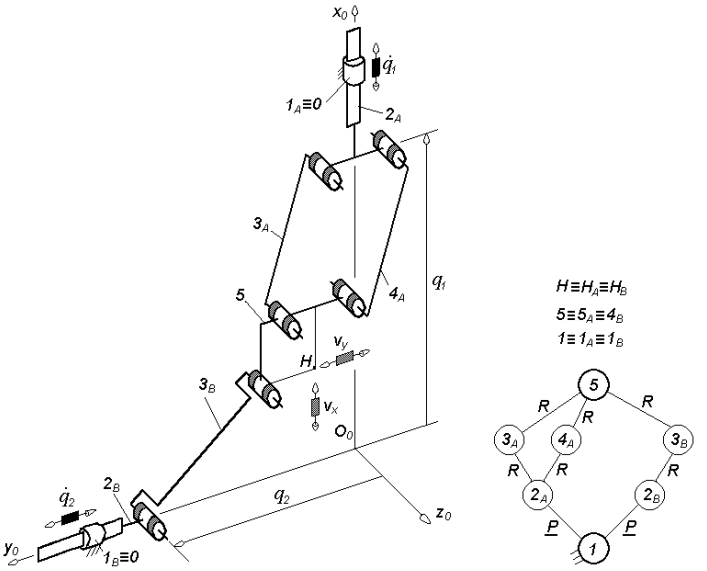

Fig. 2.4. $\underline{P}Pa$-$\underline{P}RR$-type translational parallel mechanism with six overconstraints and linear motors on the fixed base, limb topologies $\underline{P} \perp Pa$ and $\underline{P} \perp R||R$

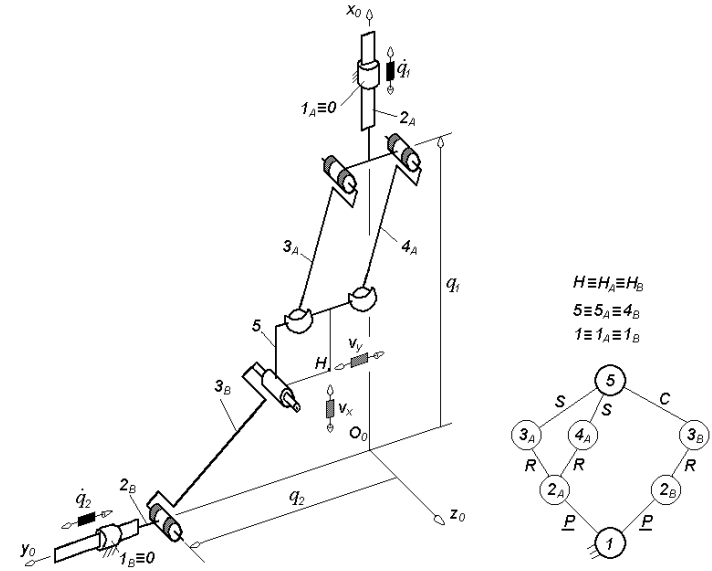

Fig. 2.5. $\underline{P}Pa^{ss}$-$\underline{P}RC$*-type translational parallel mechanism with one overconstraint and linear motors on the fixed base, limb topologies $\underline{P} \perp Pa^{ss}$ and $\underline{P} \perp R||C$*

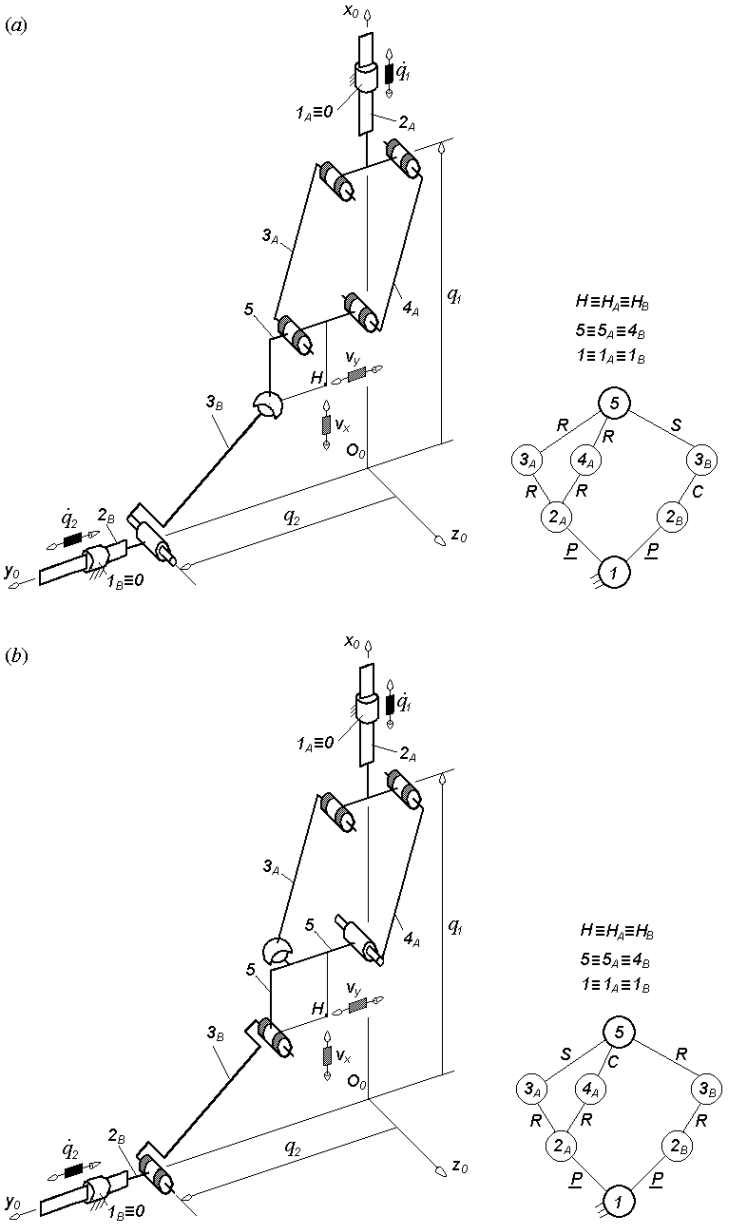

Fig. 2.6. Translational parallel mechanisms with three overconstraints and linear motors on the fixed base of types $\underline{P}Pa$-$\underline{P}C^*S^*$ (**a**) and $\underline{P}Pa^*$-$\underline{P}RR$ (**b**), limb topologies $\underline{P} \perp Pa$ and $\underline{P} \perp C^*S^*$ (**a**), $\underline{P} \perp Pa^*$ and $\underline{P} \perp R||R$ (**b**)

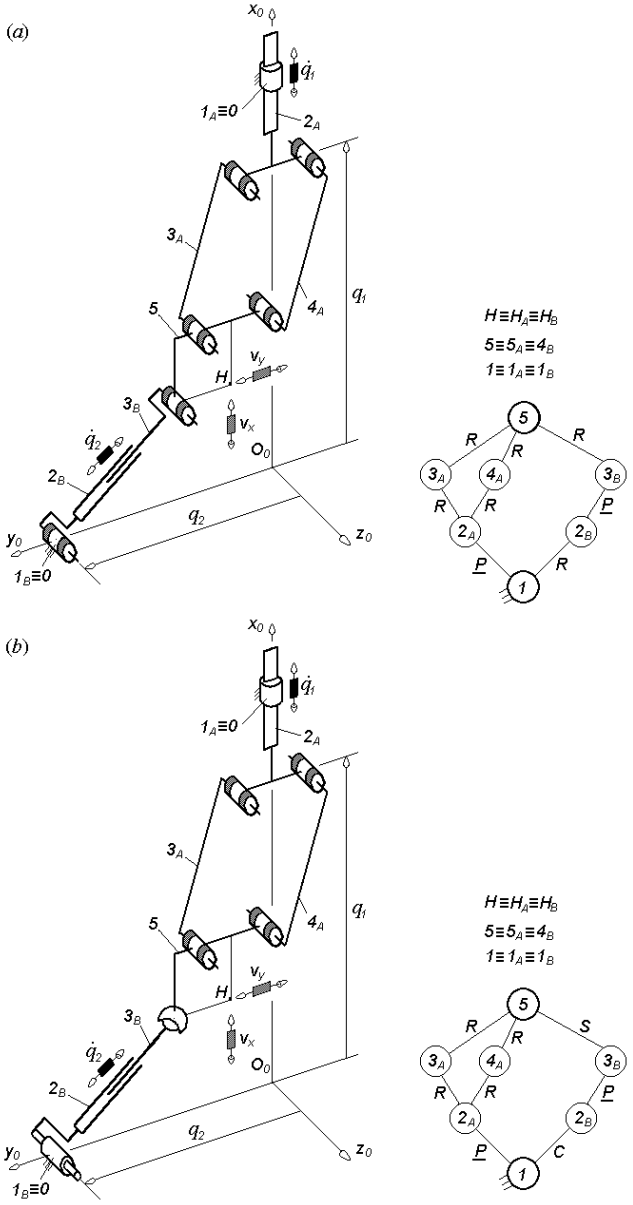

Fig. 2.7. Translational parallel mechanisms of types: $\underline{P}Pa$-$R\underline{P}R$ with six overconstraints (**a**) and $\underline{P}Pa$-$C^*\underline{P}S^*$ with three overconstraints (**b**), limb topologies $\underline{P} \perp Pa$ and $R \perp \underline{P} \perp {}^{\parallel}R$ (**a**), $\underline{P} \perp Pa$ and $C^* \perp \underline{P}S^*$ (**b**)

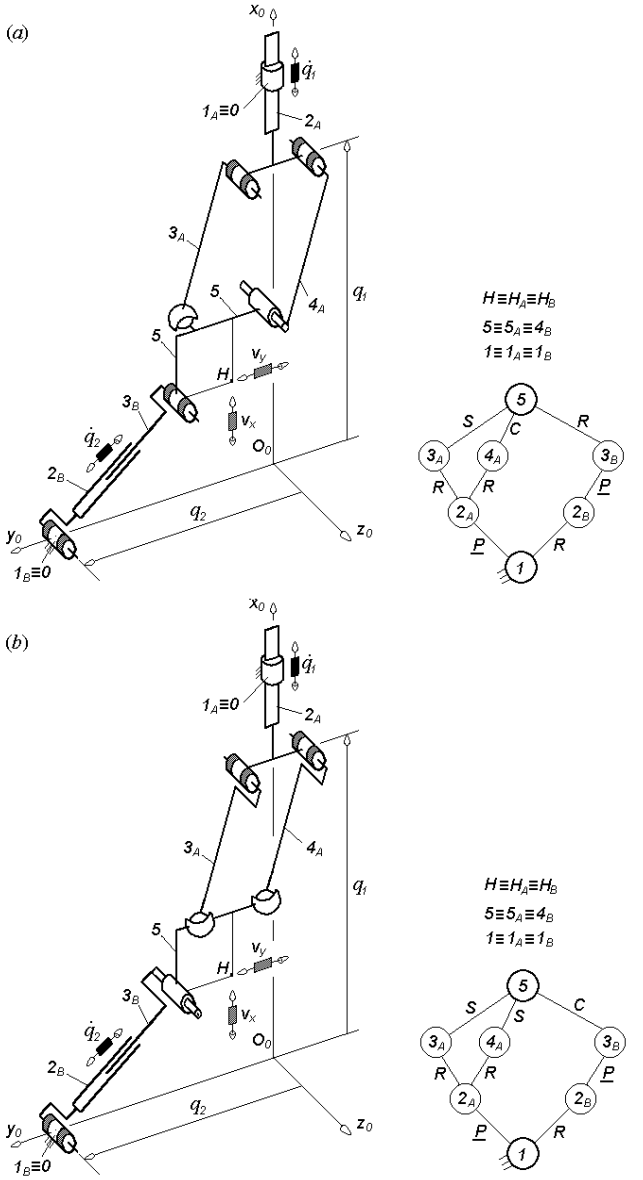

Fig. 2.8. Translational parallel mechanisms of types $\underline{P}Pa^*$-$R\underline{P}R$ with three overconstraints (**a**) and $\underline{P}Pa^{ss}$-$R\underline{P}C^*$ with one overconstraint (**b**), limb topologies $\underline{P} \perp Pa^*$ and $R \perp \underline{P} \perp {}^{\|}R$ (**a**), $\underline{P} \perp Pa^{ss}$ and $R \perp \underline{P} \perp {}^{\|}C^*$ (**b**)

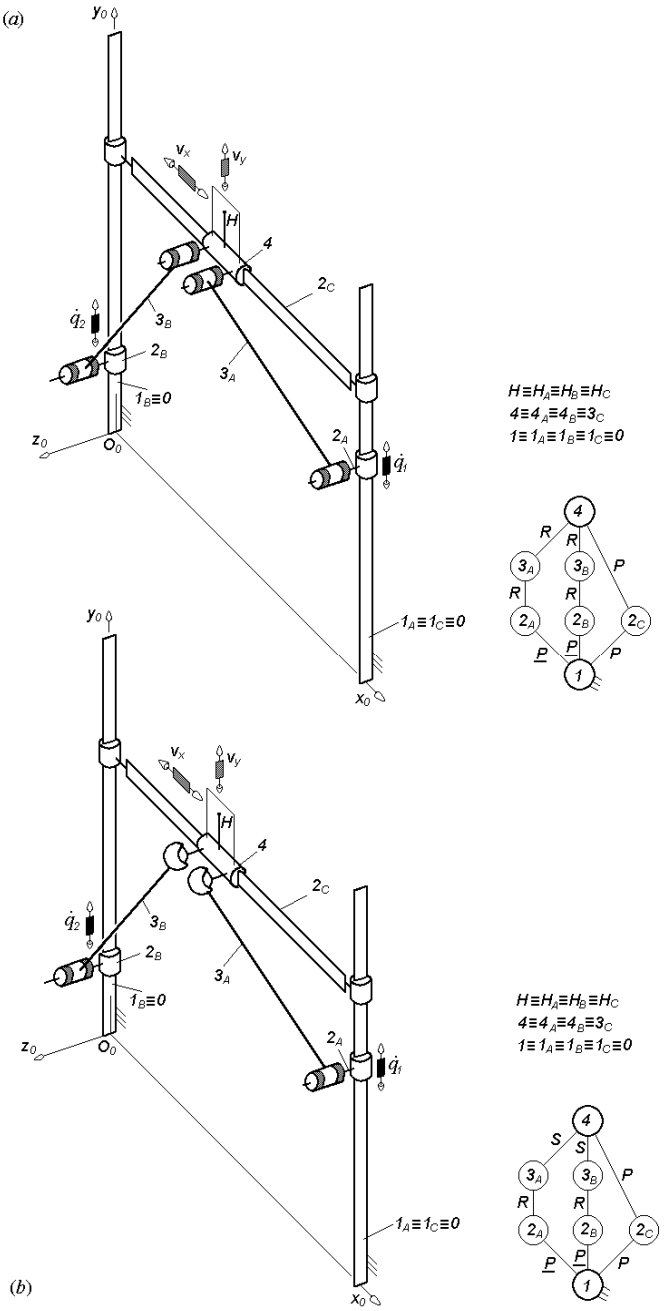

Fig. 2.9. Translational parallel mechanisms with an additional unactuated limb of types *2PRR-PP* (**a**) and *2PRS*-PP* (**b**), limb topologies $\underline{P} \perp R||R$ and $P \perp P$ (**a**), $\underline{P} \perp R\text{-}S^*$ and $P \perp P$ (**b**)

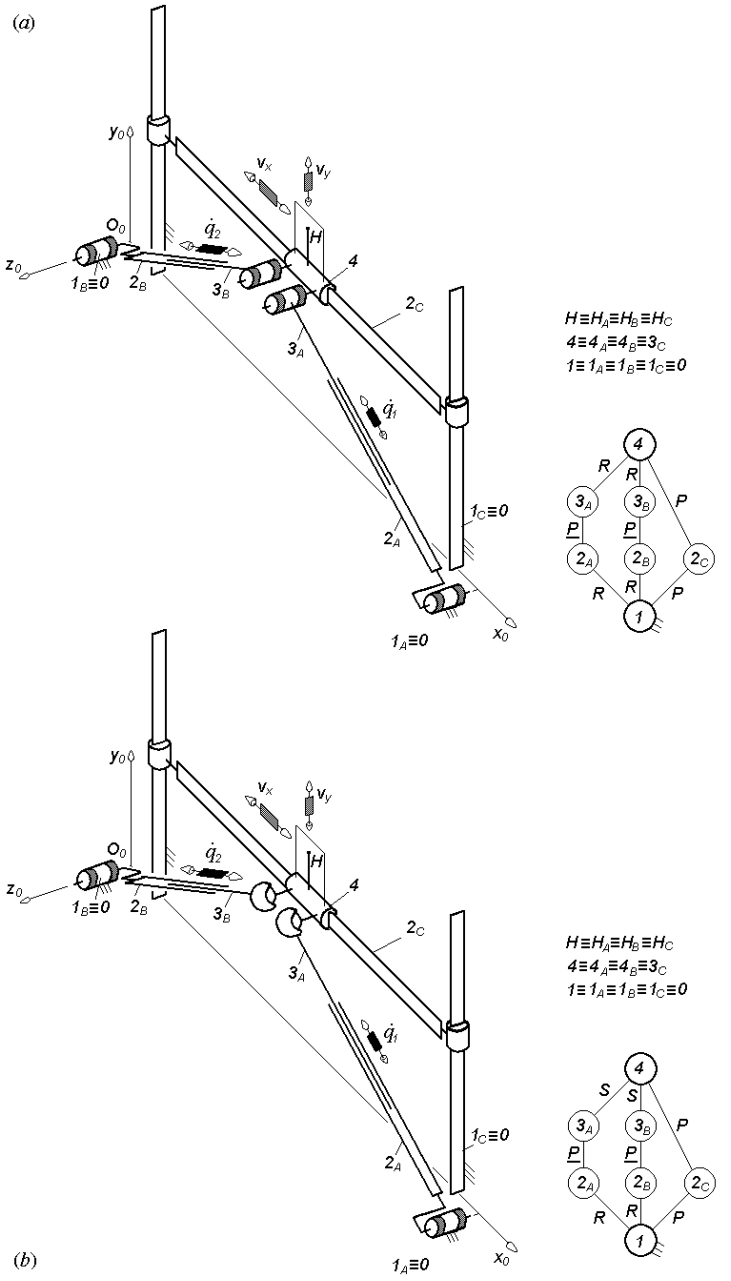

Fig. 2.10. Translational parallel mechanisms with an additional unactuated limb of types *2RPR-PP* (**a**) and *2RPS*-PP* (**b**), limb topologies $R \perp \underline{P} \perp \parallel R$ and $P \perp P$ (**a**), $R \perp \underline{P}$-S^* and $P \perp P$ (**b**)

Solutions with rotating actuators

In the basic solution with *rotating actuators* and coupled motions $F \leftarrow G_1–G_2$, the moving platform $n \equiv n_{Gi}$ is connected to the reference link $1 \equiv 1_{Gi} \equiv 0$ by two limbs of type $Pa||Pa$. Two planar parallelogram closed loops are combined in each limb. The solution is denoted by $2\underline{Pa}Pa$-type and has the two rotating actuators mounted on the fixed base. The axes of the revolute pairs of the parallelogram loops are perpendicular to the motion plane of the moving platform.

The example in Fig. 2.11 has the same arrangement of joints $Pa_z||Pa_z$ in both limbs. The structural diagram in Fig. 2.11 and Eq. (1.9) indicates that the mechanism has five independent closed loops $(q = 5)$. For this solution, Eqs. (1.2)–(1.8) and (1.17) give the following structural parameters: $M_{Gi} = S_{Gi} = 2$, $(R_{G1}) = (\boldsymbol{v}_x,\boldsymbol{v}_y)$, $(R_{G2}) = (\boldsymbol{v}_x,\boldsymbol{v}_y)$, $(R_F) = (\boldsymbol{v}_x,\boldsymbol{v}_y)$, $S_F = 2$, $M_F = 2$, $N_F = 16$ and $T_F = 0$. (see Table 2.4).

A wide range of overconstrained solutions with coupled motions and linear motors combined in two complex limbs with parallelogram loops can be derived from the solution in Fig. 2.11. They have $1 \le N_F < 16$ and may integrate up to three idle mobilities in each parallelogram loop and up to four idle mobilities outside the parallelogram loop. The idle mobilities integrated outside the parallelogram loops are three orthogonal rotations and one translation perpendicular to the motion plane of the moving platform.

For example, four idle mobilities are introduced outside the parallelogram loops in Fig. 2.12a and three idle mobilities are introduced in each parallelogram loop in Fig. 2.12b.

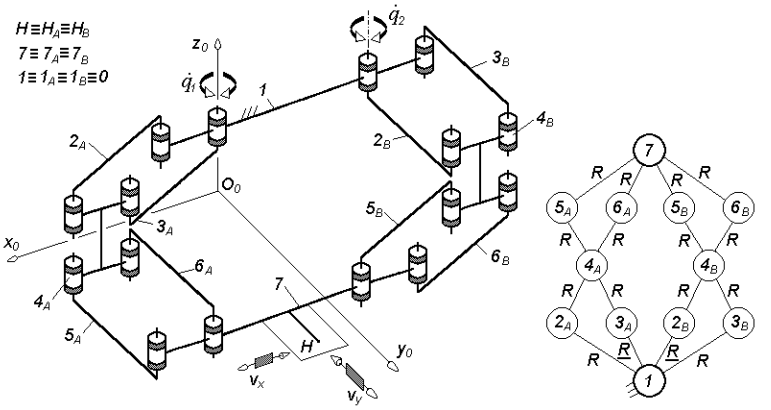

Fig. 2.11. $2\underline{Pa}Pa$-type translational parallel mechanism with coupled motions and sixteen overconstraints, limb topology $\underline{Pa}||Pa$

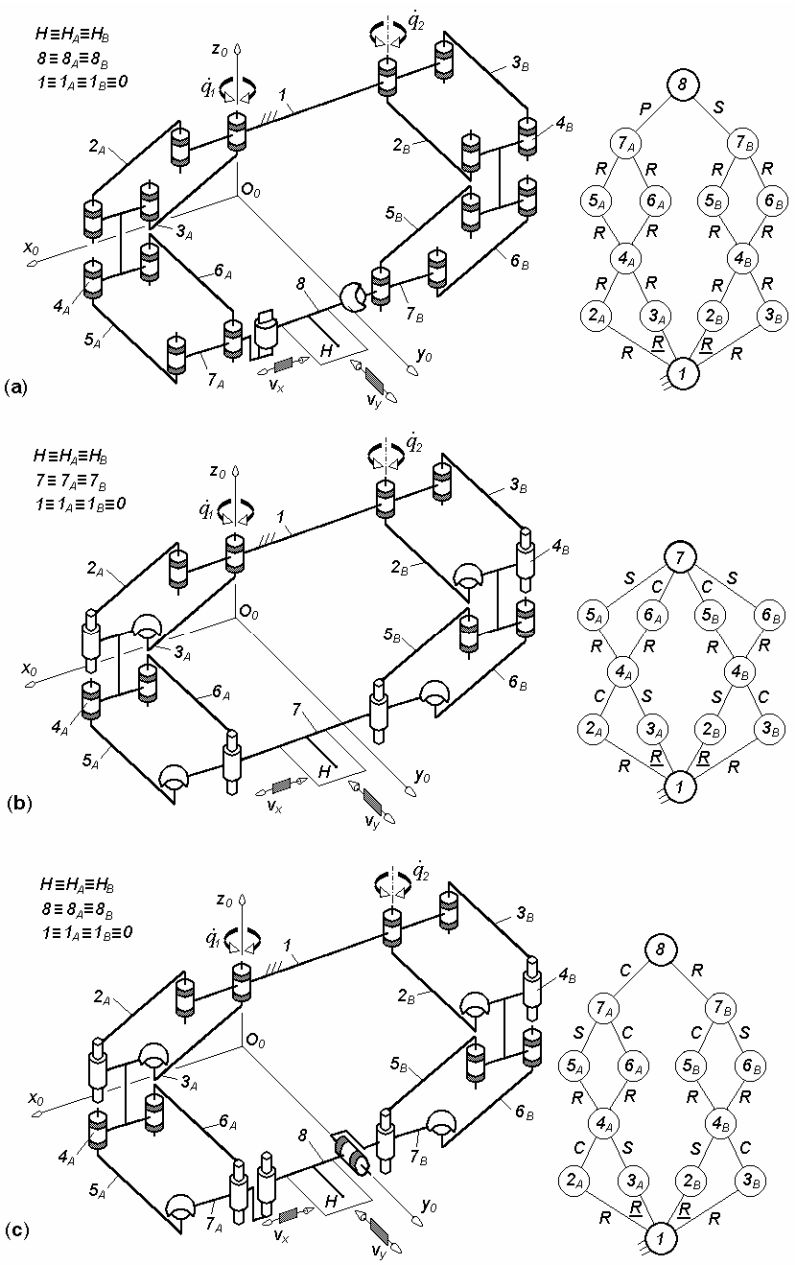

Fig. 2.12. Translational parallel mechanisms of types *PaPaP*-PaPaS** with twelve overconstraints (**a**), *2Pa*Pa** with four overconstraints (**b**) and *Pa*Pa*C*-Pa*Pa*R** with one overconstraint (**c**), limb topologies *Pa||Pa||P*-Pa||PaS** (**a**), *Pa*||Pa** (**b**), *Pa*||Pa*||C** and *Pa*||Pa* ⊥ R** (**c**)

Table 2.4. Structural parameters[a] of translational parallel mechanisms in Figs. 2.11 and 2.12

No.	Structural parameter	Solution *2PaPa*- Fig. 2.11	*PaPaP*-* *PaPaS** Fig. 2.12a	*2Pa*Pa** Fig. 2.12b	*Pa*Pa*C*-* *Pa*Pa*R** Fig. 2.12c
1	m	12	14	12	14
2	p_1	8	9	8	9
3	p_2	8	9	8	9
4	p	16	18	16	18
5	q	5	5	5	5
6	k_1	0	0	0	0
7	k_2	2	2	2	2
8	k	2	2	2	2
9	(R_{G1})	$(\boldsymbol{v}_x, \boldsymbol{v}_y)$	$(\boldsymbol{v}_x, \boldsymbol{v}_y, \boldsymbol{v}_z)$	$(\boldsymbol{v}_x, \boldsymbol{v}_y)$	$(\boldsymbol{v}_x, \boldsymbol{v}_y, v_z, \boldsymbol{\omega}_\delta)$
10	(R_{G2})	$(\boldsymbol{v}_x, \boldsymbol{v}_y)$	$(\boldsymbol{v}_x, \boldsymbol{v}_y, \boldsymbol{\omega}_\alpha, \boldsymbol{\omega}_\beta, \boldsymbol{\omega}_\delta)$	$(\boldsymbol{v}_x, \boldsymbol{v}_y)$	$(\boldsymbol{v}_x, \boldsymbol{v}_y, \boldsymbol{\omega}_\beta)$
11	S_{G1}	2	3	2	4
12	S_{G2}	2	5	2	3
13	r_{G1}	6	6	12	12
14	r_{G2}	6	6	12	12
15	M_{G1}	2	3	2	4
16	M_{G2}	2	5	2	3
17	(R_F)	$(\boldsymbol{v}_x, \boldsymbol{v}_y)$	$(\boldsymbol{v}_x, \boldsymbol{v}_y)$	$(\boldsymbol{v}_x, \boldsymbol{v}_y)$	$(\boldsymbol{v}_x, \boldsymbol{v}_y)$
18	S_F	2	2	2	2
19	r_1	12	12	24	24
20	r_F	14	18	26	29
21	M_F	2	2	2	2
22	N_F	16	12	4	1
23	T_F	0	0	0	0
24	$\sum_{j=1}^{p_1} f_j$	8	9	14	16
25	$\sum_{j=1}^{p_2} f_j$	8	11	14	15
26	$\sum_{j=1}^{p} f_j$	16	20	28	31

[a]See footnote of Table 2.1 for the nomenclature of structural parameters

In the example in Fig. 2.12c three idle mobilities are introduced outside the parallelogram loops and twelve inside the parallelogram loops. The structural parameters of the solutions illustrated in Figs. 2.11 and 2.12 are presented in Table 2.4.

As we have shown, the number of overconstraints could be further reduced by replacing one limb by a simple open kinematic chain with $2 < M_{Gi} = S_{Gi} < 6$ that integrates velocities $\boldsymbol{v}_x$ and $\boldsymbol{v}_y$ as the basis of its operational space.

In this way, a wide range of overconstrained translational parallel robots with rotating actuators and $0 < N_F \leq 9$ could be obtained. They have three independent loops ($q = 3$). For example, the solution in Fig. 2.13 is obtained by replacing G_2-limb in Fig. 2.11 by a planar kinematic chain $\underline{R}RR$-type ($\underline{R}_z||R_z||R_z$). Equations (1.2)–(1.8) and (1.17) give the following structural parameters for the parallel mechanisms in Fig. 2.13: $M_{G1} = S_{G1} = 2$, $M_{G2} = S_{G2} = 3$, $(R_{G1}) = (\boldsymbol{v}_x, \boldsymbol{v}_y)$, $(R_{G2}) = (\boldsymbol{v}_x, \boldsymbol{v}_y, \boldsymbol{\omega}_\delta)$, $(R_F) = (\boldsymbol{v}_x, \boldsymbol{v}_y)$, $S_F = 2$, $M_F = 2$, $N_F = 9$ and $T_F = 0$ (see Table 2.5).

Overconstrained solutions with $0 < N_F < 9$ can be derived from the solution in Fig. 2.13 by introducing up to three idle mobilities in each parallelogram loop and up to three idle mobilities outside the parallelogram loops. The idle mobilities integrated inside and outside the parallelogram loops could be two orthogonal rotations and one translation perpendicular to the motion plane of the moving platform.

For example, three idle mobilities are introduced outside the parallelogram loops in Fig. 2.14a and six idle mobilities are introduced in the parallelogram loops in Fig. 2.14b. In the example in Fig. 2.14c two idle mobilities are introduced outside the parallelogram loops and six in the parallelogram loops. The structural parameters of the solutions illustrated in Figs. 2.13 and 2.14 are presented in Table 2.5.

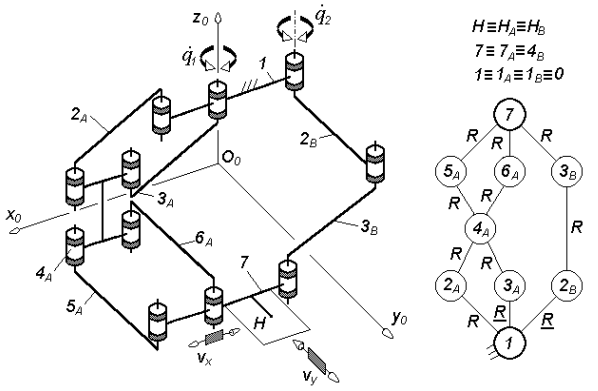

Fig. 2.13. $\underline{Pa}Pa$-$\underline{R}RR$-type translational parallel mechanism with coupled motions and nine overconstraints, limb topologies $\underline{Pa}||Pa$ and $\underline{R}||R||R$

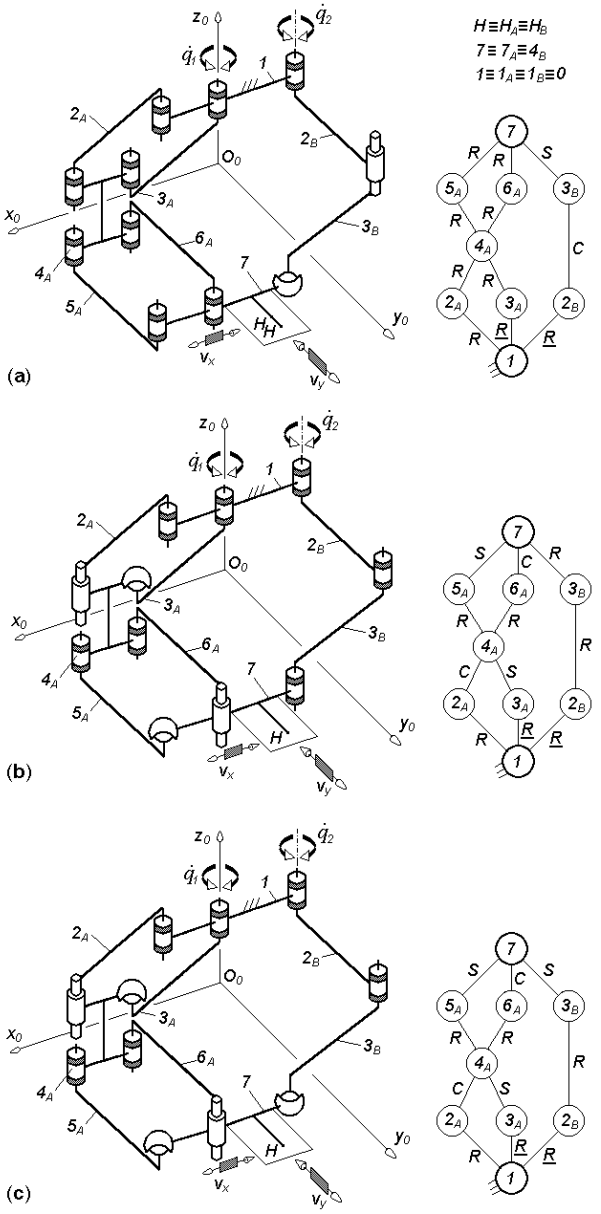

Fig. 2.14. Translational parallel mechanisms of types <u>*Pa*</u>*Pa*-<u>*R*</u>*C**S** with six overconstraints (**a**), <u>*Pa*</u>**Pa**-<u>*R*</u>*RR* with three overconstraints (**b**) and <u>*Pa*</u>**Pa**-<u>*R*</u>*RS** with one overconstraint (**c**), limb topologies <u>*Pa*</u>||*Pa* and <u>*R*</u>||*C**-*S** (**a**), <u>*Pa*</u>*||*Pa** and <u>*R*</u>||*R*||*R* (**b**), <u>*Pa*</u>*||*Pa** and <u>*R*</u>||*R*-*S** (**c**)

Table 2.5. Structural parameters[a] of translational parallel mechanisms in Figs. 2.13 and 2.14

No.	Structural parameter	Solution *PaPa-RRR* Fig. 2.13	*PaPa- RC*S** Fig. 2.14a	*Pa*Pa*-RRR* Fig. 2.14b	*Pa*Pa*- RRS** Fig. 2.14c
1	m	9	9	9	9
2	p_1	8	8	8	8
3	p_2	3	3	3	3
4	p	11	11	11	11
5	q	3	3	3	3
6	k_1	1	1	1	1
7	k_2	1	1	1	1
8	k	2	2	2	2
9	(R_{G1})	$(\boldsymbol{v}_x, \boldsymbol{v}_y)$	$(\boldsymbol{v}_x, \boldsymbol{v}_y)$	$(\boldsymbol{v}_x, \boldsymbol{v}_y)$	$(\boldsymbol{v}_x, \boldsymbol{v}_y)$
10	(R_{G2})	$(\boldsymbol{v}_x, \boldsymbol{v}_y, \boldsymbol{\omega}_\delta)$	$(\boldsymbol{v}_x, \boldsymbol{v}_y, \boldsymbol{v}_z, \boldsymbol{\omega}_\alpha, \boldsymbol{\omega}_\beta, \boldsymbol{\omega}_\delta)$	$(\boldsymbol{v}_x, \boldsymbol{v}_y, \boldsymbol{\omega}_\delta)$	$(\boldsymbol{v}_x, \boldsymbol{v}_y, \boldsymbol{\omega}_\alpha, \boldsymbol{\omega}_\beta, \boldsymbol{\omega}_\delta)$
11	S_{G1}	2	2	2	2
12	S_{G2}	3	6	3	5
13	r_{G1}	6	6	12	12
14	r_{G2}	0	0	0	10
15	M_{G1}	2	2	2	2
16	M_{G2}	3	6	3	5
17	(R_F)	$(\boldsymbol{v}_x, \boldsymbol{v}_y)$	$(\boldsymbol{v}_x, \boldsymbol{v}_y)$	$(\boldsymbol{v}_x, \boldsymbol{v}_y)$	$(\boldsymbol{v}_x, \boldsymbol{v}_y)$
18	S_F	2	2	2	2
19	r_1	6	6	12	12
20	r_F	9	12	15	17
21	M_F	2	2	2	2
22	N_F	9	6	3	1
23	T_F	0	0	0	0
24	$\sum_{j=1}^{p_1} f_j$	8	8	14	14
25	$\sum_{j=1}^{p_2} f_j$	3	6	3	5
26	$\sum_{j=1}^{p} f_j$	11	14	17	19

[a]See footnote of Table 2.1 for the nomenclature of structural parameters

Solutions of type $F \leftarrow G_1$–G_2–G_3 with an additional unactuated limb can also be derived by using two simple actuated limbs with $2 < M_{Gi} = S_{Gi} < 6$ and an unactuated limb $P \perp P$-type. The directions of the two prismatic pairs are parallel to the plane of motion of the moving platform. Actuated limbs G_1 and G_2 must integrate velocities $\boldsymbol{v}_x$ and $\boldsymbol{v}_y$ in the bases of their operational spaces. The three limbs form $q = 2$ independent loops and must meet the following conditions: $M_F = S_F = 2$ and $(R_F) = (R_{G1} \cap R_{G2} \cap R_{G2}) = (\boldsymbol{v}_x, \boldsymbol{v}_y)$.

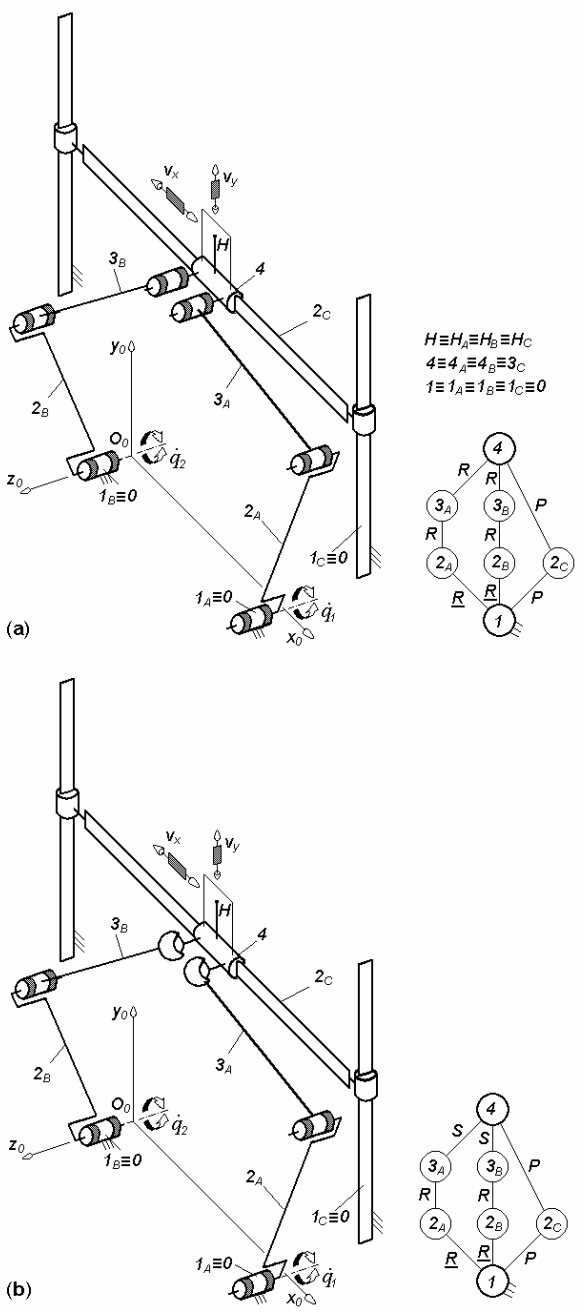

Fig. 2.15. Translational parallel mechanisms with an additional unactuated limb of types *2RRR-PP* (**a**) and *2RRS*-PP* (**b**), limb topologies $\underline{R}||R||R$ and $P \perp P$ (**a**), $\underline{R}||R$-S^* and $P \perp P$ (**b**)

Equation (1.16) indicates that the overconstrained solutions of these *T2*-type translational parallel robots with coupled motions and an additional unactuated limb have $\sum_1^p f_i < 14$. Various solutions with identical or different limb architectures can be generated. For example the solution in Fig. 2.15a has two actuated limbs of type *RRR* and six overconstraints. The solution in Fig. 2.15b has two overconstraints. These two solutions have the same structural parameters as their counterparts with linear motors (see Table 2.3).

Solutions with linear and rotating actuators

The basic solution with linear and rotating actuators and coupled motions $F \leftarrow G_1–G_2$ has a moving platform $n \equiv n_{Gi}$ connected to a reference link $1 \equiv 1_{Gi} \equiv 0$ by two limbs of types $P \perp Pa$ and $Pa||Pa$. This solution is denoted by <u>*P*</u>*Pa*-<u>*Pa*</u>*Pa* and has one linear and one rotating actuator situated on the fixed base. The linear actuator may have any direction parallel to the plane of motion of the moving platform. The axis of the actuated revolute pair is perpendicular to the motion plane of the moving platform.

The example in Fig. 2.16 has the following arrangement of joints: $P_x \perp Pa_z$ in G_1-limb and $Pa_z||Pa_z$ in G_2-limb. The structural diagram in Fig. 2.16 and Eq. (1.9) indicates that the mechanism has four independent closed loops $(q = 4)$. Equations (1.2)–(1.8) and (1.17) give the following structural parameters for the parallel mechanisms in Fig. 2.16: $M_{Gi} = S_{Gi} = 2$, $(R_{G1}) = (\boldsymbol{v}_x,\boldsymbol{v}_y)$, $(R_{G2}) = (\boldsymbol{v}_x,\boldsymbol{v}_y)$, $(R_F) = (\boldsymbol{v}_x,\boldsymbol{v}_y)$, $S_F = 2$, $M_F = 2$, $N_F = 13$ and $T_F = 0$ (see Table 2.6).

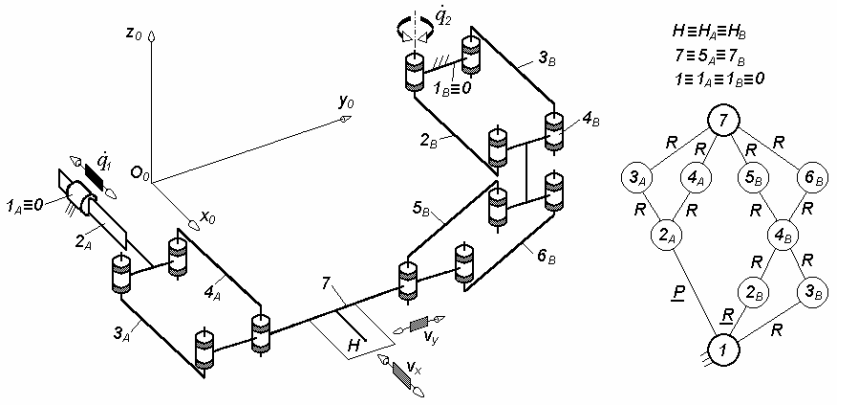

Fig. 2.16. <u>*P*</u>*Pa*-<u>*Pa*</u>*Pa*-type translational parallel mechanism with coupled motions and thirteen overconstraints, limb topologies <u>*P*</u> $\perp$ *Pa* and <u>*Pa*</u>||*Pa*

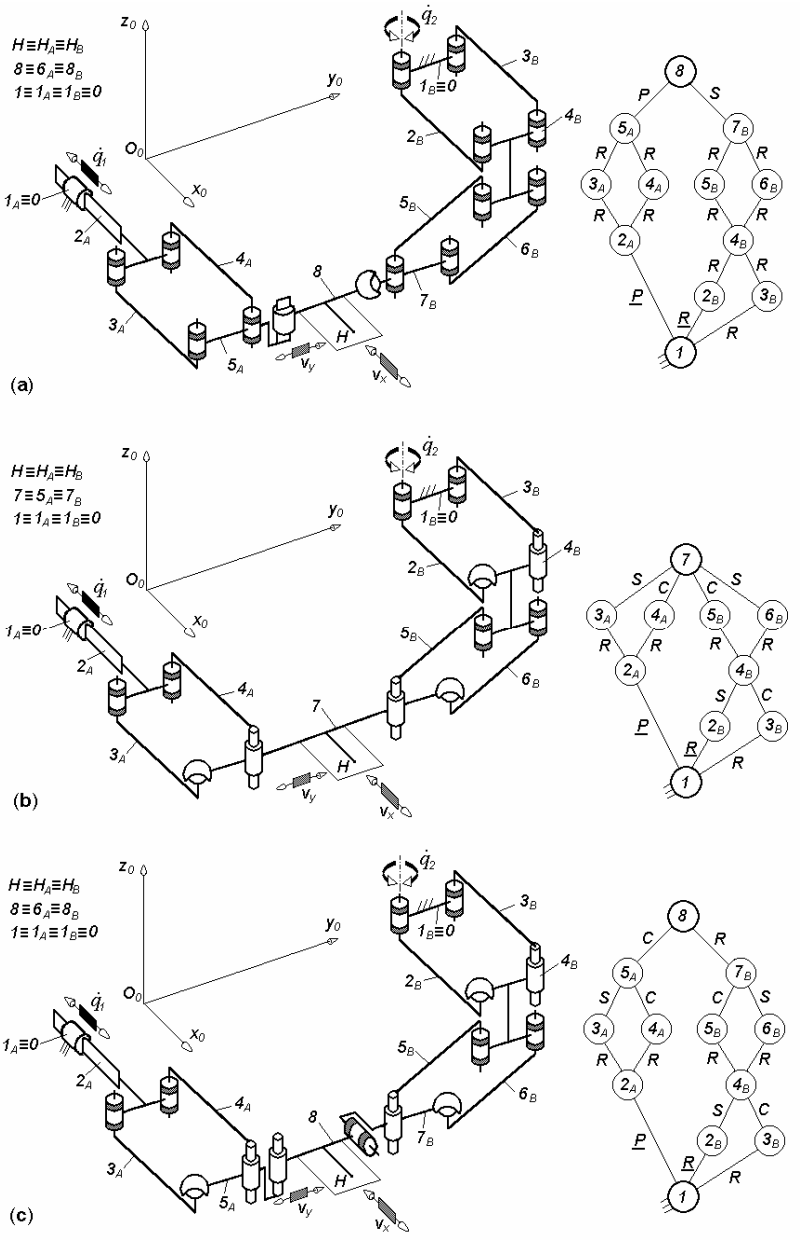

Fig. 2.17. Translational parallel mechanisms of types $\underline{P}PaP^*$-$\underline{Pa}PaS^*$ with nine overconstraints (**a**), $\underline{P}Pa^*$-$\underline{Pa}^*Pa^*$ with four overconstraints (**b**) and $\underline{P}Pa^*C^*$-$\underline{Pa}^*Pa^*R^*$ with one overconstraint (**c**), limb topologies $\underline{P} \perp Pa||P^*$ and $\underline{Pa}||Pa$-S^* (**a**), $\underline{P} \perp Pa^*$ and $\underline{Pa}^*||Pa^*$ (**b**), $\underline{P} \perp Pa^*||C^*$ and $\underline{Pa}^*||Pa^* \perp R^*$ (**c**)

Table 2.6. Structural parameters[a] of translational parallel mechanisms in Figs. 2.16 and 2.17

No.	Structural parameter	Solution *PPa*- *PaPa* Fig. 2.16	*PPaP**- *PaPaS** Fig. 2.17a	*PPa**- *Pa*Pa** Fig. 2.17b	*PPa*C**- *Pa*Pa*R** Fig. 2.17c
1	m	10	12	10	12
2	p_1	5	6	5	6
3	p_2	8	9	8	9
4	p	13	15	13	15
5	q	4	4	4	4
6	k_1	0	0	0	0
7	k_2	2	2	2	2
8	k	2	2	2	2
9	(R_{G1})	$(\boldsymbol{v}_x, \boldsymbol{v}_y)$	$(\boldsymbol{v}_x, \boldsymbol{v}_y, \boldsymbol{v}_z)$	$(\boldsymbol{v}_x, \boldsymbol{v}_y)$	$(\boldsymbol{v}_x, \boldsymbol{v}_y, v_z, \boldsymbol{\omega}_\delta)$
10	(R_{G2})	$(\boldsymbol{v}_x, \boldsymbol{v}_y)$	$(\boldsymbol{v}_x, \boldsymbol{v}_y, \boldsymbol{\omega}_\alpha, \boldsymbol{\omega}_\beta, \boldsymbol{\omega}_\delta)$	$(\boldsymbol{v}_x, \boldsymbol{v}_y)$	$(\boldsymbol{v}_x, \boldsymbol{v}_y, \boldsymbol{\omega}_\beta)$
11	S_{G1}	2	3	2	4
12	S_{G2}	2	5	2	3
13	r_{G1}	3	3	6	6
14	r_{G2}	6	6	12	12
15	M_{G1}	2	3	2	4
16	M_{G2}	2	5	2	3
17	(R_F)	$(\boldsymbol{v}_x, \boldsymbol{v}_y)$	$(\boldsymbol{v}_x, \boldsymbol{v}_y)$	$(\boldsymbol{v}_x, \boldsymbol{v}_y)$	$(\boldsymbol{v}_x, \boldsymbol{v}_y)$
18	S_F	2	2	2	2
19	r_1	9	9	18	18
20	r_F	11	15	20	23
21	M_F	2	2	2	2
22	N_F	13	9	4	1
23	T_F	0	0	0	0
24	$\sum_{j=1}^{p_1} f_j$	5	6	8	10
25	$\sum_{j=1}^{p_2} f_j$	8	11	14	15
26	$\sum_{j=1}^{p} f_j$	13	17	22	25

[a]See footnote of Table 2.1 for the nomenclature of structural parameters

A wide range of overconstrained solutions with coupled motions and linear and rotating actuators integrated in two complex limbs with parallelogram loops can be derived from the solution in Fig. 2.16. They have $0 < N_F < 13$ and could integrate up to three idle mobilities in each parallelogram loop and up to four idle mobilities outside the parallelogram loop as presented in the previous sections. For example, four idle mobilities are introduced outside the parallelogram loops in Fig. 2.17a and three idle

mobilities are introduced in each parallelogram loop in Fig. 2.17b. In the example in Fig. 2.17c three idle mobilities are introduced outside the parallelogram loops and nine inside the parallelogram loops. The structural parameters of the solutions illustrated in Figs. 2.16 and 2.17 are presented in Table 2.6. One limb in Fig. 2.16 can be replaced by a simple open kinematic chain with $2 < M_{Gi} = S_{Gi} < 6$ that integrates the velocities $\boldsymbol{v}_x$ and $\boldsymbol{v}_y$ in the basis of its operational space. In this way, a large diversity of overconstrained translational parallel robots with $0 < N_F < 10$ actuated by linear and rotating motors can be obtained. They have three independent closed loops ($q = 3$) when G_1-limb is replaced (Fig. 2.18) and $q = 2$ when G_2-limb is replaced (Fig. 2.19).

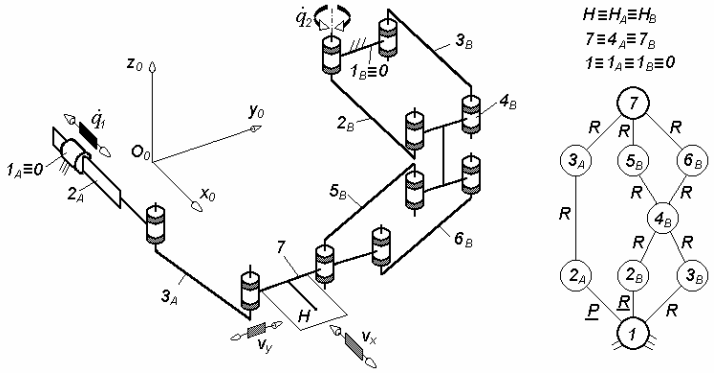

Fig. 2.18. *PRR-PaPa*-type translational parallel mechanism with nine overconstraints, limb topologies $\underline{P} \perp R||R$ and $\underline{Pa}||Pa$

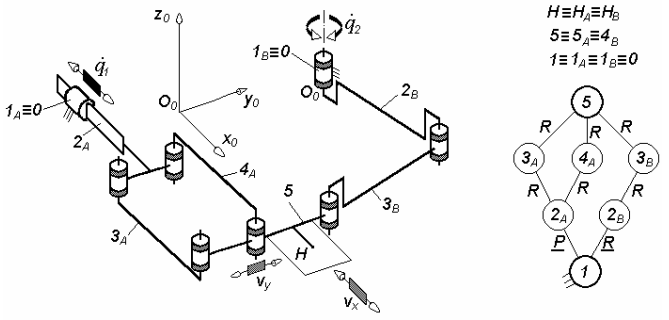

Fig. 2.19. *PPa-RRR*-type translational parallel mechanism with six overconstraints, limb topologies $\underline{P} \perp Pa\text{-}\underline{R}||R||R$

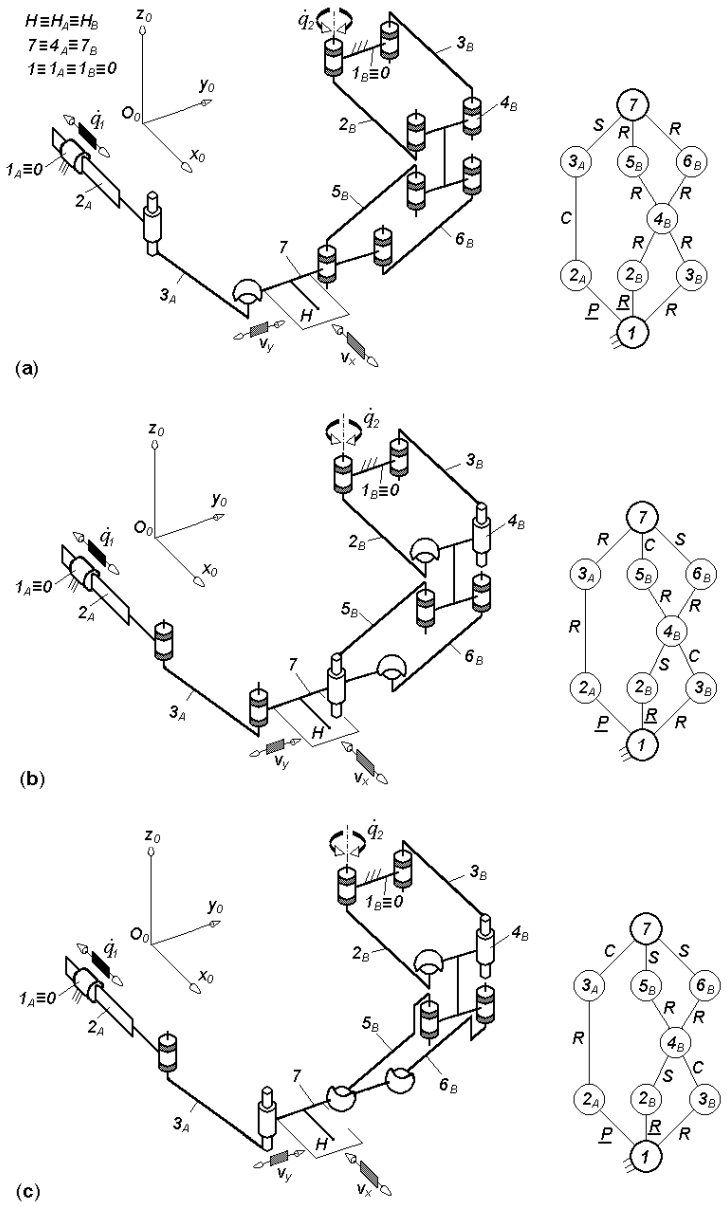

Fig. 2.20. Translational parallel mechanisms of types $\underline{P}C^*S^*$-$\underline{Pa}Pa$ with six overconstraints (**a**), $\underline{P}RR$-$\underline{Pa}^*Pa^*$ with three overconstraints (**b**) and $\underline{P}RC^*$-$\underline{Pa}^*Pa^{ss}$ with one overconstraint (**c**), limb topologies $\underline{P} \perp C^*$-S^* and $\underline{Pa}||Pa$ (**a**), $\underline{P} \perp R||R$ and $\underline{Pa}^*||Pa^*$ (**b**), $\underline{P} \perp R||C^*$ and $\underline{Pa}^*||Pa^{ss}$ (**c**)

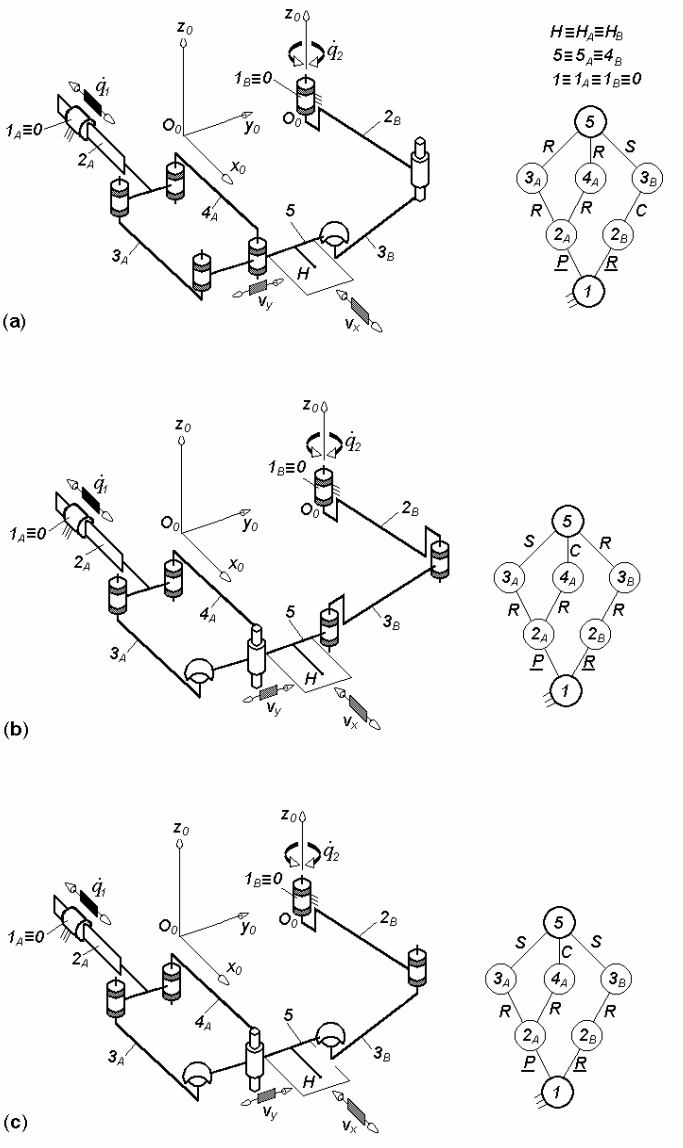

Fig. 2.21. Translational parallel mechanisms of types $\underline{P}Pa$-$\underline{R}C$*S* with three overconstraints (**a**), $\underline{P}Pa$*-$\underline{R}RR$ with three overconstraints (**b**) and $\underline{P}Pa$*-$\underline{R}RS$* with one overconstraint (**c**), limb topologies $\underline{P} \perp Pa$ and $\underline{R}||C$*-S* (**a**), $\underline{P} \perp Pa$* and $\underline{R}||R||R$ (**b**), $\underline{P} \perp Pa$* and $\underline{R}||R$-S*(**c**)

For example, the solution in Fig. 2.18 is obtained by replacing G_1-limb in Fig. 2.16 by a planar kinematic chain $\underline{P}_y R_z R_z$-type. Equations (1.2)–(1.8) and (1.17) give the following structural parameters for the solution in Fig. 2.18: $M_{G1} = S_{G1} = 3$, $M_{G2} = S_{G2} = 2$, $(R_{G1}) = (\boldsymbol{v}_x, \boldsymbol{v}_y, \boldsymbol{\omega}_\delta)$, $(R_{G2}) = (\boldsymbol{v}_x, \boldsymbol{v}_y)$, $(R_F) = (\boldsymbol{v}_x, \boldsymbol{v}_y)$, $S_F = 2$, $M_F = 2$, $N_F = 9$ and $T_F = 0$. The solution in Fig. 2.19 is obtained by replacing G_2-limb in Fig. 2.16 by a planar kinematic chain $\underline{R}_z R_z R_z$-type. The solution in Fig. 2.19 has the following structural parameters: $M_{G1} = S_{G1} = 2$, $M_{G2} = S_{G2} = 3$, $(R_{G1}) = (\boldsymbol{v}_x, \boldsymbol{v}_y)$, $(R_{G2}) = (\boldsymbol{v}_x, \boldsymbol{v}_y, \boldsymbol{\omega}_\delta)$, $(R_F) = (\boldsymbol{v}_x, \boldsymbol{v}_y)$, $S_F = 2$, $M_F = 2$, $N_F = 6$ and $T_F = 0$.

A wide range of overconstrained solutions with coupled motions and linear and rotating actuators can be derived from solutions in Figs. 2.18 and 2.19. They have $0 < N_F < 9$ and could integrate up to three idle mobilities in each parallelogram loop and up to three idle mobilities outside the parallelogram loops. For example, three idle mobilities are introduced outside the parallelogram loops in Figs. 2.20a and 2.21a, and three idle mobilities inside each parallelogram loop in Figs. 2.20b and 2.21b.

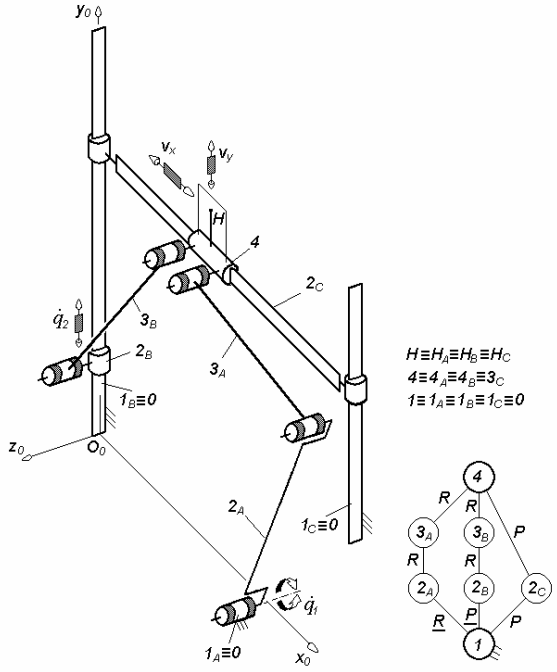

Fig. 2.22. $\underline{R}RR$-$\underline{P}RR$-PP-type translational parallel mechanism with an additional unactuated limb and six overconstraints, limb topologies $\underline{R}||R||R$, $\underline{P} \perp R||R$ and $P \perp P$

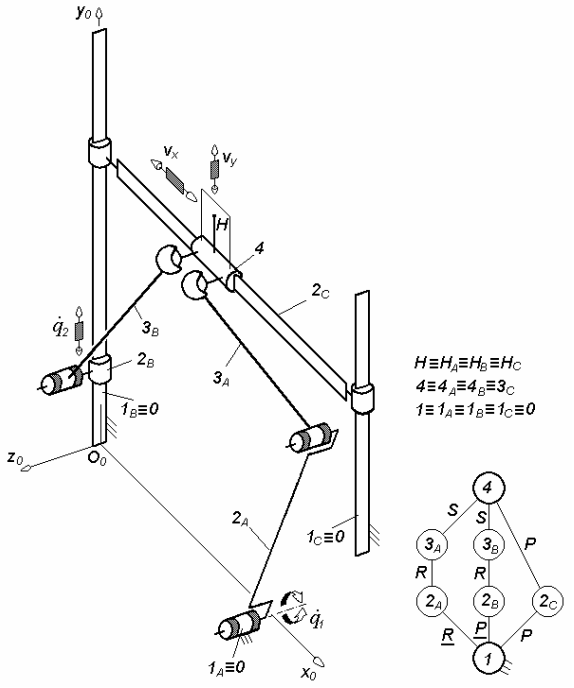

Fig. 2.23. *RRS*-PRS*-PP*-type translational parallel mechanism with an additional unactuated limb and two overconstraints, limb topologies $\underline{R}||R\text{-}S^*$, $\underline{P} \perp R\text{-}S^*$ and $P \perp P$

Two idle mobilities are introduced outside the parallelogram loops and three inside each parallelogram loop in Figs. 2.20c and 2.21c. The structural parameters of the solutions illustrated in Figs. 2.18 and 2.20 are obtained by similarity with their counterparts using rotating actuators (see Table 2.5). The solutions in Figs. 2.19 and 2.21 have the same structural parameters as their counterparts with linear actuators (see Table 2.2).

Solutions of type $F \leftarrow G_1\text{–}G_2\text{–}G_3$ with an additional unactuated limb and two limbs actuated by linear and rotating motors can also be generated. For example, the solution in Fig. 2.22 with six overconstraints has the actuated limbs of types $\underline{R}_z R_z R_z$ and $\underline{P}_y R_z R_z$. The solution in Fig. 2.23 with two overconstraints has the actuated limbs of type *RRS* and *PRS*. These solutions have the same structural parameters as their counterparts with linear motors (see Table 2.3).

2.1.2 Non overconstrained solutions

Equation (1.15) indicates that *non overconstrained* solutions of *T2*-type translational parallel robots with coupled motions and q independent loops meet the condition $\sum_1^p f_i = 2 + 6q$. Various solutions fulfil this condition along with $M_F = S_F = 2$ and $(R_F) = (\boldsymbol{v}_x, \boldsymbol{v}_y)$. They can have identical limbs or limbs with different structures and may be actuated by linear or rotating motors.

Solutions with linear actuators

Non overconstrained solutions $F \leftarrow G_1 – G_2$ with linear actuators and coupled motions have $\sum_1^p f_i = 20$ when two complex limbs are used. They can be derived from the solution in Fig. 2.1 by introducing ten idle mobilities: four outside the parallelogram loops and six inside the parallelogram loops. For example the solution in Fig. 2.24 with G_1-limb $\underline{P}Pa^{ss}$-type and G_2-limb $\underline{P}C^*Pa^{ss}$-type has $M_{G1} = S_{G1} = 3$, $M_{G2} = S_{G2} = 5$, $(R_{G1}) = (\boldsymbol{v}_x, \boldsymbol{v}_y, \boldsymbol{\omega}_\beta)$, $(R_{G2}) = (\boldsymbol{v}_x, \boldsymbol{v}_y, \boldsymbol{v}_z, \boldsymbol{\omega}_\alpha, \boldsymbol{\omega}_\delta)$, $(R_F) = (\boldsymbol{v}_x, \boldsymbol{v}_y)$, $M_F = S_F = 2$, $N_F = 0$ and $T_F = 0$.

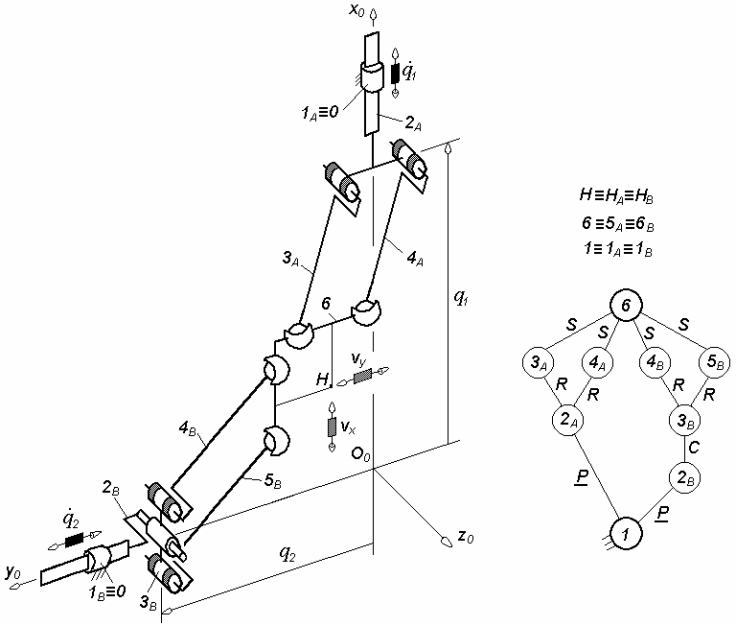

Fig. 2.24. $\underline{P}Pa^{ss}$-$\underline{P}C^*Pa^{ss}$-type non overconstrained translational parallel mechanism, limb topologies $\underline{P} \perp Pa^{ss}$ and $\underline{P} \perp C^* || Pa^{ss}$

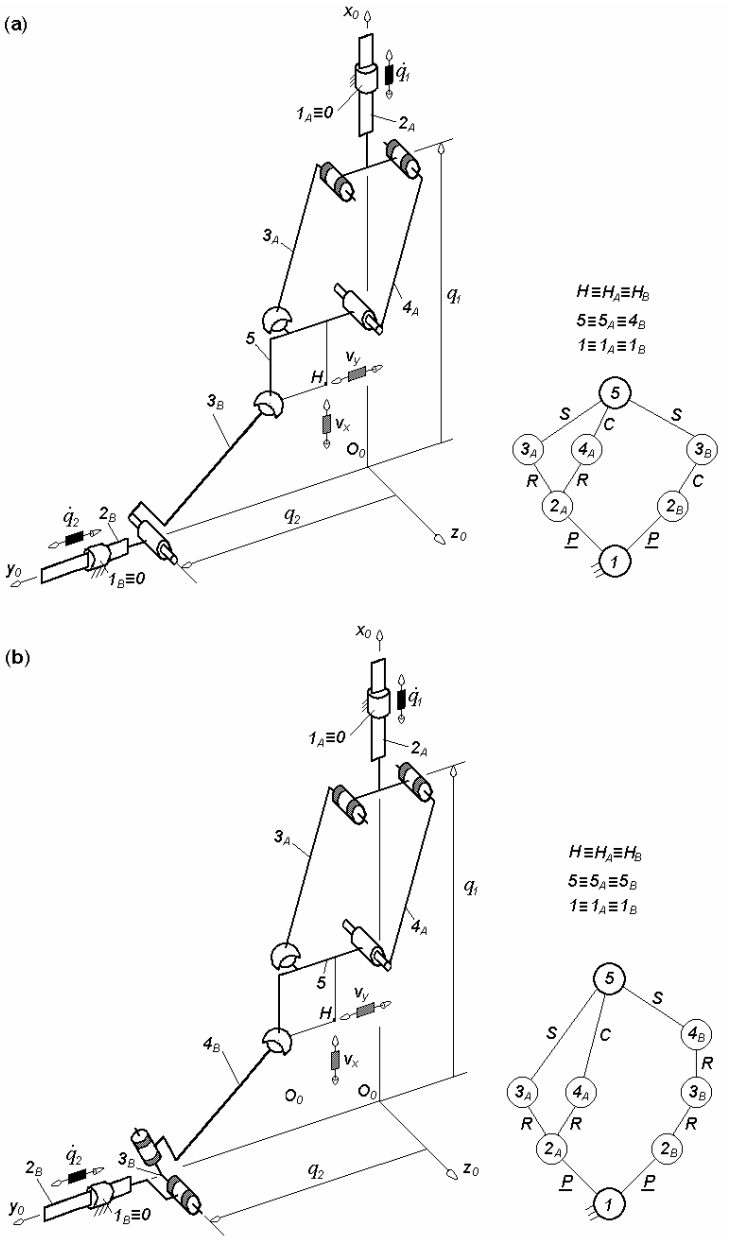

Fig. 2.25. Non overconstrained translational parallel mechanisms of types $\underline{P}Pa^*$-$\underline{P}C^*S^*$ (**a**) and $\underline{P}Pa^*$-$\underline{P}U^*S^*$ (**b**), limb topologies $\underline{P} \perp Pa^*$ and $\underline{P} \perp C^*$-S^* (**a**), $\underline{P} \perp Pa^*$ and $\underline{P} \perp U^*S^*$ (**b**)

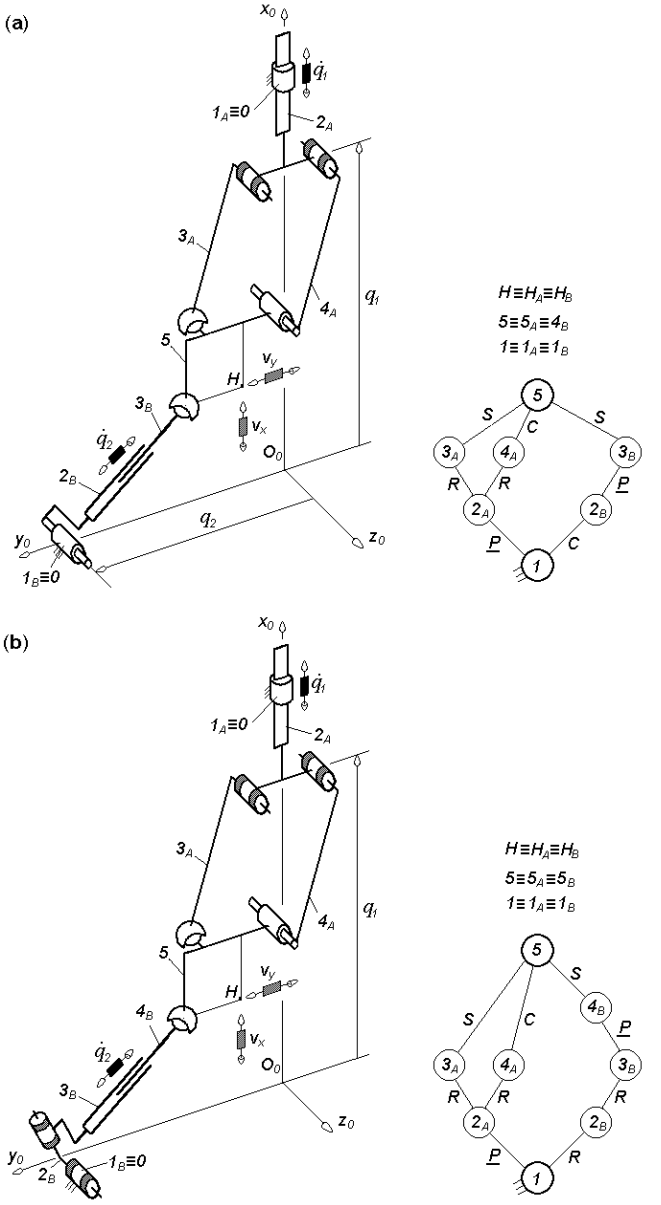

Fig. 2.26. Non overconstrained translational parallel mechanisms of types $\underline{P}Pa^*$-$C^*\underline{P}S^*$ (**a**) and $\underline{P}Pa^*$-$U^*\underline{P}S^*$ (**b**), limb topology $\underline{P} \perp Pa^*$ and $C^* \perp \underline{P}$-S^* (**a**), $\underline{P} \perp Pa^*$ and $U^* \perp \underline{P}$-S^* (**b**)

Table 2.7. Structural parameters[a] of translational parallel mechanisms in Figs. 2.24–2.26

No.	Structural parameter	Solution $\underline{P}Pa^{ss}$-$\underline{P}C$*Pa^{ss} (Fig. 2.24)	$\underline{P}Pa$*-$\underline{P}C$*S* $\underline{P}Pa$*-C*$\underline{P}S$* (Figs. 2.25a, 2.26a)	$\underline{P}Pa$*-$\underline{P}U$*S* $\underline{P}Pa$*-U*$\underline{P}S$* (Figs. 2.25b, 2.26b)
1	m	9	7	8
2	p_1	5	5	5
3	p_2	6	3	4
4	p	11	8	9
5	q	3	2	2
6	k_1	0	1	1
7	k_2	2	1	1
8	k	2	2	2
9	(R_{G1})	$(\boldsymbol{v}_x, \boldsymbol{v}_y, \boldsymbol{\omega}_\beta)$	$(\boldsymbol{v}_x, \boldsymbol{v}_y)$	$(\boldsymbol{v}_x, \boldsymbol{v}_y)$
10	(R_{G2})	$(\boldsymbol{v}_x, \boldsymbol{v}_y, \boldsymbol{v}_z, \boldsymbol{\omega}_\alpha, \boldsymbol{\omega}_\delta)$	$(\boldsymbol{v}_x, \boldsymbol{v}_y, \boldsymbol{v}_z, \boldsymbol{\omega}_\alpha, \boldsymbol{\omega}_\beta, \boldsymbol{\omega}_\delta)$	$(\boldsymbol{v}_x, \boldsymbol{v}_y, \boldsymbol{v}_z, \boldsymbol{\omega}_\alpha, \boldsymbol{\omega}_\beta, \boldsymbol{\omega}_\delta)$
11	S_{G1}	3	2	2
12	S_{G2}	5	6	6
13	r_{G1}	6	6	6
14	r_{G2}	6	0	0
15	M_{G1}	3	2	2
16	M_{G2}	5	6	6
17	(R_F)	$(\boldsymbol{v}_x, \boldsymbol{v}_y)$	$(\boldsymbol{v}_x, \boldsymbol{v}_y)$	$(\boldsymbol{v}_x, \boldsymbol{v}_y)$
18	S_F	2	2	2
19	r_1	12	6	6
20	r_F	18	12	12
21	M_F	2	2	2
22	N_F	0	0	0
23	T_F	0	0	0
24	$\sum_{j=1}^{p_1} f_j$	9	8	8
25	$\sum_{j=1}^{p_2} f_j$	11	6	6
26	$\sum_{j=1}^{p} f_j$	20	14	14

[a]See footnote of Table 2.1 for the nomenclature of structural parameters

Non overconstrained solutions $F \leftarrow G_1$–G_2 with linear actuators and coupled motions have $\sum_1^p f_i = 14$ when one simple and one complex limb are used. They can be derived from the solution in Fig. 2.4 by introducing six idle mobilities: three outside and three inside the parallelogram loop. For example, the solution in Fig. 2.25a has G_1-limb of type $\underline{P}Pa$* and G_2-limb

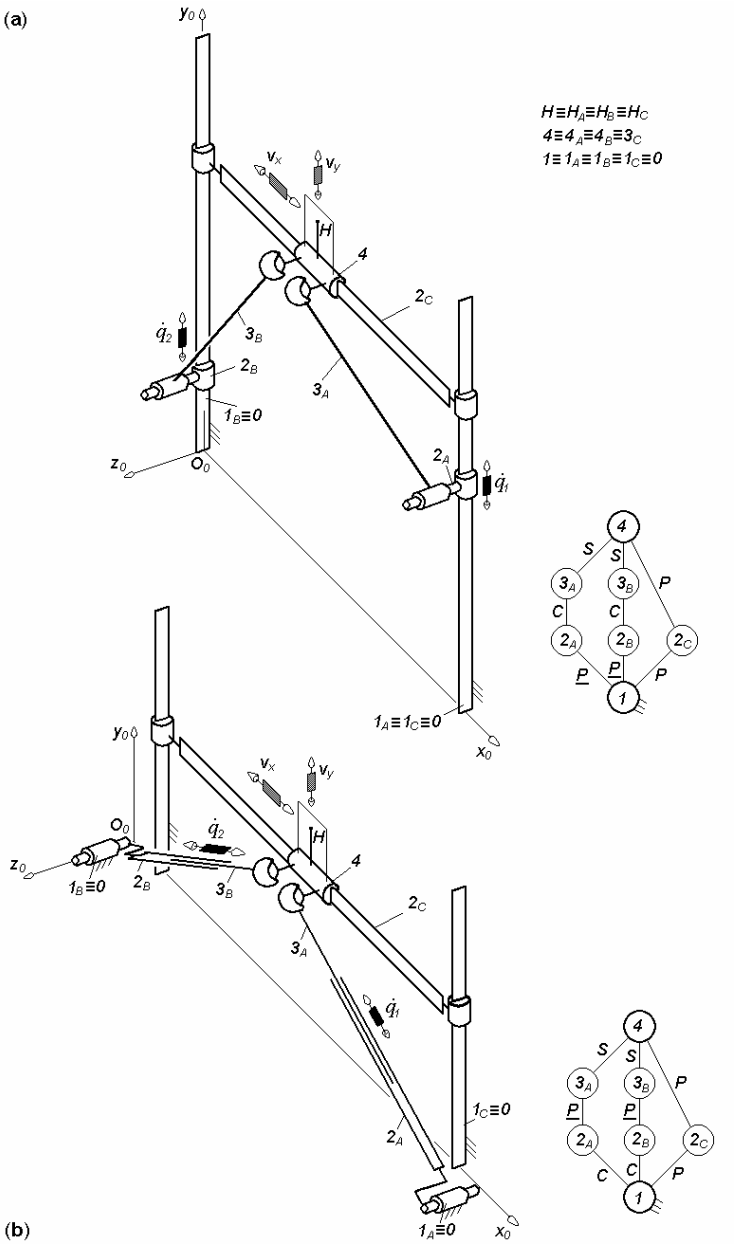

Fig. 2.27. Non overconstrained translational parallel mechanisms with an additional unactuated limb of types *2PC*S*-PP* (**a**) and *2C*PS*-PP* (**b**), limb topologies $\underline{P} \perp C^*\text{-}S^*$ and $P \perp P$ (**a**), $C^* \perp \underline{P}\text{-}S^*$ and $P \perp P$ (**b**)

of type $\underline{P}C^*S^*$. The solution in Fig. 2.25b has G_1-limb of type $\underline{P}Pa^*$ and $G2$-limb of type $U^*\underline{P}S^*$. Both solutions have the following structural parameters $M_{G1} = S_{G1} = 2$, $M_{G2} = S_{G2} = 6$, $(R_F) = (\boldsymbol{v}_x, \boldsymbol{v}_y)$, $(R_{G1}) = (\boldsymbol{v}_x, \boldsymbol{v}_y)$, $(R_{G2}) = (\boldsymbol{v}_x, \boldsymbol{v}_y, \boldsymbol{v}_z, \boldsymbol{\omega}_\alpha, \boldsymbol{\omega}_\beta, \boldsymbol{\omega}_\delta)$, $M_F = S_F = 2$, $N_F = 0$ and $T_F = 0$.

Non overconstrained solutions with linear actuators non adjacent to the fixed base can be derived from the overconstrained solutions presented in Fig. 2.7a by introducing three idle mobilities inside and three outside the parallelogram loop. For example, the solution in Fig. 2.26a has G_1-limb of type $\underline{P}Pa^*$ and G_2-limb of type $C^*\underline{P}S^*$. The solution in Fig. 2.26b has G_1-limb of type $\underline{P}Pa^*$ and G_2-limb of type $U^*\underline{P}S^*$. Both solutions have $M_{G1} = S_{G1} = 2$, $M_{G2} = S_{G2} = 6$, $(R_{G1}) = (\boldsymbol{v}_x, \boldsymbol{v}_y)$, $(R_{G2}) = (\boldsymbol{v}_x, \boldsymbol{v}_y, \boldsymbol{v}_z, \boldsymbol{\omega}_\alpha, \boldsymbol{\omega}_\beta, \boldsymbol{\omega}_\delta)$, $(R_F) = (\boldsymbol{v}_x, \boldsymbol{v}_y)$, $M_F = S_F = 2$, $N_F = 0$ and $T_F = 0$. The structural parameters of the solutions illustrated in Figs. 2.24–2.26 are presented in Table 2.7.

Non overconstrained solutions of type $F \leftarrow G_1$–G_2–G_3 with an additional *unactuated limb* can be derived from the overconstrained solutions presented in Figs. 2.9a and 2.10a. The solutions in Fig. 2.27 have an unactuated simple limb $\underline{P}P$-type and two actuated simple limbs $\underline{P}C^*S^*$-type (Fig. 2.27a) and $C^*\underline{P}S^*$-type (Fig. 2.27b). For both solutions have $M_{G1} = S_{G1} = 6$, $M_{G2} = S_{G2} = 6$, $M_{G3} = S_{G3} = 2$, $(R_{G1}) = (R_{G2}) = (\boldsymbol{v}_x, \boldsymbol{v}_y, \boldsymbol{v}_z, \boldsymbol{\omega}_\alpha, \boldsymbol{\omega}_\beta, \boldsymbol{\omega}_\delta)$, $(R_{G3}) = (\boldsymbol{v}_x, \boldsymbol{v}_y)$, $(R_F) = (\boldsymbol{v}_x, \boldsymbol{v}_y)$, $M_F = S_F = 2$, $N_F = 0$ and $T_F = 0$.

Solutions with rotating actuators

Non overconstrained solutions $F \leftarrow G_1$–G_2 with rotating actuators and coupled motions have $\sum_1^p f_i = 32$ when two complex limbs are used.

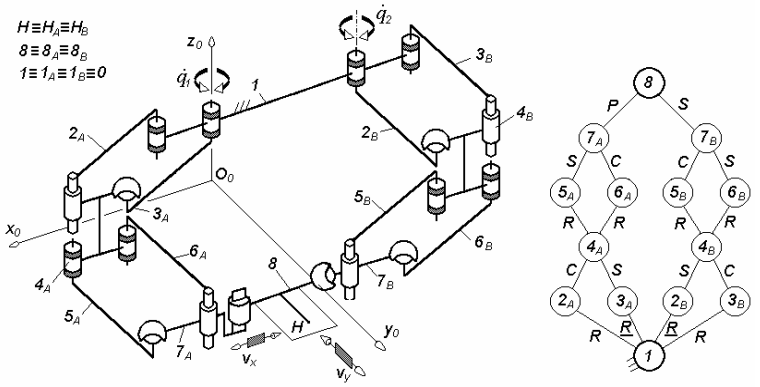

Fig. 2.28. $\underline{Pa}^*Pa^*P^*$-$\underline{Pa}^*Pa^*S^*$-type non overconstrained translational parallel mechanism, limb topologies $\underline{Pa}^*||Pa^*||P^*$-$\underline{Pa}^*||Pa^*S^*$

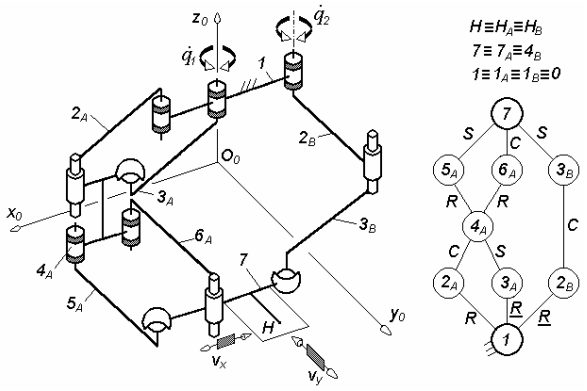

Fig. 2.29. *Pa*Pa*-RC*S**-type non overconstrained translational parallel mechanism, limb topologies *Pa*||Pa** and *R||C*-S**

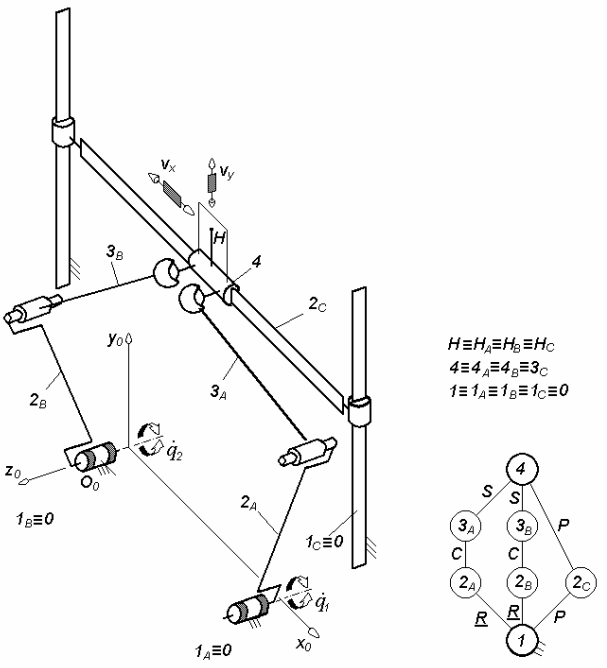

Fig. 2.30. *2RC*S*-PP*-type non overconstrained translational parallel mechanism with an additional unactuated limb, limb topologies *R||C*-S** and $P \perp P$

Table 2.8. Structural parameters[a] of translational parallel mechanisms in Figs. 2.28–2.30

No.	Structural parameter	Solution *Pa*Pa*P*- *Pa*Pa*S* Fig. 2.28	*Pa*Pa*-*RC*S* Fig. 2.29	*2RC*S*-PP Fig. 2.30
1	m	14	9	7
2	p_1	9	8	3
3	p_2	9	3	3
4	p_3	–	–	2
5	p	18	11	8
6	q	5	3	2
7	k_1	0	1	3
8	k_2	2	1	0
9	k	2	2	3
10	(R_{G1})	$(\boldsymbol{v}_x, \boldsymbol{v}_y, \boldsymbol{v}_z)$	$(\boldsymbol{v}_x, \boldsymbol{v}_y)$	$(\boldsymbol{v}_x, \boldsymbol{v}_y, \boldsymbol{v}_z, \boldsymbol{\omega}_\alpha, \boldsymbol{\omega}_\beta, \boldsymbol{\omega}_\delta)$
11	(R_{G2})	$(\boldsymbol{v}_x, \boldsymbol{v}_y, \boldsymbol{\omega}_\alpha, \boldsymbol{\omega}_\beta, \boldsymbol{\omega}_\delta)$	$(\boldsymbol{v}_x, \boldsymbol{v}_y, \boldsymbol{v}_z, \boldsymbol{\omega}_\alpha, \boldsymbol{\omega}_\beta, \boldsymbol{\omega}_\delta)$	$(\boldsymbol{v}_x, \boldsymbol{v}_y, \boldsymbol{v}_z, \boldsymbol{\omega}_\alpha, \boldsymbol{\omega}_\beta, \boldsymbol{\omega}_\delta)$
12	(R_{G3})	–	–	$(\boldsymbol{v}_x, \boldsymbol{v}_y)$
13	S_{G1}	3	2	6
14	S_{G2}	5	6	6
15	S_{G3}	–	–	2
16	r_{G1}	12	12	0
17	r_{G2}	12	0	0
18	r_{G3}	–	–	0
19	M_{G1}	3	2	6
20	M_{G2}	5	6	6
21	M_{G3}	–	–	2
22	(R_F)	$(\boldsymbol{v}_x, \boldsymbol{v}_y)$	$(\boldsymbol{v}_x, \boldsymbol{v}_y)$	$(\boldsymbol{v}_x, \boldsymbol{v}_y)$
23	S_F	2	2	2
24	r_1	24	12	0
25	r_F	30	18	12
26	M_F	2	2	2
27	N_F	0	0	0
28	T_F	0	0	0
29	$\sum_{j=1}^{p_1} f_j$	15	14	6
30	$\sum_{j=1}^{p_2} f_j$	17	6	6
31	$\sum_{j=1}^{p_3} f_j$	–	–	2
32	$\sum_{j=1}^{p} f_j$	32	20	14

[a]See footnote of Table 2.1 for the nomenclature of structural parameters

They can be derived from the solution in Fig. 2.11 by introducing sixteen idle mobilities: four outside and twelve inside the parallelogram loops. For example the solution in Fig. 2.28 has G_1-limb of type $\underline{Pa}$*Pa*P* and G_2-limb of type $\underline{Pa}$*Pa*S* with $M_{G1} = S_{G1} = 3$, $M_{G2} = S_{G2} = 5$, $(R_{G1}) = (\boldsymbol{v}_x, \boldsymbol{v}_y, \boldsymbol{v}_z)$, $(R_{G2}) = (\boldsymbol{v}_x, \boldsymbol{v}_y, \boldsymbol{\omega}_\alpha, \boldsymbol{\omega}_\beta, \boldsymbol{\omega}_\delta)$, $(R_F) = (\boldsymbol{v}_x, \boldsymbol{v}_y)$, $M_F = S_F = 2$, $N_F = 0$ and $T_F = 0$.

Non overconstrained solutions $F \leftarrow G_1$–G_2 with rotating actuators and coupled motions have $\sum_1^p f_i = 20$ when a simple and a complex limb are used. They can be derived from the solution in Fig. 2.13 by introducing nine idle mobilities: three outside and six inside the parallelogram loops. For example, the solution in Fig. 2.29 with G_1-limb of type $\underline{Pa}$*Pa* and G_2-limb of type $\underline{R}$C*S* has the following structural parameters: $M_{G1} = S_{G1} = 2$, $M_{G2} = S_{G2} = 6$, $(R_{G1}) = (\boldsymbol{v}_x, \boldsymbol{v}_y)$, $(R_{G2}) = (\boldsymbol{v}_x, \boldsymbol{v}_y, \boldsymbol{v}_z, \boldsymbol{\omega}_\alpha, \boldsymbol{\omega}_\beta, \boldsymbol{\omega}_\delta)$, $(R_F) = (\boldsymbol{v}_x, \boldsymbol{v}_y)$, $M_F = S_F = 2$, $N_F = 0$ and $T_F = 0$.

Non overconstrained solutions of type $F \leftarrow G_1$–G_2–G_3 with an additional unactuated limb and rotating actuators can be derived from the overconstrained solution in Fig. 2.15a. For example, the solution in Fig. 2.30 has an unactuated simple limb $\underline{P}P$-type and two actuated simple limbs $\underline{R}C$*S*-type. This solution has the following structural parameters: $M_{G1} = S_{G1} = 6$, $M_{G2} = S_{G2} = 6$, $M_{G3} = S_{G3} = 2$, $(R_{G1}) = (R_{G2}) = (\boldsymbol{v}_x, \boldsymbol{v}_y, \boldsymbol{v}_z, \boldsymbol{\omega}_\alpha, \boldsymbol{\omega}_\beta, \boldsymbol{\omega}_\delta)$, $(R_{G3}) = (\boldsymbol{v}_x, \boldsymbol{v}_y)$, $(R_F) = (\boldsymbol{v}_x, \boldsymbol{v}_y)$, $M_F = S_F = 2$, $N_F = 0$ and $T_F = 0$.

The structural parameters of the solutions illustrated in Figs. 2.28–2.30 are presented in Table 2.8.

Solutions with linear and rotating actuators

Non overconstrained solutions $F \leftarrow G_1$–G_2 with linear and rotating actuators and coupled motions have $\sum_1^p f_i = 26$ when two complex limbs are used. They can be derived from the solution in Fig. 2.16 by introducing thirteen idle mobilities: four outside and nine inside the parallelogram loops. For example, the solution in Fig. 2.31 has G_1-limb of type $\underline{P}Pa$*P* and G_2-limb of type $\underline{Pa}$*Pa*S* with $M_{G1} = S_{G1} = 3$, $M_{G2} = S_{G2} = 5$, $(R_{G1}) = (\boldsymbol{v}_x, \boldsymbol{v}_y, \boldsymbol{v}_z)$, $(R_{G2}) = (\boldsymbol{v}_x, \boldsymbol{v}_y, \boldsymbol{\omega}_\alpha, \boldsymbol{\omega}_\beta, \boldsymbol{\omega}_\delta)$, $(R_F) = (\boldsymbol{v}_x, \boldsymbol{v}_y)$, $M_F = S_F = 2$, $N_F = 0$ and $T_F = 0$.

Non overconstrained solutions $F \leftarrow G_1$–G_2 with linear and rotating actuators and coupled motions have $\sum_1^p f_i = 20$ when a simple limb is actuated by

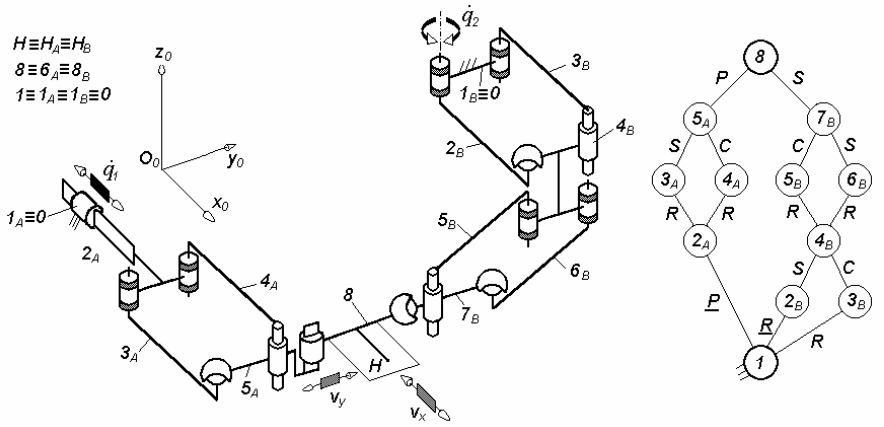

Fig. 2.31. *PPa*P*-Pa*Pa*S**-type non overconstrained translational parallel mechanism, limb topologies $\underline{P} \perp Pa^* || P^*$ and $\underline{Pa}^* \perp Pa^* S^*$

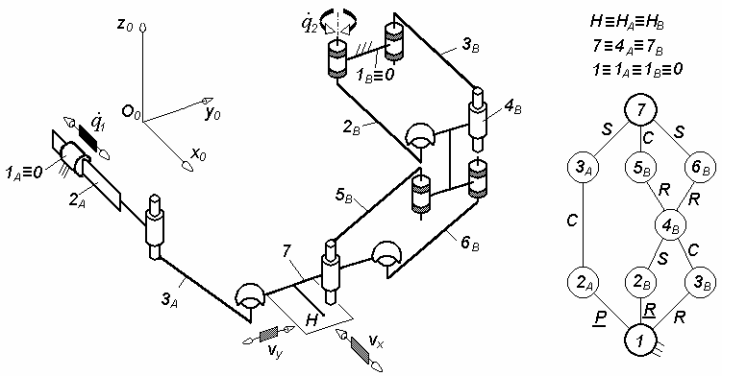

Fig. 2.32. *PC*S*-Pa*Pa**-type non overconstrained translational parallel mechanism, limb topologies $\underline{P} \perp C^* S^*$ and $\underline{Pa}^* || Pa^*$

a linear motor and a complex limb by a rotating motor. They can be derived from the solution in Fig. 2.18 by introducing nine idle mobilities: three outside and six inside the parallelogram loops. For example, the solution in Fig. 2.32 has G_1-limb of type $\underline{P}C^*S^*$ and G_2-limb of type $\underline{Pa}^*Pa^*$ with $M_{G1} = S_{G1} = 6$, $M_{G2} = S_{G2} = 2$, $(R_{G1}) = (\boldsymbol{v}_x, \boldsymbol{v}_y, \boldsymbol{v}_z, \boldsymbol{\omega}_\alpha, \boldsymbol{\omega}_\beta, \boldsymbol{\omega}_\delta)$, $(R_{G2}) = (\boldsymbol{v}_x, \boldsymbol{v}_y)$, $(R_F) = (\boldsymbol{v}_x, \boldsymbol{v}_y)$, $M_F = S_F = 2$, $N_F = 0$ and $T_F = 0$.

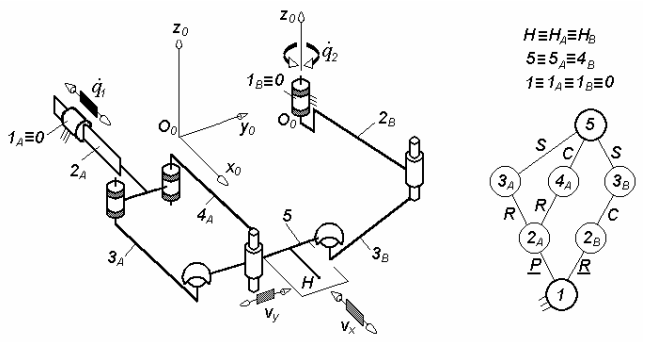

Fig. 2.33. $\underline{P}Pa^*$-$\underline{R}C^*S^*$-type non overconstrained translational parallel mechanism, limb topologies $\underline{P} \perp Pa^*$ and $\underline{R}||C^*$-S^*

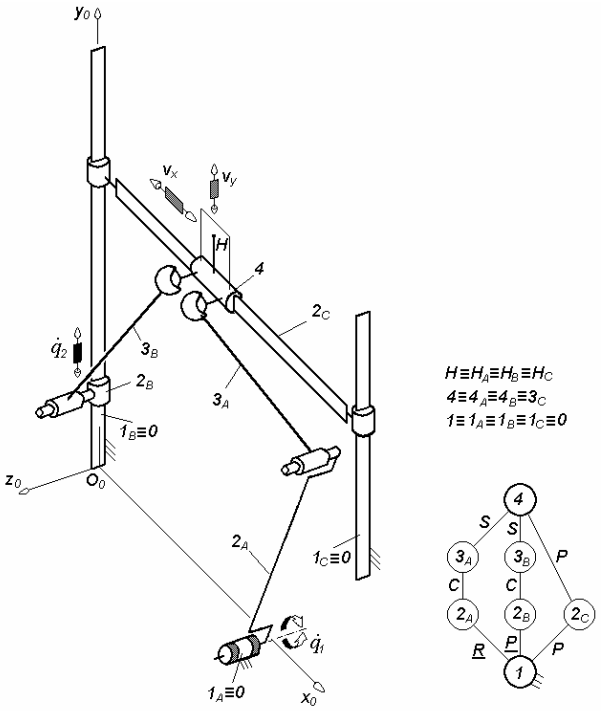

Fig. 2.34. $\underline{R}C^*S^*$-$\underline{P}C^*S^*$-PP-type non overconstrained translational parallel mechanism with an additional unactuated limb, limb topologies $\underline{R}||C^*$-S^*, $\underline{P} \perp C^*$-S^* and $P \perp P$

Table 2.9. Structural parameters[a] of translational parallel mechanisms in Figs. 2.31–2.33

No.	Structural parameter	Solution *PPa*P*-Pa*Pa*S** Fig. 2.31	*PC*S*-Pa*Pa** Fig. 2.32	*PPa*-RC*S** Fig. 2.33
1	m	12	9	7
2	p_1	6	3	5
3	p_2	9	8	3
4	p	15	11	8
5	q	4	3	2
6	k_1	0	1	1
7	k_2	2	1	1
8	k	2	2	2
9	(R_{G1})	$(\boldsymbol{v}_x, \boldsymbol{v}_y, \boldsymbol{v}_z)$	$(\boldsymbol{v}_x, \boldsymbol{v}_y, \boldsymbol{v}_z, \boldsymbol{\omega}_\alpha, \boldsymbol{\omega}_\beta, \boldsymbol{\omega}_\delta)$	$(\boldsymbol{v}_x, \boldsymbol{v}_y)$
10	(R_{G2})	$(\boldsymbol{v}_x, \boldsymbol{v}_y, \boldsymbol{\omega}_\alpha, \boldsymbol{\omega}_\beta, \boldsymbol{\omega}_\delta)$	$(\boldsymbol{v}_x, \boldsymbol{v}_y)$	$(\boldsymbol{v}_x, \boldsymbol{v}_y, \boldsymbol{v}_z, \boldsymbol{\omega}_\alpha, \boldsymbol{\omega}_\beta, \boldsymbol{\omega}_\delta)$
11	S_{G1}	3	6	2
12	S_{G2}	5	2	6
13	r_{G1}	6	0	6
14	r_{G2}	12	12	0
15	M_{G1}	3	6	2
16	M_{G2}	5	2	6
17	(R_F)	$(\boldsymbol{v}_x, \boldsymbol{v}_y)$	$(\boldsymbol{v}_x, \boldsymbol{v}_y)$	$(\boldsymbol{v}_x, \boldsymbol{v}_y)$
18	S_F	2	2	2
19	r_1	18	12	6
20	r_F	24	18	12
20	M_F	2	2	2
21	N_F	0	0	0
22	T_F	0	0	0
23	$\sum_{j=1}^{p_1} f_j$	9	6	8
24	$\sum_{j=1}^{p_2} f_j$	17	14	6
25	$\sum_{j=1}^{p} f_j$	26	20	14

[a]See footnote of Table 2.1 for the nomenclature of structural parameters

Non overconstrained solutions $F \leftarrow G_1$–G_2 with linear and rotating actuators and coupled motions have $\sum_1^p f_i = 14$ when a complex limb is actuated by a linear motor and a simple limb by a rotating motor. They can be derived from the solution in Fig. 2.19 by introducing six idle mobilities: three outside and three inside the parallelogram loop. For example, the solution in Fig. 2.33 has G_1-limb of type *PPa** and G_2-limb of type *RC*S** with the following structural parameters: $M_{G1} = S_{G1} = 2$, $M_{G2} = S_{G2} = 6$,

$(R_{G1}) = (\boldsymbol{v}_x, \boldsymbol{v}_y)$, $(R_{G2}) = (\boldsymbol{v}_x, \boldsymbol{v}_y, \boldsymbol{v}_z, \boldsymbol{\omega}_\alpha, \boldsymbol{\omega}_\beta, \boldsymbol{\omega}_\delta)$, $(R_F) = (\boldsymbol{v}_x, \boldsymbol{v}_y)$, $M_F = S_F = 2$, $N_F = 0$ and $T_F = 0$. The structural parameters of the solutions illustrated in Figs. 2.31–2.33 are presented in Table 2.9.

Non overconstrained solutions of type $F \leftarrow G_1$–G_2–G_3 with an additional unactuated limb and linear and rotating actuators can be derived from the overconstrained solution in Fig. 2.22. For example, the solution in Fig. 2.34 has an unactuated simple limb *P*P-type and two simple actuated limbs *R*C*S*- and *P*C*S*-type. The solution in Fig. 2.34 is characterised by the following structural parameters: $M_{G1} = S_{G1} = 6$, $M_{G2} = S_{G2} = 6$, $M_{G3} = S_{G3} = 2$, $(R_{G1}) = (R_{G2}) = (\boldsymbol{v}_x, \boldsymbol{v}_y, \boldsymbol{v}_z, \boldsymbol{\omega}_\alpha, \boldsymbol{\omega}_\beta, \boldsymbol{\omega}_\delta)$, $(R_{G3}) = (\boldsymbol{v}_x, \boldsymbol{v}_y)$, $(R_F) = (\boldsymbol{v}_x, \boldsymbol{v}_y)$, $M_F = S_F = 2$, $N_F = 0$ and $T_F = 0$. The solution in Figs. 2.30 and 2.34 have the same structural parameters (see Table 2.8).

2.2 *T2*-type translational parallel robots with decoupled motions

T2-type translational parallel robots with *decoupled motions* and linear or rotating actuators with various degrees of overconstraint can be generated. In these solutions one of the operational velocities depends on just one actuated joint velocity and the other depends of both actuated joint velocities: $v_1 = v_1(\dot{q}_1)$ and $v_2 = v_2(\dot{q}_1, \dot{q}_2)$. We consider $v_1 = v_x$ and $v_2 = v_y$.

2.2.1 Overconstrained solutions

The *overconstrained* solutions of *T2*-type translational parallel robots with decoupled motions and q independent loops meet the same condition $\sum_1^p f_i < 2 + 6q$ as their counterparts with coupled motions.

Solutions with linear actuators

T2-type translational parallel robots with decoupled motions and *linear actuators* can be derived from their counterparts with coupled motions by replacing a *PPa*-limb by a *PP*-limb as illustrated in Figs. 2.35–2.37. These solutions have two limbs which could be one simple and one complex (Fig. 2.35) or both simple limbs (Figs. 2.36 and 2.37). The complex limb G_2 combines a closed parallelogram loop. The linear actuators can be mounted on the fixed base (Figs. 2.35–2.37) or on a moving link (Fig. 2.37).

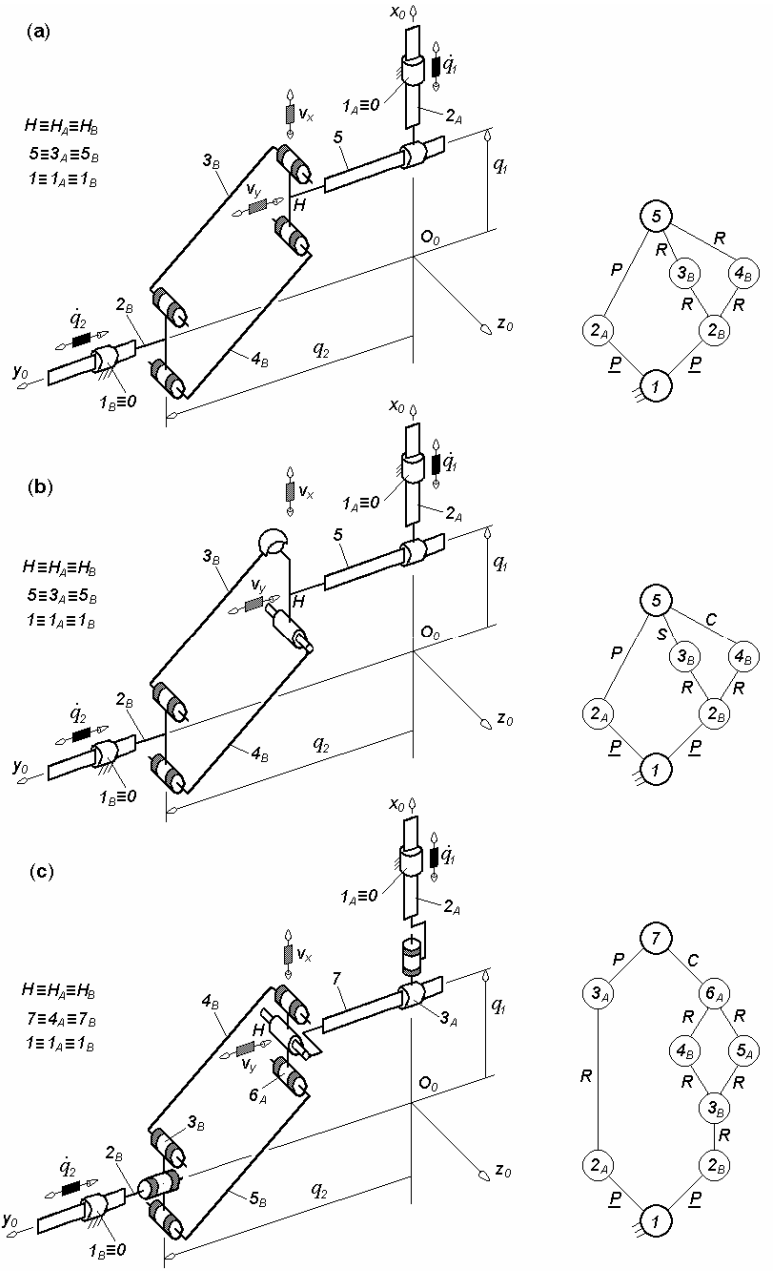

Fig. 2.35. Translational parallel mechanisms of types $\underline{P}P$-$\underline{P}Pa$ with seven overconstraints (**a**), $\underline{P}P$-$\underline{P}Pa^*$ with four overconstraints (**b**) and $\underline{P}R^*P$-$\underline{P}R^*PaC^*$ with three overconstraints (**c**), limb topologies $\underline{P} \perp P$ and $\underline{P} \perp Pa$ (**a**), $\underline{P} \perp P$ and $\underline{P} \perp Pa^*$ (**b**), $\underline{P}||R^* \perp P$ and $\underline{P}||R^* \perp Pa||C^*$ (**c**)

Table 2.10. Structural parameters[a] of translational parallel mechanisms in Fig. 2.35

No.	Structural parameter	Solution <u>*PP*</u>-<u>*P*</u>*Pa* Fig. 2.35a	<u>*PP*</u>-<u>*P*</u>*Pa** Fig. 2.35b	<u>*P*</u>*R**P*-<u>*P*</u>*R**Pa*C* Fig. 2.35c
1	m	6	6	9
2	p_1	2	2	3
3	p_2	5	5	7
4	p	7	7	10
5	q	2	2	2
6	k_1	1	1	1
7	k_2	1	1	1
8	k	2	2	2
9	(R_{G1})	$(\boldsymbol{v}_x, \boldsymbol{v}_y)$	$(\boldsymbol{v}_x, \boldsymbol{v}_y)$	$(\boldsymbol{v}_x, \boldsymbol{v}_y, \boldsymbol{\omega}_\alpha)$
10	(R_{G2})	$(\boldsymbol{v}_x, \boldsymbol{v}_y)$	$(\boldsymbol{v}_x, \boldsymbol{v}_y)$	$(\boldsymbol{v}_x, \boldsymbol{v}_y, \boldsymbol{v}_z, \boldsymbol{\omega}_\beta, \boldsymbol{\omega}_\delta)$
11	S_{G1}	2	2	3
12	S_{G2}	2	2	5
13	r_{G1}	0	0	0
14	r_{G2}	3	6	3
15	M_{G1}	2	2	3
16	M_{G2}	2	2	5
17	(R_F)	$(\boldsymbol{v}_x, \boldsymbol{v}_y)$	$(\boldsymbol{v}_x, \boldsymbol{v}_y)$	$(\boldsymbol{v}_x, \boldsymbol{v}_y)$
18	S_F	2	2	2
19	r_1	3	6	3
20	r_F	5	8	9
21	M_F	2	2	2
22	N_F	7	4	3
23	T_F	0	0	0
24	$\sum_{j=1}^{p_1} f_j$	2	2	3
25	$\sum_{j=1}^{p_2} f_j$	5	8	8
26	$\sum_{j=1}^{p} f_j$	7	10	11

[a]See footnote of Table 2.1 for the nomenclature of structural parameters

The overconstrained solutions with a simple and a complex limb integrating a parallelogram loop have $1 \leq N_F \leq 7$. These solutions could combine up to three idle mobilities in the parallelogram loop and up to four idle mobilities outside it. The structural parameters of the solutions illustrated in Fig. 2.35 are presented in Table 2.10.

A large variety of *T2*-type translational parallel robots with decoupled motions and linear actuators can be obtained by associating a simple limb G_1 of type <u>*PP*</u> with any simple G_2 - limb that integrates velocities $\boldsymbol{v}_x$ and $\boldsymbol{v}_y$ in

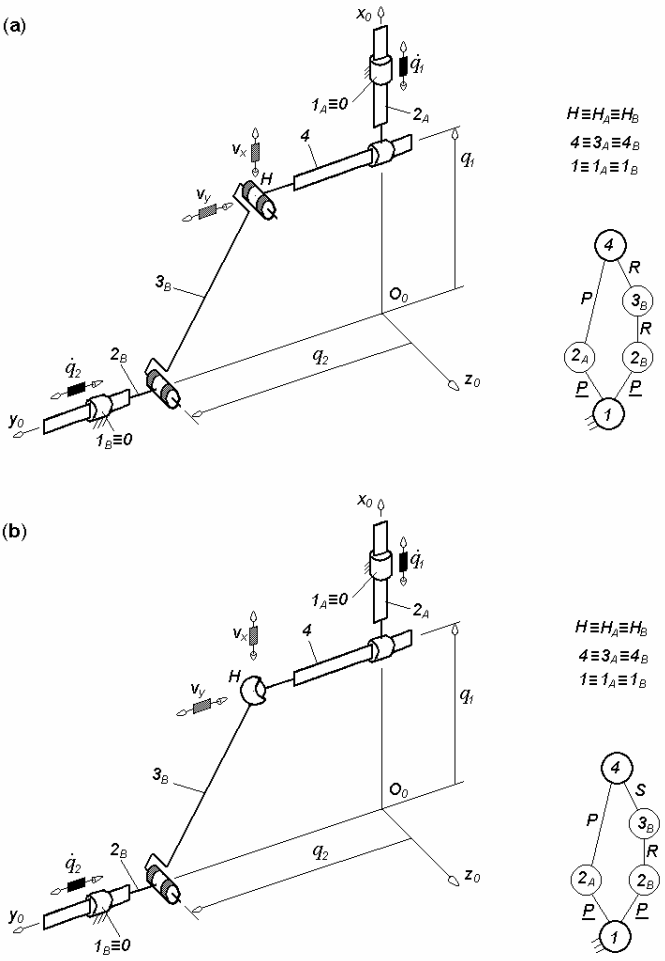

Fig. 2.36. Translational parallel mechanisms of types $\underline{P}P$-$\underline{P}RR$ with three overconstraints (**a**) and $\underline{P}P$-$\underline{P}RS$* with one overconstraint (**b**), limb topologies $\underline{P} \perp P$ and $\underline{P} \perp R||R$ (**a**) $\underline{P} \perp P$ and $\underline{P} \perp R$-S* (**b**)

the basis of its operational velocity vector space. G_2-limb can have $2 < M_{Gi} = S_{Gi} < 6$. The overconstrained solutions with decoupled motions and two simple limbs have $1 \le N_F \le 3$ and may integrate up to three idle mobilities.

For the solutions with two simple limbs in Figs. 2.36a and 2.37a, Eqs. (1.2)–(1.8) and (1.17) give the following structural parameters: $M_{G1} = S_{G1} = 2$, $M_{G2} = S_{G2} = 3$, $(R_{G1}) = (\boldsymbol{v}_x, \boldsymbol{v}_y)$, $(R_{G2}) = (\boldsymbol{v}_x, \boldsymbol{v}_y, \boldsymbol{\omega}_\delta)$, $(R_F) = (\boldsymbol{v}_x, \boldsymbol{v}_y)$, $M_F = S_F = 2$, $N_F = 3$ and $T_F = 0$ (see Table 2.11).

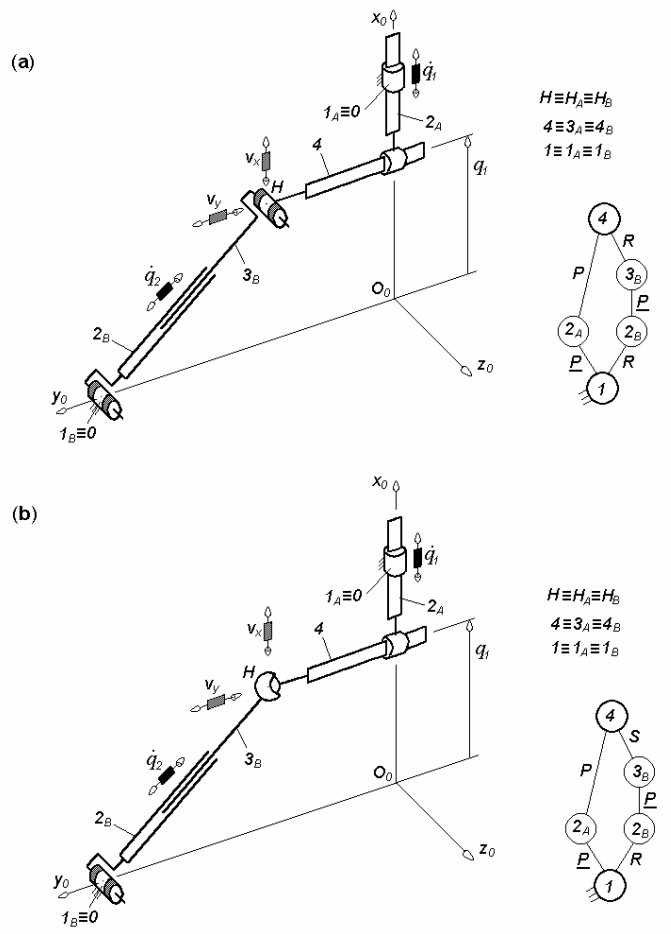

Fig. 2.37. Translational parallel mechanisms of types $\underline{P}P$-$R\underline{P}R$ with three overconstraints (**a**) and $\underline{P}P$-$R\underline{P}S$* with one overconstraint (**b**), limb topologies: $\underline{P} \perp P\text{-}R \perp \underline{P} \perp {}^{\parallel}R$ (**a**) and $\underline{P} \perp P\text{-}R \perp \underline{P}S$ (**b**)

For the solutions with two simple limbs in Figs. 2.36b and 2.37b, Eqs. (1.2)–(1.8) and (1.17) give the following parameters: $M_{G1} = S_{G1} = 2$, $M_{G2} = S_{G2} = 5$, $(R_{G1}) = (\boldsymbol{v}_x, \boldsymbol{v}_y)$, $(R_{G2}) = (\boldsymbol{v}_x, \boldsymbol{v}_y, \boldsymbol{\omega}_\alpha, \boldsymbol{\omega}_\beta, \boldsymbol{\omega}_\delta)$, $(R_F) = (\boldsymbol{v}_x, \boldsymbol{v}_y)$, $M_F = S_F = 2$, $N_F = 1$ and $T_F = 0$ (see Table 2.11).

Table 2.11. Structural parameters[a] of translational parallel mechanisms in Figs. 2.36–2.37

No.	Structural parameter	Solution *PP*-*PRR* (Fig. 2.36a) *PP*-*RPR* (Fig. 2.37a)	*PP*-*PRS** (Fig. 2.36b) *PP*-*RPS** (Fig. 2.37b)
1	m	5	5
2	p_1	2	2
3	p_2	3	3
4	p	5	5
5	q	1	1
6	k_1	2	2
7	k_2	0	0
8	k	2	2
9	(R_{G1})	$(\boldsymbol{v}_x, \boldsymbol{v}_y)$	$(\boldsymbol{v}_x, \boldsymbol{v}_y)$
10	(R_{G2})	$(\boldsymbol{v}_x, \boldsymbol{v}_y, \omega_\delta)$	$(\boldsymbol{v}_x, \boldsymbol{v}_y, \omega_\alpha, \omega_\beta, \omega_\delta)$
11	S_{G1}	2	2
12	S_{G2}	3	5
13	r_{G1}	0	0
14	r_{G2}	0	0
15	M_{G1}	2	2
16	M_{G2}	3	5
17	(R_F)	$(\boldsymbol{v}_x, \boldsymbol{v}_y)$	$(\boldsymbol{v}_x, \boldsymbol{v}_y)$
18	S_F	2	2
19	r_1	0	0
20	r_F	3	5
21	M_F	2	2
22	N_F	3	1
23	T_F	0	0
24	$\sum_{j=1}^{p_1} f_j$	2	2
25	$\sum_{j=1}^{p_2} f_j$	3	5
26	$\sum_{j=1}^{p} f_j$	5	7

[a]See footnote of Table 2.1 for the nomenclature of structural parameters

Solutions with rotating actuators

T2-type translational parallel robots with decoupled motions and rotating actuators can be derived from their counterparts with coupled motions by replacing a *PaPa*-limb by a *PaP*-limb as illustrated in Figs. 2.38 and 2.39. These solutions have two complex limbs (Fig. 2.38) or a complex and a simple limb (Figs. 2.39).

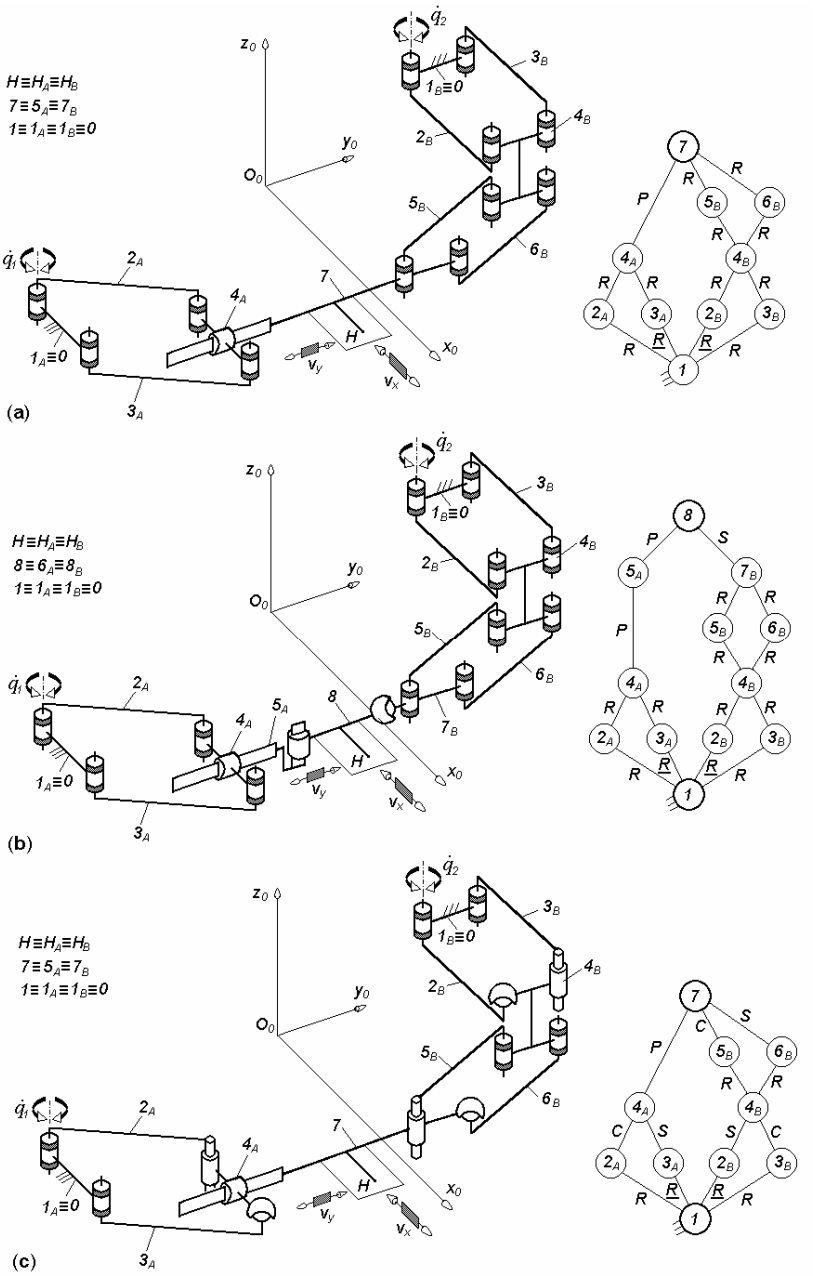

Fig. 2.38. Translational parallel mechanisms of types <u>*Pa*</u>*P*-<u>*Pa*</u>*Pa* with thirteen overconstraints (**a**), <u>*Pa*</u>*PP**-<u>*Pa*</u>*PaS** with nine overconstraints (**b**) and <u>*Pa*</u>**P*-<u>*Pa*</u>**Pa** with four overconstraints (**c**), limb topologies <u>*Pa*</u> $\perp$ *P* and <u>*Pa*</u>||*Pa* (**a**), <u>*Pa*</u> $\perp$ *P* $\perp$ *P** and <u>*Pa*</u>||*PaS** (**b**), <u>*Pa*</u>* $\perp$ *P* and <u>*Pa*</u>*||*Pa** (**c**)

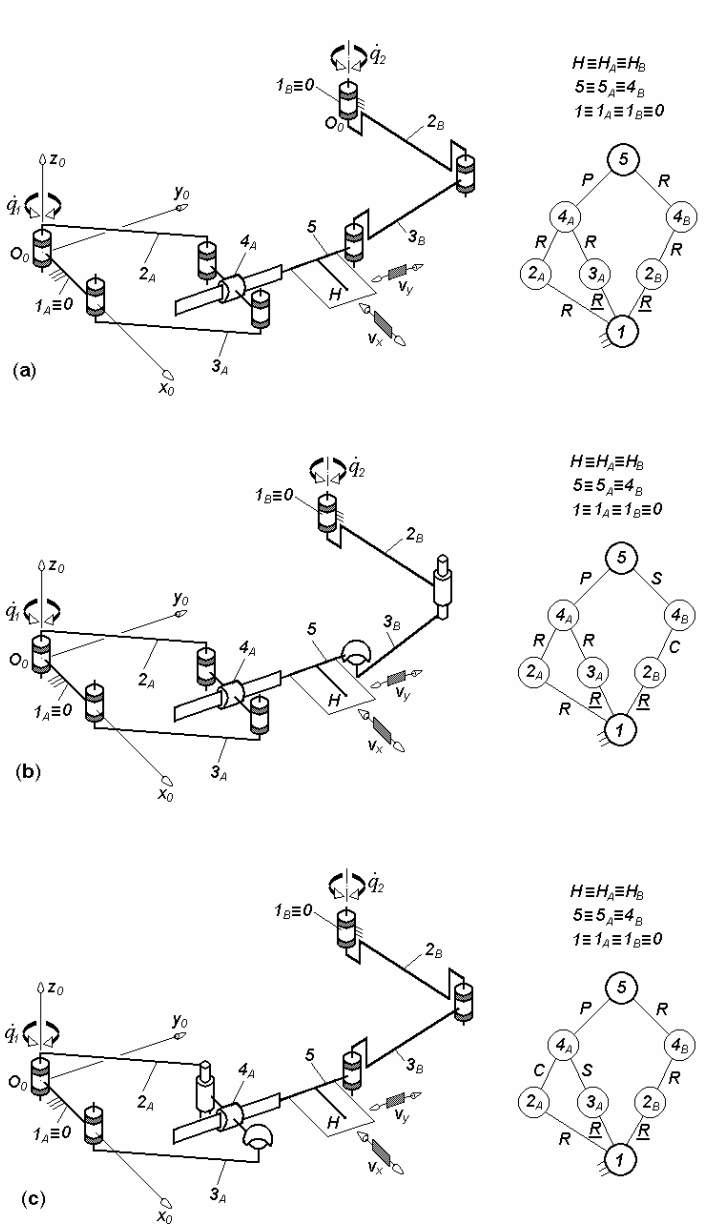

Fig. 2.39. Translational parallel mechanisms of types $\underline{Pa}P\text{-}\underline{R}RR$ with six overconstraints (**a**) $\underline{Pa}P\text{-}\underline{R}C^*S^*$ with three overconstraints (**b**) and $\underline{Pa}^*P\text{-}\underline{R}RR$ with three overconstraints (**c**), limb topologies $\underline{Pa} \perp P$ and $\underline{R}||R||R$ (**a**) $\underline{Pa} \perp P$ and $\underline{R}||C^*S^*$ (**b**), $\underline{Pa}^* \perp P$ and $\underline{R}||R||R$ (**c**)

The overconstrained solutions with two complex limbs have $1 \leq N_F \leq 13$. The complex limb G_1 combines one closed parallelogram loop and complex limb G_2 two parallelogram loops (Fig. 2.38a). These solutions could combine up to three idle mobilities in each parallelogram loop (Fig. 2.38c) and up to four idle mobilities outside them (Fig. 2.38b).

A large variety of *T2*-type translational parallel robots with decoupled motions and rotating actuators can be generated by associating the complex limb G_1 of type $\underline{Pa}P$ with any simple G_2-limb that integrates velocities $\boldsymbol{v}_x$ and $\boldsymbol{v}_y$ in the basis of its operational velocity vector space along with a constant orientation of the moving platform. G_2-limb can have $2 < M_{Gi} = S_{Gi} < 6$. For example, in Fig. 2.39a, a planar simple limb $\underline{R}RR$-type with $M_{Gi} = S_{Gi} = 3$ is used.

The overconstrained solutions with decoupled motions and a complex and a simple limb have $1 \leq N_F \leq 6$ and may integrate up to three idle mobilities inside and three others outside the parallelogram loop (Fig. 2.39b and c).

The solutions illustrated in Fig. 2.38 have the same structural parameters as those in Figs. 2.16, 2.17a and b (see Table 2.6). The solutions in Fig. 2.39 have the same structural parameters as those in Figs. 2.4, 2.5a and b (see Table 2.2).

Solutions with rotating and linear actuators

Basic solutions of overconstrained *T2*-type translational parallel robots with decoupled motions actuated by rotating and linear motors have two complex limbs of types $\underline{Pa}P$ and $\underline{P}Pa$ (Fig. 2.40a). They have $1 \leq N_F \leq 10$. Each complex limb combines one closed parallelogram loop. These solutions may integrate up to three idle mobilities in each parallelogram loop (Fig. 2.40c) and up to four idle mobilities outside them (Fig. 2.40b). The solutions illustrated in Figs. 2.40a and c have the same structural parameters as those in Figs. 2.1 and 2.2b (see Table 2.1). The solution in Fig. 2.40b has the following structural parameters: $M_{G1} = S_{G1} = 3$, $M_{G2} = S_{G2} = 5$, $(R_{G1}) = (\boldsymbol{v}_x, \boldsymbol{v}_y, \boldsymbol{v}_z)$, $(R_{G2}) = (\boldsymbol{v}_x, \boldsymbol{v}_y, \boldsymbol{\omega}_\alpha, \boldsymbol{\omega}_\beta, \boldsymbol{\omega}_\delta)$, $(R_F) = (\boldsymbol{v}_x, \boldsymbol{v}_y)$, $M_F = S_F = 2$, $N_F = 6$ and $T_F = 0$.

A large variety of overconstrained *T2*-type translational parallel robots with decoupled motions actuated by rotating and linear motors can be set up by associating a complex limb G_1 of type $\underline{Pa}P$ with any simple G_2-limb that integrates velocities $\boldsymbol{v}_x$ and $\boldsymbol{v}_y$ in the basis of its operational velocity space. G_2-limb can have $2 < M_{Gi} = S_{Gi} < 6$. For example, simple planar limbs with $M_{Gi} = S_{Gi} = 3$ of type $\underline{P}RR$ is used in Fig. 2.41a and $R\underline{P}R$ in Fig. 2.42a.

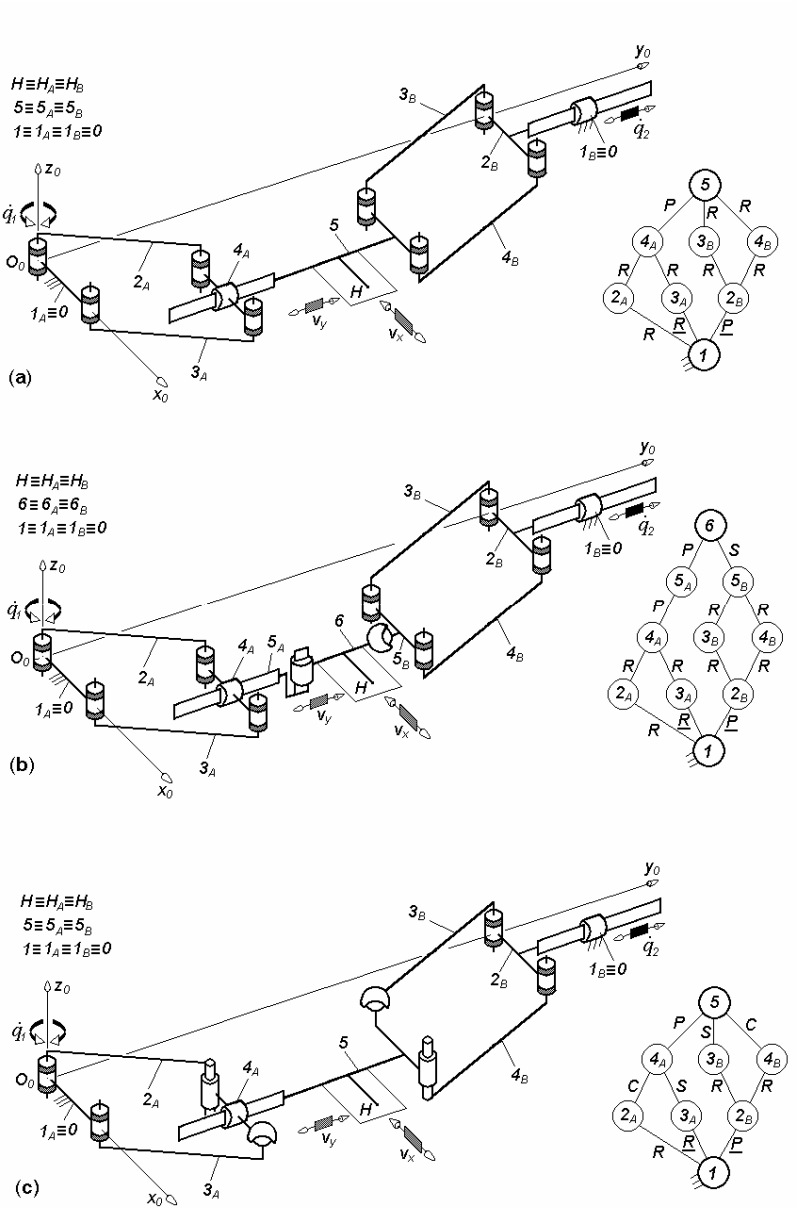

Fig. 2.40. Translational parallel mechanisms of types $\underline{Pa}P\text{-}\underline{P}Pa$ with ten overconstraints (**a**) $\underline{Pa}PP^*\text{-}\underline{P}PaS^*$ with six overconstraints (**b**) and $\underline{Pa}^*P\text{-}\underline{P}Pa^*$ with four overconstraints (**c**), limb topologies $\underline{Pa} \perp P$ and $\underline{P} \perp Pa$ (**a**), $\underline{Pa} \perp P \perp P^*$ and $\underline{P} \perp PaS^*$ (**b**), $\underline{Pa}^* \perp P$ and $\underline{P} \perp Pa^*$ (**c**)

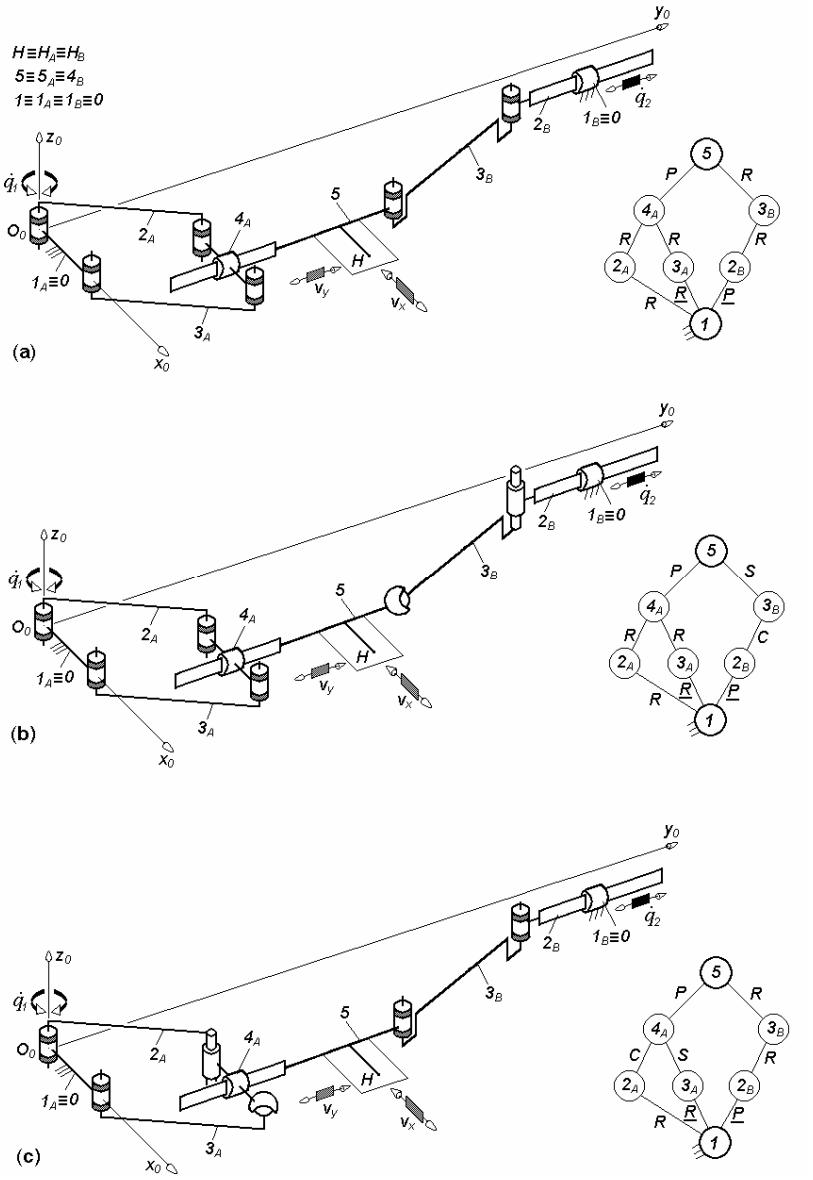

Fig. 2.41. Translational parallel mechanisms of types <u>*Pa*</u>*P*-<u>*P*</u>*RR* with six overconstraints (**a**), <u>*Pa*</u>*P*-<u>*P*</u>*C***S** with three overconstraints (**b**) and <u>*Pa*</u>**P*-<u>*P*</u>*RR* with three overconstraints (**c**), limb topologies <u>*Pa*</u> ⊥ *P* and <u>*P*</u> ⊥ *R*||*R* (**a**), <u>*Pa*</u> ⊥ *P* and <u>*P*</u> ⊥ *C**-*S** (**b**), <u>*Pa*</u>* ⊥ *P* and <u>*P*</u> ⊥ *R*||*R* (**c**)

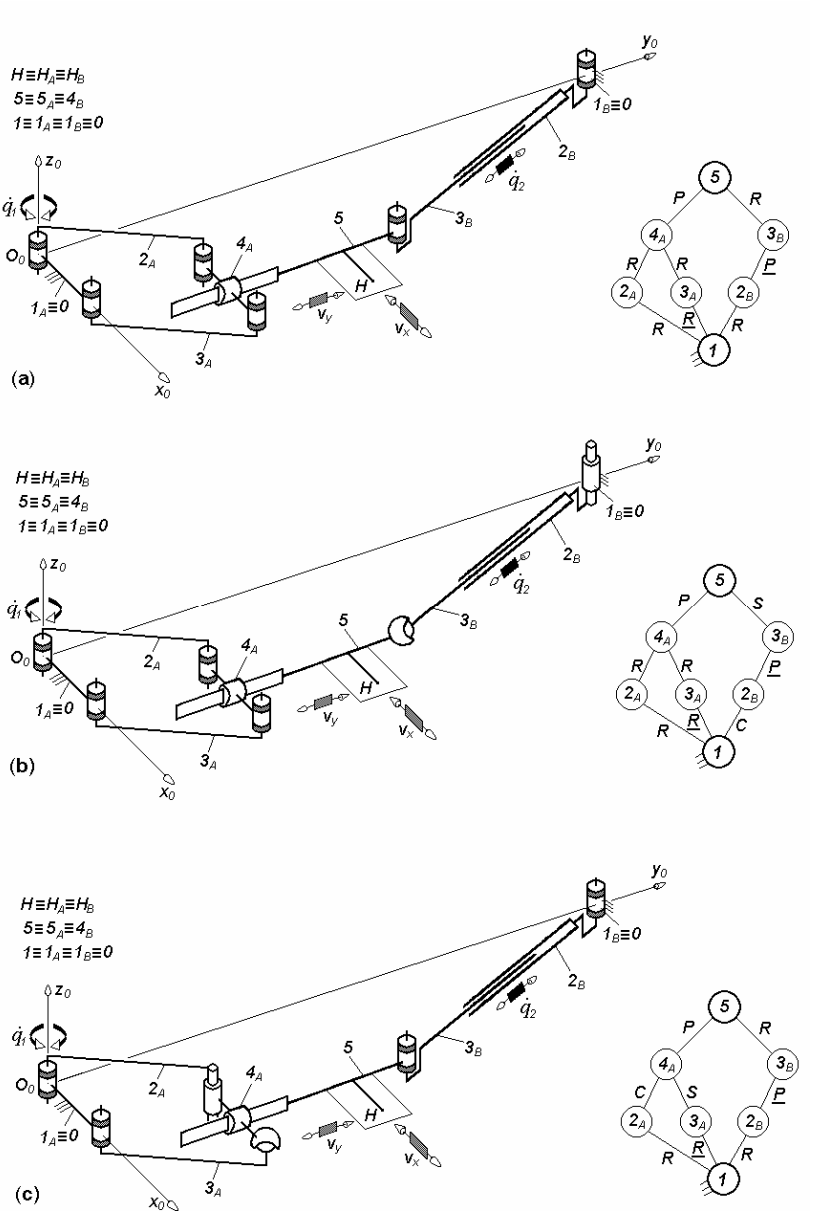

Fig. 2.42. Translational parallel mechanisms of types $\underline{Pa}P$-$R\underline{P}R$ with six overconstraints (**a**), $\underline{Pa}P$-$C^*\underline{P}S^*$ with three overconstraints (**b**) and $\underline{Pa}^*P$-$R\underline{P}R$ with three overconstraints (**c**), limb topologies $\underline{Pa} \perp P$ and $R \perp \underline{P} \perp {}^{\parallel}R$ (**a**), $\underline{Pa} \perp P$ and $C^* \perp \underline{P}$-S^* (**b**), $\underline{Pa}^* \perp P$ and $R \perp \underline{P} \perp {}^{\parallel}R$ (**c**)

These overconstrained solutions with decoupled motions and a complex and a simple limb have $1 \le N_F \le 6$ and could combine up to three idle mobilities outside the parallelogram loop (Figs. 2.41b and 2.42b) and other three idle mobilities inside the parallelogram loop (Figs. 2.41c and 2.42c).

The solutions in Figs. 2.41 and 2.42 have the same structural parameters as those in Figs. 2.4, 2.5a and b (see Table 2.2).

2.2.2 Non overconstrained solutions

Non overconstrained solutions of *T2*-type translational parallel robots with decoupled motions and q independent loops meet the same condition $\sum_1^p f_i = 2 + 6q$ as their counterparts with coupled motions.

Solutions with linear actuators

Non overconstrained solutions $F \leftarrow G_1$–G_2 with *linear actuators* and decoupled motions have $\sum_1^p f_i = 14$ when one complex limb is used. They are derived from the solution in Fig. 2.35a by introducing ten idle mobilities: four outside and three inside the parallelogram loop. Structural parameters of solutions in Figs. 2.43 and 2.44 are presented in Table 2.12.

Non overconstrained solutions $F \leftarrow G_1$–G_2 with linear actuators and decoupled motions have $\sum_1^p f_i = 8$ when two simple limbs are used. They

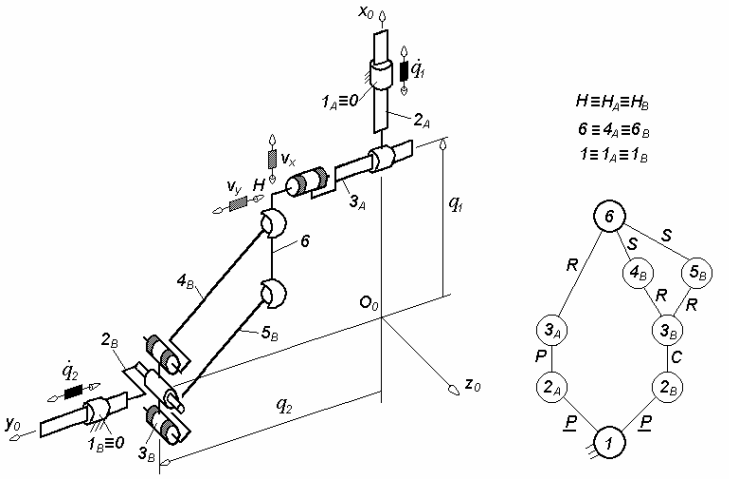

Fig. 2.43. $\underline{P}PR^*$-$\underline{P}C^*Pa^{ss}$-type non overconstrained translational parallel mechanism, limb topologies $\underline{P} \perp P||R^*$ and $\underline{P} \perp C^*||Pa^{ss}$

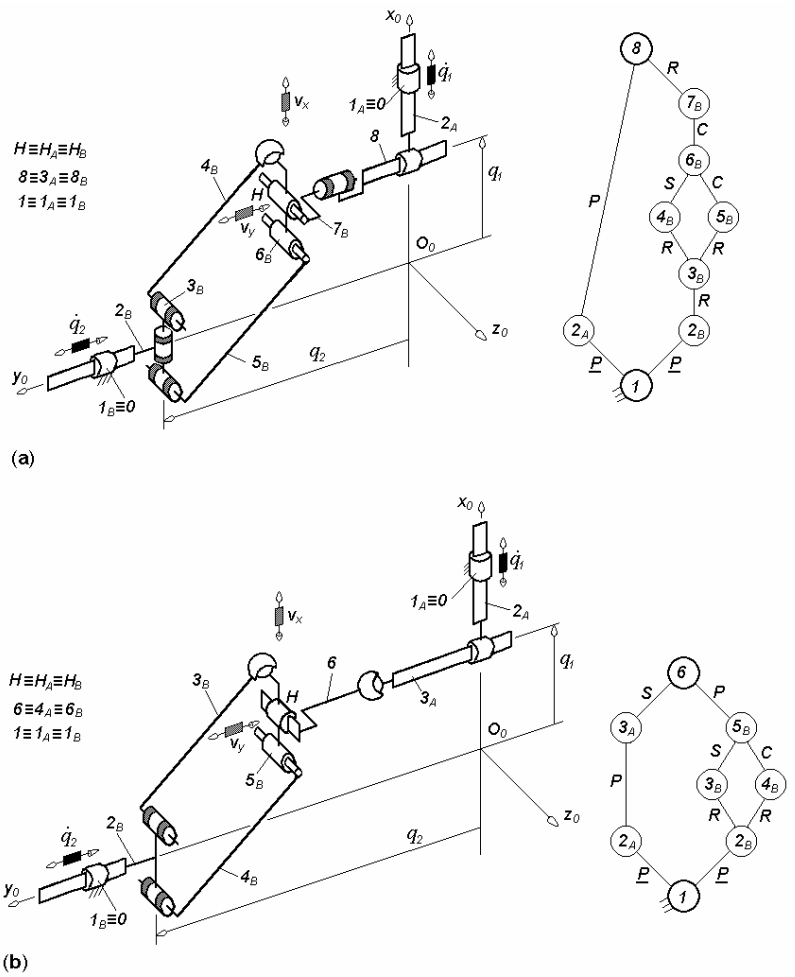

Fig. 2.44. Non overconstrained translational parallel mechanisms of types $\underline{P}P$-$\underline{P}R$*Pa*C*R* (**a**) and $\underline{P}PS$*-$\underline{P}Pa$*P* (**b**), limb topologies $\underline{P} \perp P$ and $\underline{P} \perp R$* $\perp^{\perp} Pa$*$||C$*$\perp R$* (**a**), $\underline{P} \perp PS$* and $\underline{P} \perp Pa$*$||P$* (**b**)

are derived from the solutions in Figs. 2.36a and 2.37a by using three idle mobilities. For example, the solutions in Fig. 2.45 have G_1-limb of type $\underline{P}P$ and G_2-limb of type $\underline{P}C$*S* (Fig. 2.45a), $\underline{P}U$*S* (Fig. 2.45b) and U*$\underline{P}S$* (Fig. 2.45c). These solutions have $M_{G1} = S_{G1} = 2$, $M_{G2} = S_{G2} = 6$, $(R_{G1}) = (\boldsymbol{v}_x, \boldsymbol{v}_y)$, $(R_{G2}) = (\boldsymbol{v}_x, \boldsymbol{v}_y, \boldsymbol{v}_z, \boldsymbol{\omega}_\alpha, \boldsymbol{\omega}_\beta, \boldsymbol{\omega}_\delta)$, $(R_F) = (\boldsymbol{v}_x, \boldsymbol{v}_y)$, $M_F = S_F = 2$, $N_F = 0$ and $T_F = 0$.

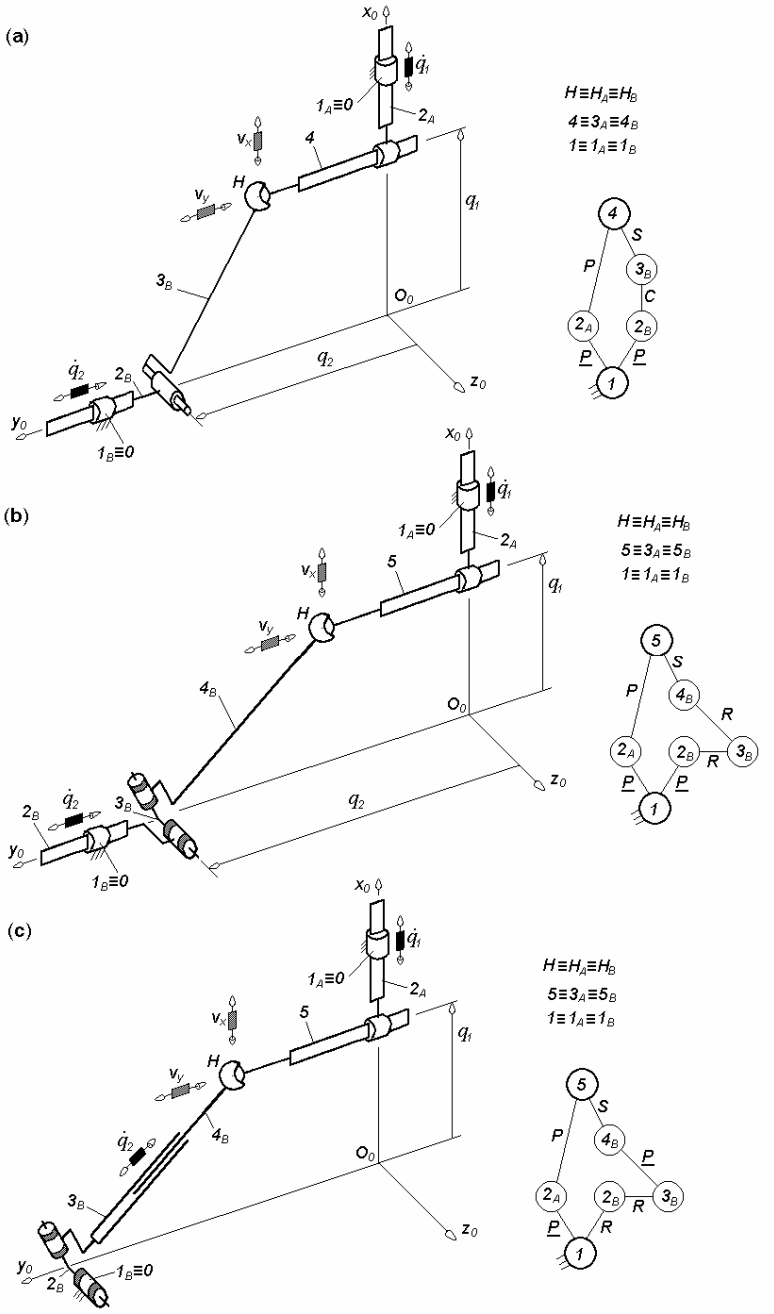

Fig. 2.45. Non overconstrained translational parallel mechanisms of types $\underline{P}P$-$\underline{P}C^*S^*$ (**a**), $\underline{P}P$-$\underline{P}U^*S^*$ (**b**) and $\underline{P}P$-$U^*\underline{P}S^*$ (**c**), limb topologies $\underline{P} \perp P$ and $\underline{P} \perp C^*$-S^* (**a**), $\underline{P} \perp P$ and $\underline{P} \perp U^*$-S^* (**b**), $\underline{P} \perp P$ and $U^* \perp \underline{P}$-S^* (**c**)

Table 2.12. Structural parameters[a] of translational parallel mechanisms in Figs. 2.43 and 2.44

No.	Structural parameter	Solution *PPR*-PC*Pa*^{ss} Fig. 2.43	*PP-PR*Pa*C*R** Fig. 2.44a	*PPS*-PPa*P** Fig. 2.44b
1	m	8	9	8
2	p_1	3	2	3
3	p_2	6	8	6
4	p	9	10	9
5	q	2	2	2
6	k_1	1	1	1
7	k_2	1	1	1
8	k	2	2	2
9	(R_{G1})	$(\boldsymbol{v}_x, \boldsymbol{v}_y, \omega_\beta)$	$(\boldsymbol{v}_x, \boldsymbol{v}_y)$	$(\boldsymbol{v}_x, \boldsymbol{v}_y, \omega_\alpha, \omega_\beta, \omega_\delta)$
10	(R_{G2})	$(\boldsymbol{v}_x, \boldsymbol{v}_y, \boldsymbol{v}_z, \boldsymbol{\omega}_\alpha, \boldsymbol{\omega}_\delta)$	$(\boldsymbol{v}_x, \boldsymbol{v}_y, \boldsymbol{v}_z, \boldsymbol{\omega}_\alpha, \boldsymbol{\omega}_\beta, \boldsymbol{\omega}_\delta)$	$(\boldsymbol{v}_x, \boldsymbol{v}_y, \boldsymbol{v}_z)$
11	S_{G1}	3	2	5
12	S_{G2}	5	6	3
13	r_{G1}	0	0	0
14	r_{G2}	6	6	6
15	M_{G1}	3	2	5
16	M_{G2}	5	6	3
17	(R_F)	$(\boldsymbol{v}_x, \boldsymbol{v}_y)$	$(\boldsymbol{v}_x, \boldsymbol{v}_y)$	$(\boldsymbol{v}_x, \boldsymbol{v}_y)$
18	S_F	2	2	2
19	r_1	6	6	6
20	r_F	12	12	12
21	M_F	2	2	2
22	N_F	0	0	0
23	T_F	0	0	0
24	$\sum_{j=1}^{p_1} f_j$	3	2	5
25	$\sum_{j=1}^{p_2} f_j$	11	12	9
26	$\sum_{j=1}^{p} f_j$	14	14	14

[a]See footnote of Table 2.1 for the nomenclature of structural parameters

Solutions with rotating actuators

Non overconstrained solutions $F \leftarrow G_1$–G_2 with *rotating actuators* and decoupled motions have $\sum_1^p f_i = 26$ when two complex limbs are used. They are derived from the solution in Fig. 2.38a by introducing thirteen idle mobilities: four outside the parallelogram loops and three inside each

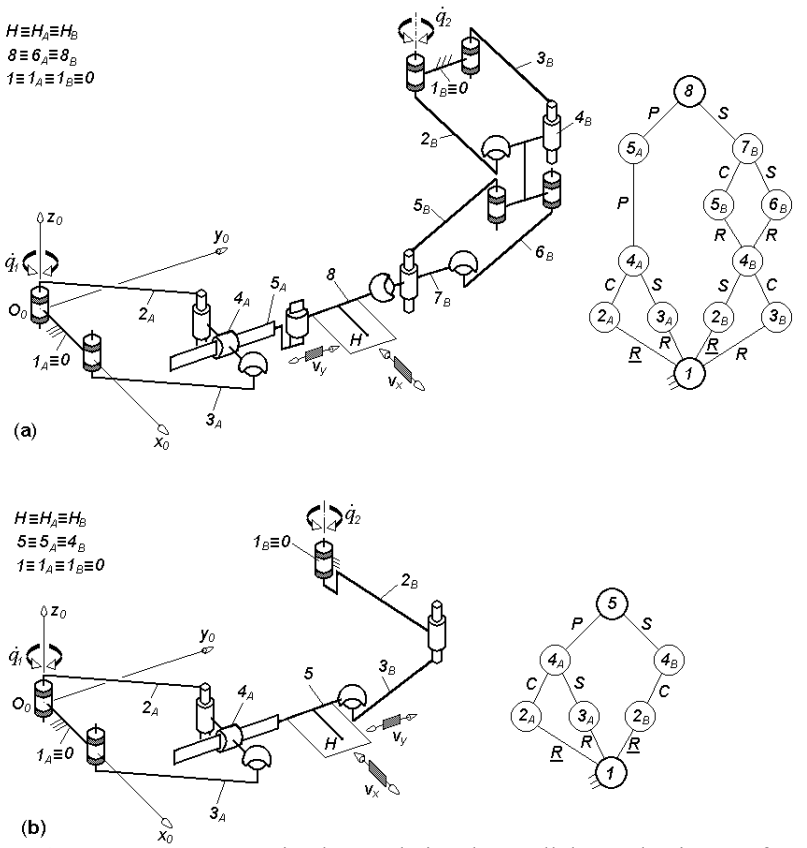

Fig. 2.46. Non overconstrained translational parallel mechanisms of types <u>*Pa*</u>**PP**-<u>*Pa*</u>**Pa***S** (**a**) and <u>*Pa*</u>**P*-<u>*R*</u>*C***S** (**b**), limb topologies <u>*Pa*</u>* ⊥ *P* ⊥ ||*P** and <u>*Pa*</u>*||*Pa***S** (**a**), <u>*Pa*</u>* ⊥ *P* and <u>*R*</u>||*C***S** (**b**)

parallelogram loop. For example, the solution in Fig. 2.46a has G_1-limb of type <u>*Pa*</u>**PP** and G_2-limb of type <u>*Pa*</u>**Pa***S**. Equations (1.2)–(1.8) and (1.17) give the following structural parameters for this solution: $M_{G1} = S_{G1} = 3$, $M_{G2} = S_{G2} = 5$, $(R_{G1}) = (\boldsymbol{v}_x, \boldsymbol{v}_y, \boldsymbol{v}_z)$, $(R_{G2}) = (\boldsymbol{v}_x, \boldsymbol{v}_y, \boldsymbol{\omega}_\alpha, \boldsymbol{\omega}_\beta, \boldsymbol{\omega}_\delta)$, $(R_F) = (\boldsymbol{v}_x, \boldsymbol{v}_y)$, $M_F = S_F = 2$, $N_F = 0$ and $T_F = 0$ (see Table 2.13).

Non overconstrained solutions $F \leftarrow G_1$–G_2 with rotating actuators and decoupled motions have $\sum_1^p f_i = 14$ when a complex and a simple limb are used. They are derived from the solution in Fig. 2.39a by introducing three idle mobilities inside and four outside the parallelogram loop. For example, the solution in Fig. 2.46b has G_1-limb of type <u>*Pa*</u>**P* and G_2-limb

Table 2.13. Structural parameters[a] of translational parallel mechanisms in Fig. 2.46

No.	Structural parameter	Solution *Pa**PP*-*Pa**Pa*S* Fig. 2.46a	*Pa**P-*RC**S* Fig. 2.46b
1	m	12	7
2	p_1	6	5
3	p_2	9	3
4	p	15	8
5	q	4	2
6	k_1	0	1
7	k_2	2	1
8	k	2	2
9	(R_{G1})	$(\boldsymbol{v}_x, \boldsymbol{v}_y, \boldsymbol{v}_z)$	$(\boldsymbol{v}_x, \boldsymbol{v}_y)$
10	(R_{G2})	$(\boldsymbol{v}_x, \boldsymbol{v}_y, \boldsymbol{\omega}_\alpha, \boldsymbol{\omega}_\beta, \boldsymbol{\omega}_\delta)$	$(\boldsymbol{v}_x, \boldsymbol{v}_y, \boldsymbol{v}_z, \boldsymbol{\omega}_\alpha, \boldsymbol{\omega}_\beta, \boldsymbol{\omega}_\delta)$
11	S_{G1}	3	2
12	S_{G2}	5	6
13	r_{G1}	6	6
14	r_{G2}	12	0
15	M_{G1}	3	2
16	M_{G2}	5	6
17	(R_F)	$(\boldsymbol{v}_x, \boldsymbol{v}_y)$	$(\boldsymbol{v}_x, \boldsymbol{v}_y)$
18	S_F	2	2
19	r_1	18	6
20	r_F	24	12
21	M_F	2	2
22	N_F	0	0
23	T_F	0	0
24	$\sum_{j=1}^{p_1} f_j$	9	8
25	$\sum_{j=1}^{p_2} f_j$	17	6
26	$\sum_{j=1}^{p} f_j$	26	14

[a]See footnote of Table 2.1 for the nomenclature of structural parameters

of type *RC**S**. Equations (1.2)–(1.8) and (1.17) give the following structural parameters for this parallel mechanism: $M_{G1} = S_{G1} = 2$, $M_{G2} = S_{G2} = 6$, $(R_{G2}) = (\boldsymbol{v}_x, \boldsymbol{v}_y, \boldsymbol{v}_z, \boldsymbol{\omega}_\alpha, \boldsymbol{\omega}_\beta, \boldsymbol{\omega}_\delta)$, $(R_{G1}) = (\boldsymbol{v}_x, \boldsymbol{v}_y)$, $(R_F) = (\boldsymbol{v}_x, \boldsymbol{v}_y)$, $M_F = S_F = 2$, $N_F = 0$ and $T_F = 0$ (see Table 2.13).

Solutions with rotating and linear actuators

Non overconstrained solutions $F \leftarrow G_1$–G_2 with rotating and linear actuators and decoupled motions have $\sum_1^p f_i = 20$ when two complex limbs are used. They are derived from the solution in Fig. 2.40a by introducing ten idle mobilities: four outside the parallelogram loops and three inside each parallelogram loop.

For example, the solution in Fig. 2.47 has G_1-limb of type $\underline{Pa}$*PP* and G_2-limb of type $\underline{Pa}$*PaS*. For this solution, Eqs. (1.2)–(1.8) and (1.17) give the following structural parameters: $M_{G1} = S_{G1} = 3$, $M_{G2} = S_{G2} = 5$, $(R_{G1}) = (\boldsymbol{v}_x, \boldsymbol{v}_y, \boldsymbol{v}_z)$, $(R_{G2}) = (\boldsymbol{v}_x, \boldsymbol{v}_y, \boldsymbol{\omega}_\alpha, \boldsymbol{\omega}_\beta, \boldsymbol{\omega}_\delta)$, $(R_F) = (\boldsymbol{v}_x, \boldsymbol{v}_y)$, $M_F = S_F = 2$, $N_F = 0$ and $T_F = 0$. The solutions in Figs. 2.46a and 2.47 have the same structural parameters (see Table 2.13).

Non overconstrained solutions $F \leftarrow G_1$–G_2 with rotating and linear actuators and decoupled motions have $\sum_1^p f_i = 14$ when a complex and a simple limb are used. They are derived from the solutions in Figs. 2.41a and 2.42a by introducing three idle mobilities in the parallelogram loop and four outside the parallelogram loop. For example, the solutions in Fig. 2.48 have G_1-limb of type $\underline{Pa}$*P and G_2-limb of type $\underline{P}C$*S* (Fig. 2.48a) or C*$\underline{P}S$* (Fig. 2.48b). Equations (1.2)–(1.8) and (1.17) give the following structural parameters for both solutions: $M_{G1} = S_{G1} = 2$, $M_{G2} = S_{G2} = 6$, $(R_{G1}) = (\boldsymbol{v}_x, \boldsymbol{v}_y)$, $(R_{G2}) = (\boldsymbol{v}_x, \boldsymbol{v}_y, \boldsymbol{v}_z, \boldsymbol{\omega}_\alpha, \boldsymbol{\omega}_\beta, \boldsymbol{\omega}_\delta)$, $(R_F) = (\boldsymbol{v}_x, \boldsymbol{v}_y)$, $M_F = S_F = 2$, $N_F = 0$ and $T_F = 0$. The solutions in Figs. 2.46b and 2.48 have the same structural parameters (see Table 2.13).

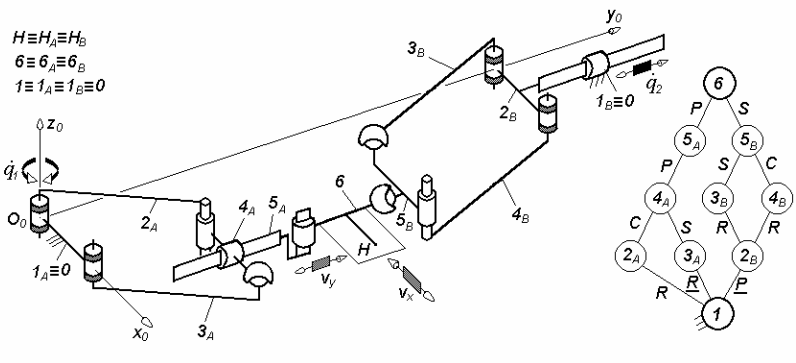

Fig. 2.47. $\underline{Pa}$*PP*-$\underline{P}Pa$*S*-type non overconstrained translational parallel mechanism, limb topologies $\underline{Pa}$*$\perp P \perp \parallel P$* and $\underline{P} \perp Pa$*-S*

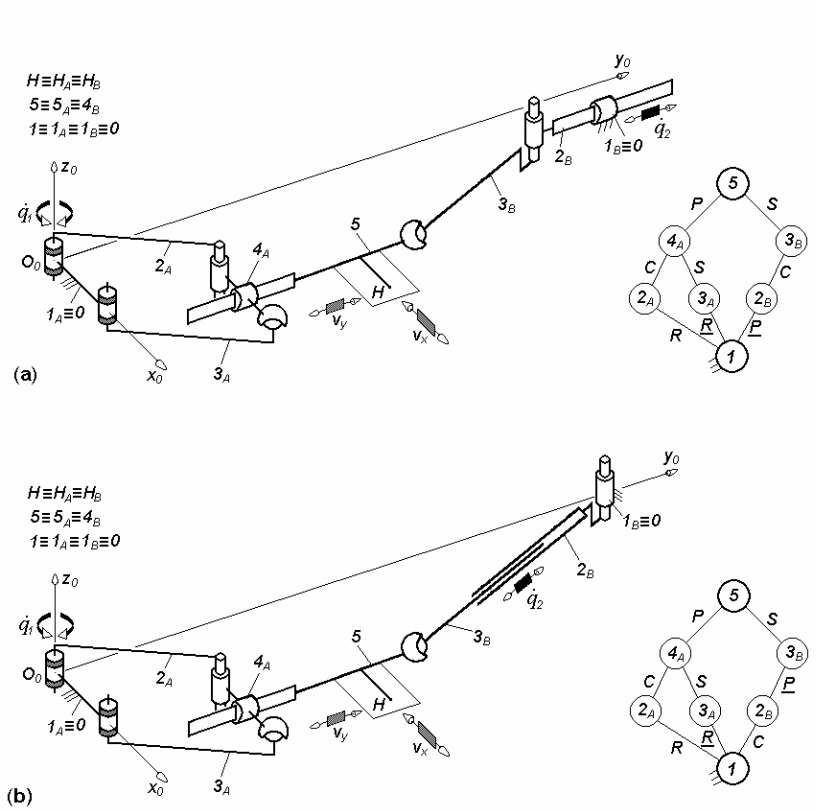

Fig. 2.48. Non overconstrained translational parallel mechanisms of types $\underline{Pa}$*P-$\underline{P}C$*S* (**a**) and $\underline{Pa}$*P-C*$\underline{P}S$* (**b**), limb topologies $\underline{Pa}^* \perp P$ and $\underline{P} \perp C^*$-S^* (**a**), $\underline{Pa}^* \perp P$ and $C^* \perp \underline{P}S^*$ (**b**)

2.3 *T2*-type translational parallel robots with uncoupled motions

T2-type translational parallel robots with *uncoupled motions* and various degrees of overconstraint can be actuated by linear or rotating motors. In these solutions, both operational velocities depend on just one actuated joint velocity: $v_1 = v_1(\dot{q}_1)$ and $v_2 = v_2(\dot{q}_2)$.

2.3.1 Overconstrained solutions

The *overconstrained* solutions of *T2*-type translational parallel robots with uncoupled motions and q independent loops meet the same condition as their counterparts with coupled and decoupled motions, that is $\sum_1^p f_i < 2 + 6q$.

Solutions with rotating actuators

Overconstrained *T2*-type translational parallel robots with uncoupled motions and *rotating actuators* can be obtained by using two limbs *PaP*-type (Fig. 2.49a). Each limb integrates a parallelogram loop and $\sum_1^p f_i < 20$.

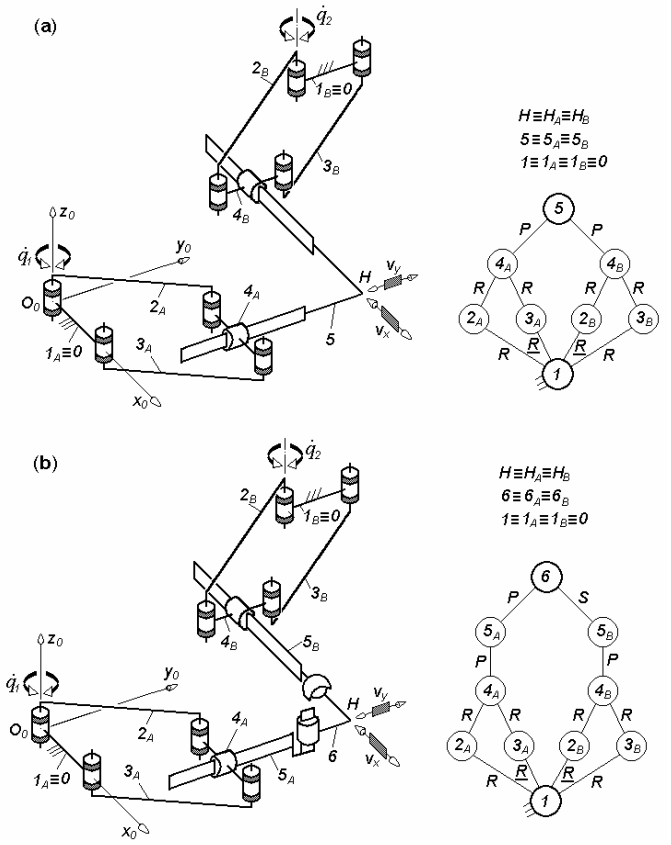

Fig. 2.49. Translational parallel mechanisms of types 2*PaP* with ten overconstraints (**a**) *PaPP**-*PaPS** with six overconstraints (**b**), limb topologies *Pa* ⊥ *P* (**a**) *Pa* ⊥ *P* ⊥ ||*P** and *Pa* ⊥ *P*-*S** (**b**)

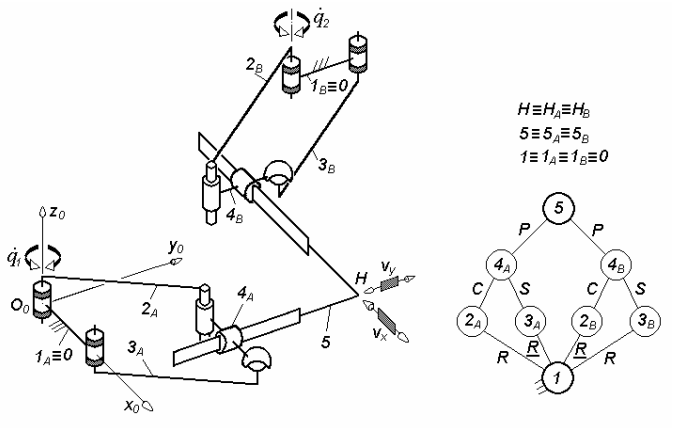

Fig. 2.50. *2Pa*P*-type translational parallel mechanism with four overconstraints, limb topology $\underline{Pa}^* \perp P$

These overconstrained solutions have $1 \le N_F \le 10$ and may integrate up to nine idle mobilities. The example presented in Fig. 2.49b integrates four idle mobilities outside the parallelogram loops and that in Fig. 2.50 has six idle mobilities inside the parallelogram loops. The solutions in Fig. 2.49a and b have the same structural parameters as their counterparts with reciprocal limb structures in Figs. 2.1 and 2.2b (see Table 2.1). Equations (1.2)–(1.8) and (1.17) give the following structural parameters for the solution *2Pa*P*-type in Fig. 2.50: $M_{G1} = S_{G1} = 3$, $M_{G2} = S_{G2} = 3$, $(R_{G1}) = (R_{G2}) = (\boldsymbol{v}_x, \boldsymbol{v}_y)$, $(R_F) = (\boldsymbol{v}_x, \boldsymbol{v}_y)$, $M_F = S_F = 2$, $N_F = 4$ and $T_F = 0$.

Solutions with rotating and linear actuators

Overconstrained *T2*-type translational parallel robots with uncoupled motions actuated by rotating and linear motors can be obtained by using a complex limb *PaP*-type and a simple one *PP*-type (Fig. 2.51a).

The complex limb integrates a parallelogram loop and $\sum_1^p f_i < 14$. The overconstrained solutions have $1 \le N_F \le 7$ and may integrate up to six idle mobilities.

The example presented in Fig. 2.51b combines three idle mobilities in the parallelogram loop and that in Fig. 2.51c has four idle mobilities outside the parallelogram loop. The solutions in Fig. 2.51a and b have the same structural parameters as their counterparts with reciprocal limb structures in Fig. 2.35a and b (see Table 2.10). Equations (1.2)–(1.8) and (1.17) give the following structural parameters for the solution *PaPP*-PPS**-type

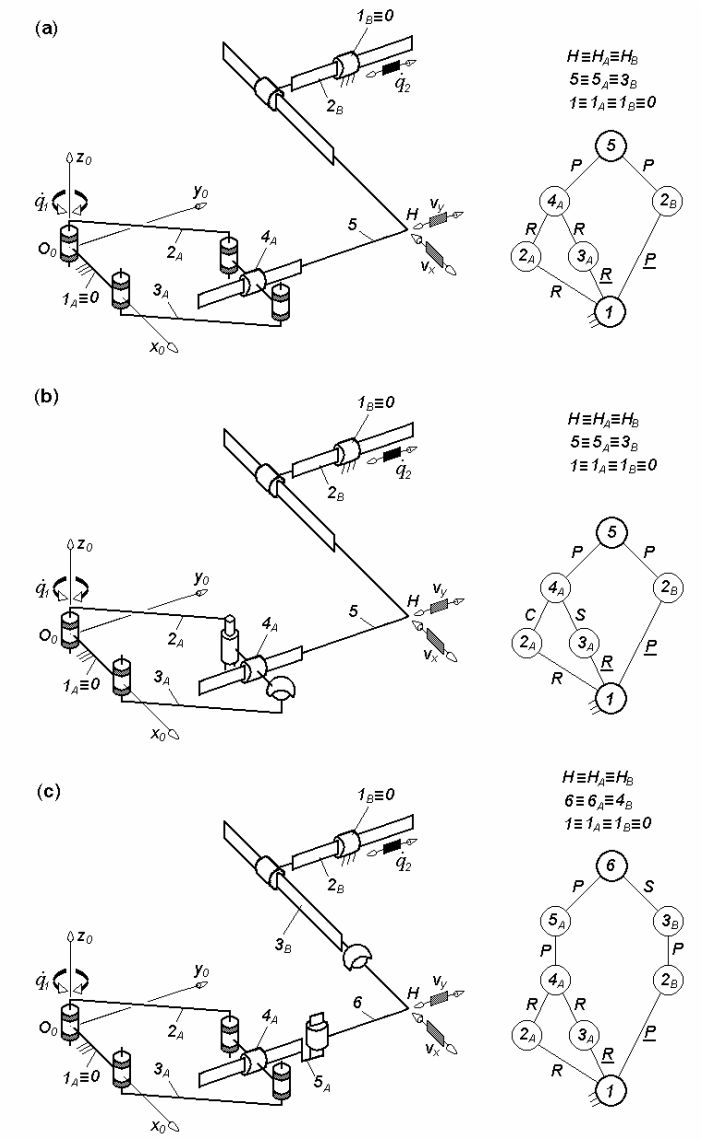

Fig. 2.51. Translational parallel mechanisms of types $\underline{Pa}P$-$\underline{P}P$ with seven overconstraints (**a**), $\underline{Pa}$*P-$\underline{P}P$ with four overconstraints (**b**) and $\underline{Pa}PP$*-$\underline{P}PS$* with three overconstraints (**c**), limb topologies $\underline{Pa} \perp P$ and $\underline{P} \perp P$ (**a**), $\underline{Pa}$* $\perp P$ and $\underline{P} \perp P$ (**b**), $\underline{Pa} \perp P \perp {}^{\parallel}P$* and $\underline{P} \perp P$-S* (**c**)

in Fig. 2.51c: $M_{G1} = S_{G1} = 3$, $M_{G2} = S_{G2} = 5$, $M_F = S_F = 2$, $(R_{G1}) = (\boldsymbol{v}_x, \boldsymbol{v}_y, \boldsymbol{v}_z)$, $(R_{G2}) = (\boldsymbol{v}_x, \boldsymbol{v}_y, \boldsymbol{\omega}_\alpha, \boldsymbol{\omega}_\beta, \boldsymbol{\omega}_\delta)$, $(R_F) = (\boldsymbol{v}_x, \boldsymbol{v}_y)$, $N_F = 0$ and $T_F = 0$.

2.3.2 Non overconstrained solutions

Non overconstrained solutions of *T2*-type translational parallel robots with uncoupled motions and q independent loops meet the same condition $\sum_1^p f_i = 2 + 6q$ as their counterparts with coupled and decoupled motions.

Solutions with rotating actuators

Non overconstrained solutions $F \leftarrow G_1 – G_2$ with *rotating actuators* and uncoupled motions have $\sum_1^p f_i = 20$. They are derived from the solution in

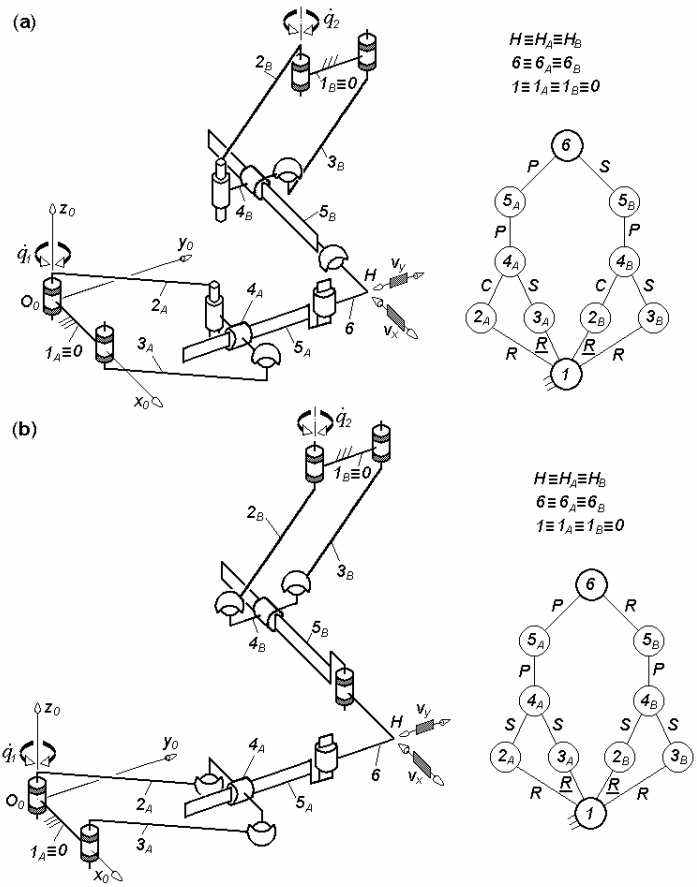

Fig. 2.52. Non overconstrained translational parallel mechanisms of types <u>*Pa*</u>**PP**-<u>*Pa*</u>**PS** (**a**) and <u>*Pa*</u>^{ss}*PP**-<u>*Pa*</u>^{ss}*PR** (**b**), limb topologies <u>*Pa*</u>* $\perp$ *P* $\perp^{\parallel}$ *P** and <u>*Pa*</u>* $\perp$ *P-S** (**a**), <u>*Pa*</u>^{ss} $\perp$ *P* $\perp^{\parallel}$ *P** and <u>*Pa*</u>^{ss} $\perp$ *P* $\perp^{\parallel}$ *R** (**b**)

Table 2.14. Structural parameters[a] of translational parallel mechanisms in Fig. 2.52

No.	Structural parameter	Solution $\underline{Pa}$*PP*-$\underline{Pa}$*PS* Fig. 2.52a	$\underline{Pa}^{ss}$PP*-$\underline{Pa}^{ss}$PR* Fig. 2.52b
1	m	10	10
2	p_1	6	6
3	p_2	6	6
4	p	12	12
5	q	3	3
6	k_1	0	0
7	k_2	2	2
8	k	2	2
9	(R_{G1})	$(\boldsymbol{v}_x, \boldsymbol{v}_y, \boldsymbol{v}_z)$	$(\boldsymbol{v}_x, \boldsymbol{v}_y, \boldsymbol{v}_z, \boldsymbol{\omega}_\beta)$
10	(R_{G2})	$(\boldsymbol{v}_x, \boldsymbol{v}_y, \boldsymbol{\omega}_\alpha, \boldsymbol{\omega}_\beta, \boldsymbol{\omega}_\delta)$	$(\boldsymbol{v}_x, \boldsymbol{v}_y, \boldsymbol{\omega}_\alpha, \boldsymbol{\omega}_\delta)$
11	S_{G1}	3	4
12	S_{G2}	5	4
13	r_{G1}	6	6
14	r_{G2}	6	6
15	M_{G1}	3	4
16	M_{G2}	5	4
17	(R_F)	$(\boldsymbol{v}_x, \boldsymbol{v}_y)$	$(\boldsymbol{v}_x, \boldsymbol{v}_y)$
18	S_F	2	2
19	r_1	12	12
20	r_F	18	18
21	M_F	2	2
22	N_F	0	0
23	T_F	0	0
24	$\sum_{j=1}^{p_1} f_j$	9	10
25	$\sum_{j=1}^{p_2} f_j$	11	10
26	$\sum_{j=1}^{p} f_j$	20	20

[a]See footnote of Table 2.1 for the nomenclature of structural parameters

Fig. 2.49a by introducing ten idle mobilities: four outside the parallelogram loops and three inside each parallelogram loop.

For example, the solution in Fig. 2.52a has G_1-limb of type $\underline{Pa}$*PP* and G_2-limb of type $\underline{Pa}$*PS*. The solution in Fig. 2.52b has G_1-limb of type $\underline{Pa}^{ss}$PP* and G_2-limb of type $\underline{Pa}^{ss}$PR*. The structural parameters of these solutions are presented in Table 2.14.

Solutions with rotating and linear actuators

Non overconstrained solutions $F \leftarrow G_1 – G_2$ with uncoupled motions actuated by rotating and linear motors have $\sum_1^p f_i = 14$. They are derived from the solution in Fig. 2.51a by introducing seven idle mobilities: four outside the parallelogram loops and three inside the parallelogram loop.

For example, the solution in Fig. 2.53a has G_1-limb of type $\underline{Pa}$*PP* and G_2-limb of type $\underline{P}PS$*. The solution in Fig. 2.53b has G_1-limb of type $\underline{Pa}^{ss}PC$* and G_2-limb of type $\underline{P}PR$*. The structural parameters of these solutions are presented in Table 2.15.

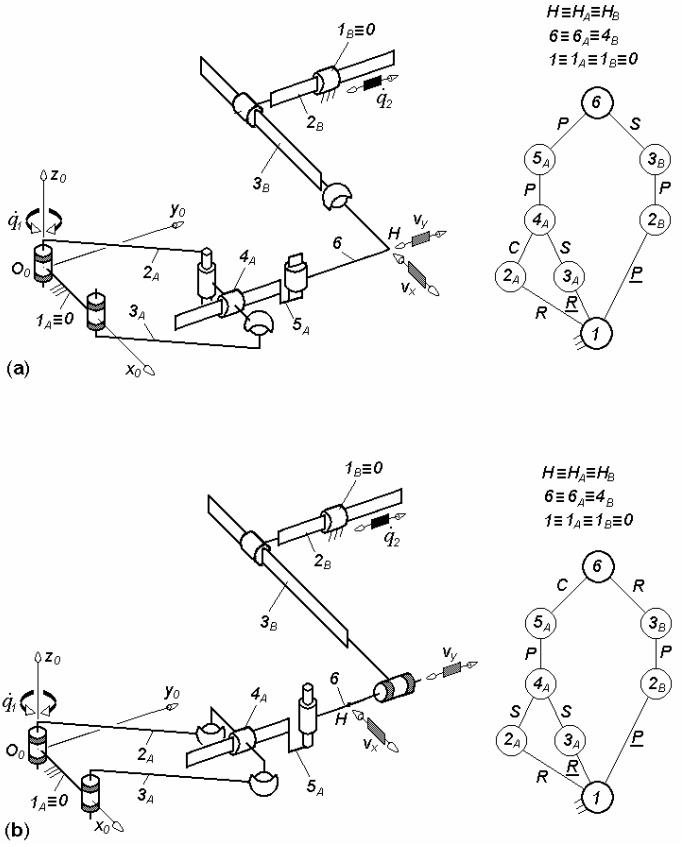

Fig. 2.53. Non overconstrained translational parallel mechanisms of types $\underline{Pa}$*PP*-$\underline{P}PS$* (**a**) and $\underline{Pa}^{ss}PC$*-$\underline{P}PR$* (**b**), limb topologies $\underline{Pa}$*$P \perp {}^{||}P$* and $\underline{P} \perp P$-S* (**a**), $\underline{Pa}^{ss} \perp P \perp {}^{||}C$* and $\underline{P} \perp P \perp {}^{||}R$* (**b**)

Table 2.15. Structural parameters[a] of translational parallel mechanisms in Fig. 2.53

No.	Structural parameter	Solution $\underline{Pa}$*PP*-$\underline{P}$PS* Fig. 2.53a	 $\underline{Pa}^{ss}$PC*-$\underline{P}$PR* Fig. 2.53b
1	m	8	8
2	p_1	6	6
3	p_2	3	3
4	p	9	9
5	q	2	2
6	k_1	1	1
7	k_2	1	1
8	k	2	2
9	(R_{G1})	$(\boldsymbol{v}_x, \boldsymbol{v}_y, \boldsymbol{v}_z)$	$(\boldsymbol{v}_x, \boldsymbol{v}_y, \boldsymbol{v}_z, \boldsymbol{\omega}_\beta, \boldsymbol{\omega}_\delta)$
10	(R_{G2})	$(\boldsymbol{v}_x, \boldsymbol{v}_y, \boldsymbol{\omega}_\alpha, \boldsymbol{\omega}_\beta, \boldsymbol{\omega}_\delta)$	$(\boldsymbol{v}_x, \boldsymbol{v}_y, \boldsymbol{\omega}_\alpha)$
11	S_{G1}	3	5
12	S_{G2}	5	3
13	r_{G1}	6	6
14	r_{G2}	0	0
15	M_{G1}	3	5
16	M_{G2}	5	3
17	(R_F)	$(\boldsymbol{v}_x, \boldsymbol{v}_y)$	$(\boldsymbol{v}_x, \boldsymbol{v}_y)$
18	S_F	2	2
19	r_1	6	6
20	r_F	12	12
21	M_F	2	2
22	N_F	0	0
23	T_F	0	0
24	$\sum_{j=1}^{p_1} f_j$	9	11
25	$\sum_{j=1}^{p_2} f_j$	5	3
26	$\sum_{j=1}^{p} f_j$	14	14

[a]See footnote of Table 2.1 for the nomenclature of structural parameters

2.4 Maximally regular *T2*-type translational parallel robots

Maximally regular T2-type translational parallel robots are actuated by linear motors and may have various degrees of overconstraint. In these solutions, both operational velocities are equal to their corresponding actuated joint velocities: $v_1 = \dot{q}_1$ and $v_2 = \dot{q}_2$. We call *Isoglide2-T2* the translational parallel mechanisms of this family.

2.4.1 Overconstrained solutions

The *overconstrained* solutions of *Isoglide2-T2* parallel robots have just one closed loop and $4 \le \sum_1^p f_i < 8$. These solutions have $1 \le N_F \le 4$ and could integrate up to four idle mobilities. The basic solution has two identical limbs $\underline{P} \perp P$-type (Fig. 2.54) and no idle mobilities. The translations in the two limbs have orthogonal directions: $\underline{P}_y P_x$-type. This solution has the following structural parameters: $M_{G1} = S_{G1} = 2$, $M_{G2} = S_{G2} = 2$, $(R_{G1}) = (R_{G2}) = (R_F) = (\boldsymbol{v}_x, \boldsymbol{v}_y)$, $M_F = S_F = 2$, $N_F = 4$ and $T_F = 0$.

There are various possibilities to introduce up to four idle mobilities. For example, solution $\underline{P}PR^*$-$\underline{P}P$-type in Fig. 2.55a is characterized by $M_{G1} = S_{G1} = 3$, $M_{G2} = S_{G2} = 2$, $(R_{G1}) = (\boldsymbol{v}_x, \boldsymbol{v}_y, \boldsymbol{\omega}_\delta)$, $(R_{G2}) = (\boldsymbol{v}_x, \boldsymbol{v}_y)$, $N_F = 3$. Solution $2\underline{P}C^*$-type in Fig. 2.55b is characterized by $M_{G1} = S_{G1} = 3$, $M_{G2} = S_{G2} = 3$, $(R_{G1}) = (\boldsymbol{v}_x, \boldsymbol{v}_y, \boldsymbol{\omega}_\alpha)$, $(R_{G2}) = (\boldsymbol{v}_x, \boldsymbol{v}_y, \boldsymbol{\omega}_\beta)$, $N_F = 2$ and solution $\underline{P}PC^*$-$\underline{P}PR^*$-type in Fig. 2.55c by $M_{G1} = S_{G1} = 4$, $M_{G2} = S_{G2} = 3$, $(R_{G1}) = (\boldsymbol{v}_x, \boldsymbol{v}_y, \boldsymbol{v}_z, \boldsymbol{\omega}_\delta)$, $(R_{G2}) = (\boldsymbol{v}_x, \boldsymbol{v}_y, \boldsymbol{\omega}_\beta)$, $N_F = 1$.

The structural parameters of the solutions in Figs. 2.54 and 2.55 are presented in Table 2.16.

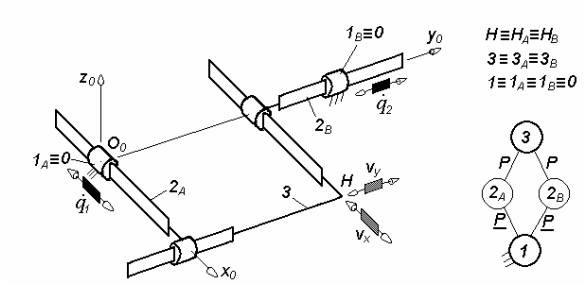

Fig. 2.54. Maximally regular $2\underline{P}P$-type translational parallel mechanism with four overconstraints, limb topology $\underline{P} \perp P$

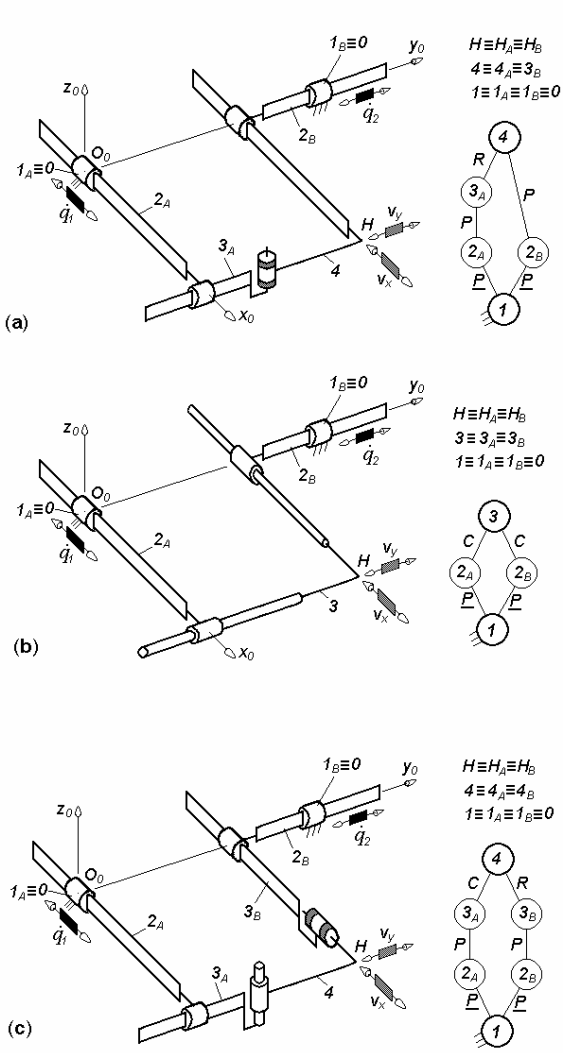

Fig. 2.55. Maximally regular parallel mechanisms of types $\underline{P}PR^*$-$\underline{P}P$ with three overconstraints (**a**), $2\underline{P}C^*$ with two overconstraints (**b**) and $\underline{P}PC^*$-$\underline{P}PR^*$ with one overconstraint (**c**), limb topologies $\underline{P} \perp P \perp^{\perp} R^*$ and $\underline{P} \perp P$ (**a**), $\underline{P} \perp C$ (**b**) $\underline{P} \perp P \perp^{\perp} C^*$ and $\underline{P} \perp P || R^*$ (**c**)

Table 2.16. Structural parameters[a] of translational parallel mechanisms in Figs. 2.54–2.55

No.	Structural parameter	Solution *2PP* Fig. 2.54	*PPR*-PP* Fig. 2.55a	*2PC** Fig. 2.55b	*PPC*-PPR** Fig. 2.55c
1	m	4	5	4	6
2	p_1	2	3	2	4
3	p_2	2	2	2	3
4	p	4	5	4	7
5	q	1	1	1	1
6	k_1	1	1	1	1
7	k_2	1	1	1	1
8	k	2	2	2	2
9	(R_{G1})	$(\boldsymbol{v}_x, \boldsymbol{v}_y)$	$(\boldsymbol{v}_x, \boldsymbol{v}_y, \boldsymbol{\omega}_\delta)$	$(\boldsymbol{v}_x, \boldsymbol{v}_y, \boldsymbol{\omega}_\beta)$	$(\boldsymbol{v}_x, \boldsymbol{v}_y, \boldsymbol{v}_y, \boldsymbol{\omega}_\delta)$
10	(R_{G2})	$(\boldsymbol{v}_x, \boldsymbol{v}_y)$	$(\boldsymbol{v}_x, \boldsymbol{v}_y)$	$(\boldsymbol{v}_x, \boldsymbol{v}_y, \boldsymbol{\omega}_\alpha)$	$(\boldsymbol{v}_x, \boldsymbol{v}_y, \boldsymbol{\omega}_\beta)$
11	S_{G1}	2	3	3	4
12	S_{G2}	2	2	3	3
13	r_{G1}	0	0	0	0
14	r_{G2}	0	0	0	0
15	M_{G1}	2	3	3	4
16	M_{G2}	2	2	3	3
17	(R_F)	$(\boldsymbol{v}_x, \boldsymbol{v}_y)$	$(\boldsymbol{v}_x, \boldsymbol{v}_y)$	$(\boldsymbol{v}_x, \boldsymbol{v}_y)$	$(\boldsymbol{v}_x, \boldsymbol{v}_y)$
18	S_F	2	2	2	2
19	r_1	0	0	0	0
20	r_F	2	3	4	5
21	M_F	2	2	2	2
22	N_F	4	3	2	1
23	T_F	0	0	0	0
24	$\sum_{j=1}^{p_1} f_j$	2	3	3	4
25	$\sum_{j=1}^{p_2} f_j$	2	2	3	3
26	$\sum_{j=1}^{p} f_j$	4	5	6	7

[a]See footnote of Table 2.1 for the nomenclature of structural parameters

2.4.2 Non overconstrained solutions

The *non overconstrained* solutions of *Isoglide2-T2* parallel robots have $\sum_1^p f_i = 8$. They are derived from the solution in Fig. 2.54 by introducing four idle mobilities as follows: one translation perpendicular to the motion

plane of the moving platform and three rotations. Various solutions exist for introducing these idle mobilities.

For example, the solution in Fig. 2.56a has G_1-limb of type $\underline{P}PP^*$ and G_2-limb of type $\underline{P}PS^*$ with $M_{G1} = S_{G1} = 3$, $M_{G2} = S_{G2} = 5$, $(R_{G1}) = (\boldsymbol{v}_x, \boldsymbol{v}_y, \boldsymbol{v}_z)$, $(R_{G2}) = (\boldsymbol{v}_x, \boldsymbol{v}_y, \boldsymbol{\omega}_\alpha, \boldsymbol{\omega}_\beta, \boldsymbol{\omega}_\delta)$. The solution in Fig. 2.56b has G_1-limb of type $\underline{P}C^*C^*$ and G_2-limb of type $\underline{P}C^*$ with $M_{G1} = S_{G1} = 5$, $M_{G2} = S_{G2} = 3$, $(R_{G1}) = (\boldsymbol{v}_x, \boldsymbol{v}_y, \boldsymbol{v}_z, \boldsymbol{\omega}_\beta, \boldsymbol{\omega}_\delta)$, $(R_{G2}) = (\boldsymbol{v}_x, \boldsymbol{v}_y, \boldsymbol{\omega}_\alpha)$. Both solutions are characterized by $(R_F) = (\boldsymbol{v}_x, \boldsymbol{v}_y)$, $M_F = S_F = 2$, $N_F = 0$ and $T_F = 0$ (see Table 2.17).

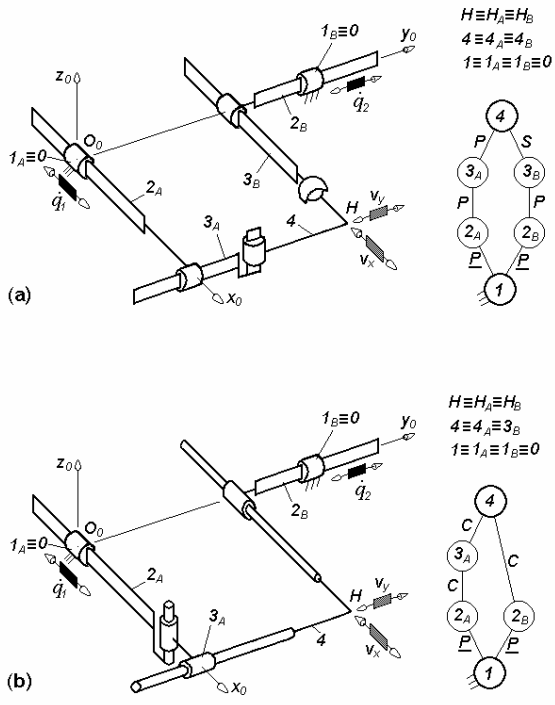

Fig. 2.56. Non overconstrained maximally regular parallel mechanisms of types $\underline{P}PP^*$-$\underline{P}PS^*$ (**a**) and $\underline{P}C^*C^*$-$\underline{P}C^*$ (**b**), limb topologies $\underline{P} \perp P \perp^{\perp} P^*$ and $\underline{P} \perp P$-S^* (**a**), $\underline{P} \perp C^*C^*$-$\underline{P} \perp C^*$ (**b**)

Table 2.17. Structural parameters[a] of translational parallel mechanisms in Fig. 2.56

No.	Structural parameter	Solution *P*PP*-*P*PS* Fig. 2.56a	*P*C*C*-*P*C* Fig. 2.56b
1	m	6	5
2	p_1	3	3
3	p_2	3	2
4	p	6	5
5	q	1	1
6	k_1	1	1
7	k_2	1	1
8	k	2	2
9	(R_{G1})	$(\boldsymbol{v}_x, \boldsymbol{v}_y, \boldsymbol{v}_z)$	$(\boldsymbol{v}_x, \boldsymbol{v}_y, \boldsymbol{v}_z, \boldsymbol{\omega}_\beta, \boldsymbol{\omega}_\delta)$
10	(R_{G2})	$(\boldsymbol{v}_x, \boldsymbol{v}_y, \boldsymbol{\omega}_\alpha, \boldsymbol{\omega}_\beta, \boldsymbol{\omega}_\delta)$	$(\boldsymbol{v}_x, \boldsymbol{v}_y, \boldsymbol{\omega}_\alpha)$
11	S_{G1}	3	5
12	S_{G2}	5	3
13	r_{G1}	0	0
14	r_{G2}	0	0
15	M_{G1}	3	5
16	M_{G2}	5	3
17	(R_F)	$(\boldsymbol{v}_x, \boldsymbol{v}_y)$	$(\boldsymbol{v}_x, \boldsymbol{v}_y)$
18	S_F	2	2
19	r_1	0	0
20	r_F	6	6
21	M_F	2	2
22	N_F	0	0
23	T_F	0	0
24	$\sum_{j=1}^{p_1} f_j$	3	6
25	$\sum_{j=1}^{p_2} f_j$	5	3
26	$\sum_{j=1}^{p} f_j$	8	8

[a]See footnote of Table 2.1 for the nomenclature of structural parameters

2.5 Other *T2*-type translational parallel robots

In the previous sections of this chapter, we have presented translational parallel robots with two degrees of freedom and a unique base of the operational velocity space for any position of the characteristic point H on the moving platform. In this section, we present translational parallel mechanisms for parallel robots with two degrees of freedom and different

bases of their operational velocity space for any position of the characteristic point H on the moving platform. These parallel mechanisms have mobility $M_F = 2$ and connectivity between the moving and fixed platforms $S_F = 2$. We note that, in this case, the moving platform performs three translations but just two of them are independent (Gao et al. 2002).

The solutions presented in this section have uncoupled motions and three legs. They are of type $F \leftarrow G_1$–G_2–G_3 in which the first two legs are actuated by rotating motors and the last leg is unactuated. The basis of the operational velocity space contains any combination of two independent translations.

2.5.1 Overconstrained solutions

The *basic overconstrained* solutions have three identical limbs each of them combining two universal joints. The distance between the centres of the two universal joints is the same in the three limbs and the fixed and the moving platforms are identical. The centers of the universal joints connecting the limbs with the fixed and the moving platforms form two identical triangles. The spatial form of this mechanism is a triangular prism. For this reason we call this solution *prism mechanism* and we denote it by *Pr*. The limbs G_1 and G_2 are actuated by rotating motors. The solution in Fig. 2.57a has one actuator on the fixed base and the second actuator is mounted on a moving link. In this solution, the axes of the first revolute joint in the actuated limbs are coplanar. Both actuators are mounted on the fixed base in Fig. 2.57b. In this case, the axes of the first revolute joints in the actuated limbs are perpendicular.

The three complex limbs form $q = 14$ independent loops and fulfil the conditions: $S_F = 2$ and $(R_F) = (R_{G1} \cap R_{G2} \cap R_{G3}) = (\boldsymbol{v}_1, \boldsymbol{v}_2)$. Two closed loops composed of two revolute joints with the same axis exist in each universal joint in Fig. 2.57. Both solutions in Fig. 2.57 have the following structural parameters: $M_{G1} = S_{G1} = 4$, $M_{G2} = S_{G2} = 4$, $M_{G3} = S_{G3} = 4$, $(R_{G1}) = (\boldsymbol{v}_1, \boldsymbol{v}_2, \boldsymbol{\omega}_\alpha, \boldsymbol{\omega}_\beta)$, $(R_{G2}) = (\boldsymbol{v}_1, \boldsymbol{v}_2, \boldsymbol{v}_3, \boldsymbol{\omega}_\alpha)$, $(R_{G3}) = (\boldsymbol{v}_1, \boldsymbol{v}_2, \boldsymbol{v}_3, \boldsymbol{\omega}_\beta)$, $(R_F) = (\boldsymbol{v}_1, \boldsymbol{v}_2)$, $M_F = S_F = 2$,

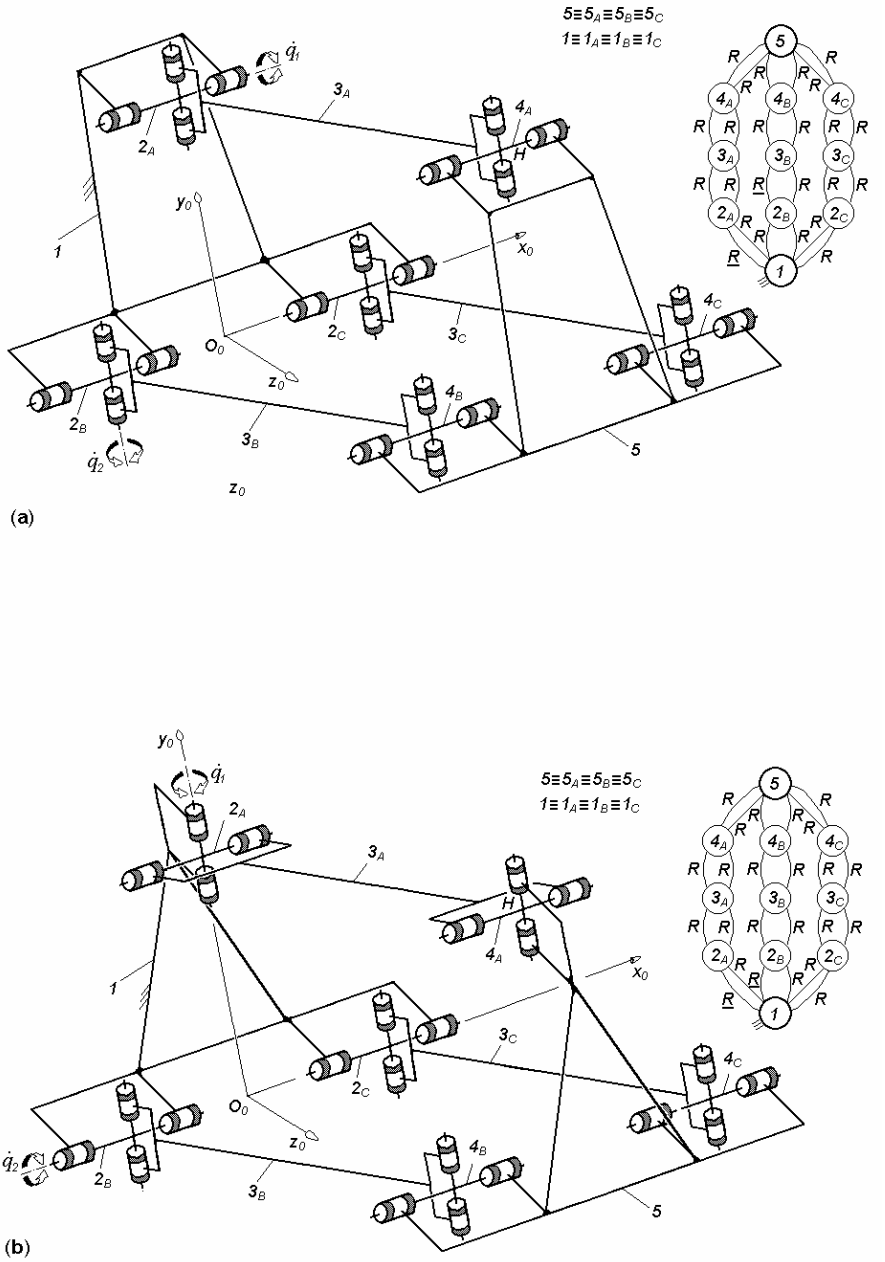

Fig. 2.57. Overconstrained *T2* parallel mechanisms with an additional unactuated limb and two revolute joints on each axis of types: $(\underline{R}RRR)^2$-$(R\underline{R}RR)^2$-$(RRRR)^2$ (**a**), $(\underline{R}RRR)^2$-$(\underline{R}RRR)^2$-$(RRRR)^2$ (**b**)

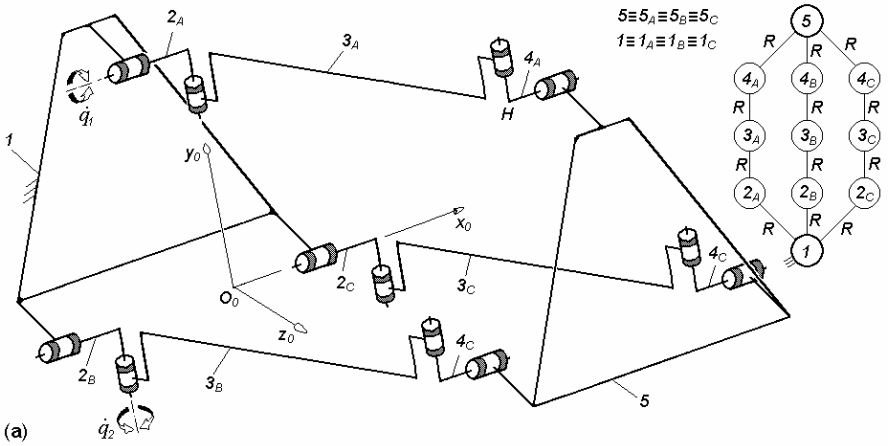

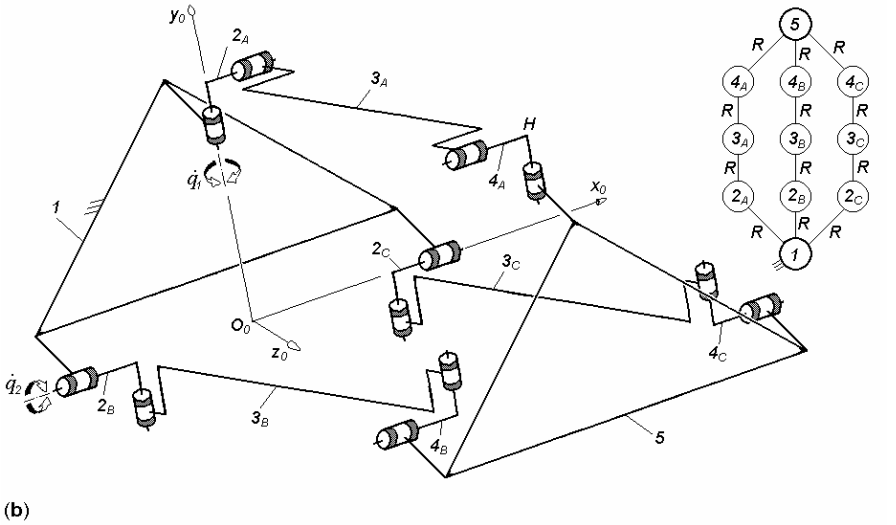

Fig. 2.58. Overconstrained *T2* parallel mechanisms with an additional unactuated limb of types: *R*RRR-*R*RRR-RRRR (**a**), *R*RRR-*R*RRR-RRRR (**b**)

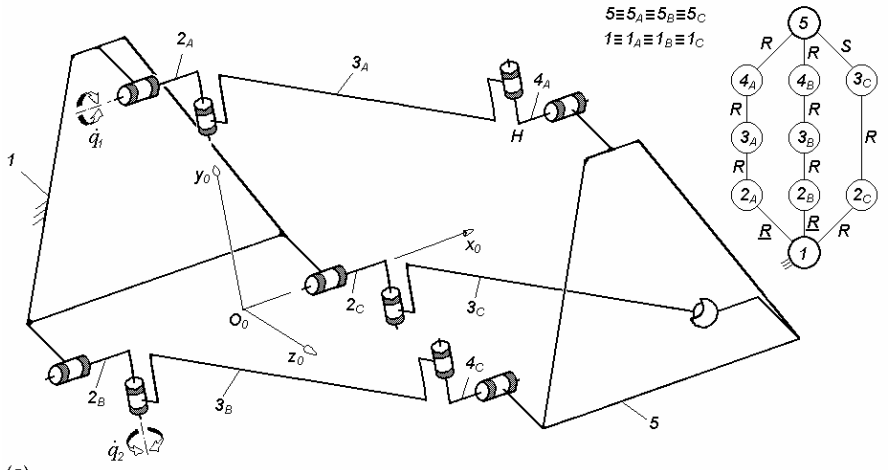

(**a**)

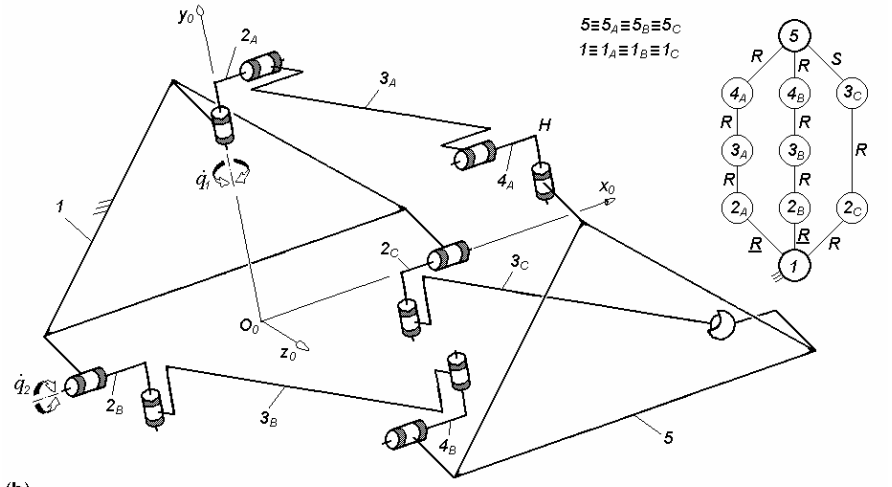

(**b**)

Fig. 2.59. Overconstrained *T2* parallel mechanisms with an additional unactuated limb of types: *RRRR-RRRR-RRS* (**a**), *RRRR-RRRR-RRS* (**b**)

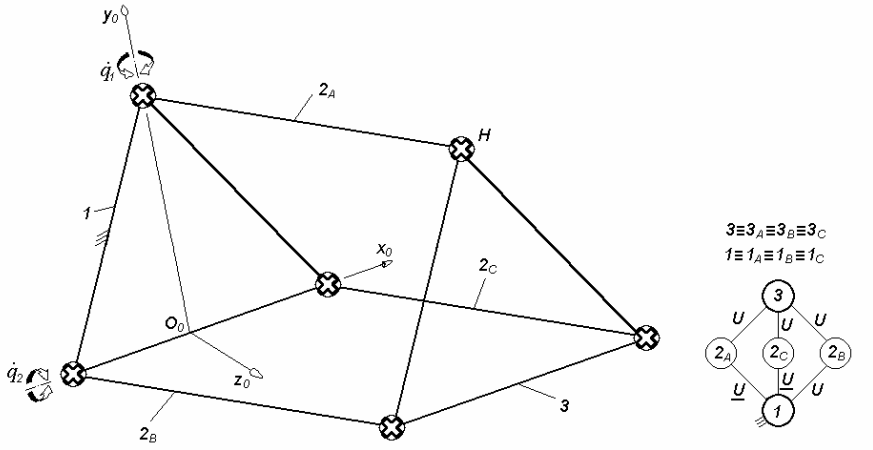

(a)

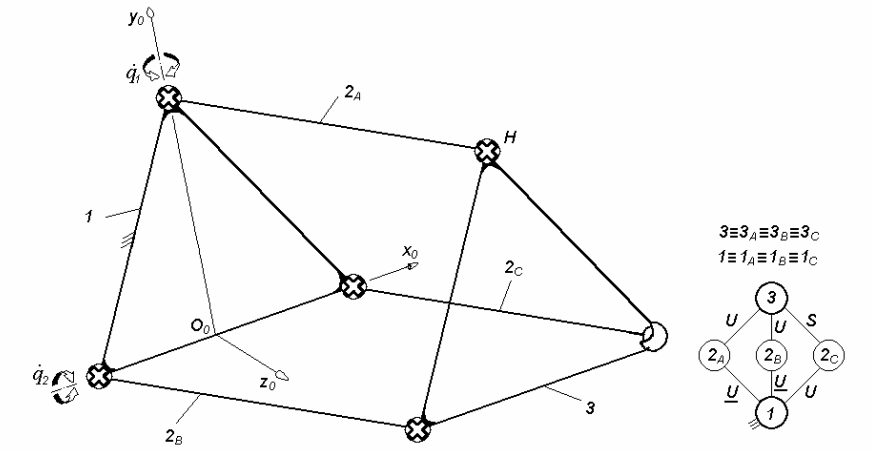

(b)

Fig. 2.60. Simplified representation of the overconstrained *T2* parallel mechanisms with an additional unactuated limb of type *Pr* (**a**) and Pr^s (**b**)

Table 2.18. Structural parameters[a] of translational parallel mechanisms in Figs. 2.57 and 2.58

No.	Structural parameter	Solution *($\underline{R}$RRR)^2-(R$\underline{R}$RR)^2-(RRRR)^2* (Fig. 2.57a) *($\underline{R}$RRR)^2-($\underline{R}$RRR)^2-(RRRR)^2* (Fig. 2.57b)	*$\underline{R}$RRR-R$\underline{R}$RR-RRRR* (Fig. 2.58a) *$\underline{R}$RRR-$\underline{R}$RRR-RRRR* (Fig. 2.58b)
1	m	11	11
2	p_1	8	4
3	p_2	8	4
4	p_3	8	4
5	p	24	12
6	q	14	2
7	k_1	0	3
8	k_2	3	0
9	k	3	3
10	(R_{G1})	($\boldsymbol{v}_1,\boldsymbol{v}_2,\boldsymbol{\omega}_\alpha,\boldsymbol{\omega}_\beta$)	($\boldsymbol{v}_1,\boldsymbol{v}_2,\boldsymbol{\omega}_\alpha,\boldsymbol{\omega}_\beta$)
11	(R_{G2})	($\boldsymbol{v}_1,\boldsymbol{v}_2,\boldsymbol{v}_3,\boldsymbol{\omega}_\alpha$)	($\boldsymbol{v}_1,\boldsymbol{v}_2,\boldsymbol{v}_3,\boldsymbol{\omega}_\alpha$)
12	(R_{G3})	($\boldsymbol{v}_1,\boldsymbol{v}_2,\boldsymbol{v}_3,\boldsymbol{\omega}_\beta$)	($\boldsymbol{v}_1,\boldsymbol{v}_2,\boldsymbol{v}_3,\boldsymbol{\omega}_\beta$)
13	S_{G1}	4	4
14	S_{G2}	4	4
15	S_{G3}	4	4
16	r_{G1}	4	0
17	r_{G2}	4	0
18	r_{G3}	4	0
19	M_{G1}	4	4
20	M_{G2}	4	4
21	M_{G3}	4	4
22	(R_F)	($\boldsymbol{v}_1,\boldsymbol{v}_2$)	($\boldsymbol{v}_1,\boldsymbol{v}_2$)
23	S_F	2	2
24	r_1	12	0
25	r_F	22	10
26	M_F	2	2
27	N_F	62	2
28	T_F	0	0
29	$\sum_{j=1}^{p_1} f_j$	8	4
30	$\sum_{j=1}^{p_2} f_j$	8	4
31	$\sum_{j=1}^{p_3} f_j$	8	4
32	$\sum_{j=1}^{p} f_j$	24	12

[a]See footnote of Table 2.1 for the nomenclature of structural parameters

Table 2.19. Structural parameters[a] of translational parallel mechanisms in Figs. 2.59 and 2.61

No.	Structural parameter	Solution *RRRR-RRRR-RRS* (Fig. 2.59a) *RRRR-RRRR-RRS* (Fig. 2.59b)	 *RRRR-RRS-RRS* (Fig. 2.61a) *RRRR-RRS-RRS* (Fig. 2.61b)
1	m	10	9
2	p_1	4	4
3	p_2	4	3
4	p_3	3	3
5	p	11	10
6	q	2	2
7	k_1	3	3
8	k_2	0	0
9	k	3	3
10	(R_{G1})	$(\boldsymbol{v}_1,\boldsymbol{v}_2,\boldsymbol{\omega}_\alpha,\boldsymbol{\omega}_\beta)$	$(\boldsymbol{v}_1,\boldsymbol{v}_2,\boldsymbol{\omega}_\alpha,\boldsymbol{\omega}_\beta)$
11	(R_{G2})	$(\boldsymbol{v}_1,\boldsymbol{v}_2,\boldsymbol{v}_3,\boldsymbol{\omega}_\alpha)$	$(\boldsymbol{v}_1,\boldsymbol{v}_2,\boldsymbol{v}_3,\boldsymbol{\omega}_\alpha,\boldsymbol{\omega}_\delta)$
12	(R_{G3})	$(\boldsymbol{v}_1,\boldsymbol{v}_2,\boldsymbol{v}_3,\boldsymbol{\omega}_\beta,\boldsymbol{\omega}_\delta)$	$(\boldsymbol{v}_1,\boldsymbol{v}_2,\boldsymbol{v}_3,\boldsymbol{\omega}_\beta,\boldsymbol{\omega}_\delta)$
13	S_{G1}	4	4
14	S_{G2}	4	5
15	S_{G3}	5	5
16	r_{G1}	0	0
17	r_{G2}	0	0
18	r_{G3}	0	0
19	M_{G1}	4	4
20	M_{G2}	4	5
21	M_{G3}	5	5
22	(R_F)	$(\boldsymbol{v}_1,\boldsymbol{v}_2)$	$(\boldsymbol{v}_1,\boldsymbol{v}_2)$
23	S_F	2	2
24	r_1	0	0
25	r_F	11	12
26	M_F	2	2
27	N_F	1	0
28	T_F	0	0
29	$\sum_{j=1}^{p_1} f_j$	4	4
30	$\sum_{j=1}^{p_2} f_j$	4	5
31	$\sum_{j=1}^{p_3} f_j$	5	5
32	$\sum_{j=1}^{p} f_j$	13	14

[a]See footnote of Table 2.1 for the nomenclature of structural parameters

$N_F = 62$ and $T_F = 0$ (see Table 2.18). Each closed loop in the universal joints introduces five overconstraints. If we consider just two revolute pairs in each universal joint, (Fig. 2.58), the number of overconstraint becomes $N_F = 2$ (see Table 2.18).

Note 1 (see Chapter 1) must be taken into account when establishing the bases of the operational velocity spaces associated with the solutions in Figs. 2.57–2.61. In accordance with this note, the bases of the vector spaces R_{Gi} in Table 2.18 are selected such as the minimum value of S_F to be obtained by Eq. (1.6). By this choice, the result of Eq. (1.2) fits in with the definition of general mobility as the minimum value of the instantaneous mobility.

Overconstrained solution with $N_F = 1$ can be derived from the basic solutions in Fig. 2.58 by replacing a universal joint by a spherical joint that combines an idle mobility (see Fig. 2.59).

The solutions in Fig. 2.59 have the following structural parameters: $M_{G1} = S_{G1} = 4$, $M_{G2} = S_{G2} = 4$, $M_{G3} = S_{G3} = 5$, $(R_{G1}) = (\boldsymbol{v}_1, \boldsymbol{v}_2, \boldsymbol{\omega}_\alpha, \boldsymbol{\omega}_\beta)$, $(R_{G2}) = (\boldsymbol{v}_1, \boldsymbol{v}_2, \boldsymbol{v}_3, \boldsymbol{\omega}_\alpha)$, $(R_{G3}) = (\boldsymbol{v}_1, \boldsymbol{v}_2, \boldsymbol{v}_3, \boldsymbol{\omega}_\beta, \boldsymbol{\omega}_\delta)$, $(R_F) = (\boldsymbol{v}_1, \boldsymbol{v}_2)$, $M_F = S_F = 2$, $N_F = 1$ and $T_F = 0$ (see Table 2.19).

Figure 2.60 represents the simplified structural diagrams of the solutions in Figs. 2.58b and 2.59b.

2.5.2 Non overconstrained solutions

Non overconstrained solutions can be derived from the solutions in Fig. 2.59 by replacing a second universal joint by a spherical joint. The two spherical joint must be introduced in two distinct legs. The solutions in Fig. 2.61 have the following structural parameters: $M_{G1} = S_{G1} = 4$, $M_{G2} = S_{G2} = 5$, $M_{G3} = S_{G3} = 5$, $(R_{G1}) = (\boldsymbol{v}_1, \boldsymbol{v}_2, \boldsymbol{\omega}_\alpha, \boldsymbol{\omega}_\beta)$, $(R_{G2}) = (\boldsymbol{v}_1, \boldsymbol{v}_2, \boldsymbol{v}_3, \boldsymbol{\omega}_\alpha, \boldsymbol{\omega}_\delta)$, $(R_{G3}) = (\boldsymbol{v}_1, \boldsymbol{v}_2, \boldsymbol{v}_3, \boldsymbol{\omega}_\beta, \boldsymbol{\omega}_\delta)$, $(R_F) = (\boldsymbol{v}_1, \boldsymbol{v}_2)$, $M_F = S_F = 2$, $N_F = 0$ and $T_F = 0$ (see Table 2.19).

Figure 2.61c represents a simplified structural diagram of the solution in Fig. 2.61b.

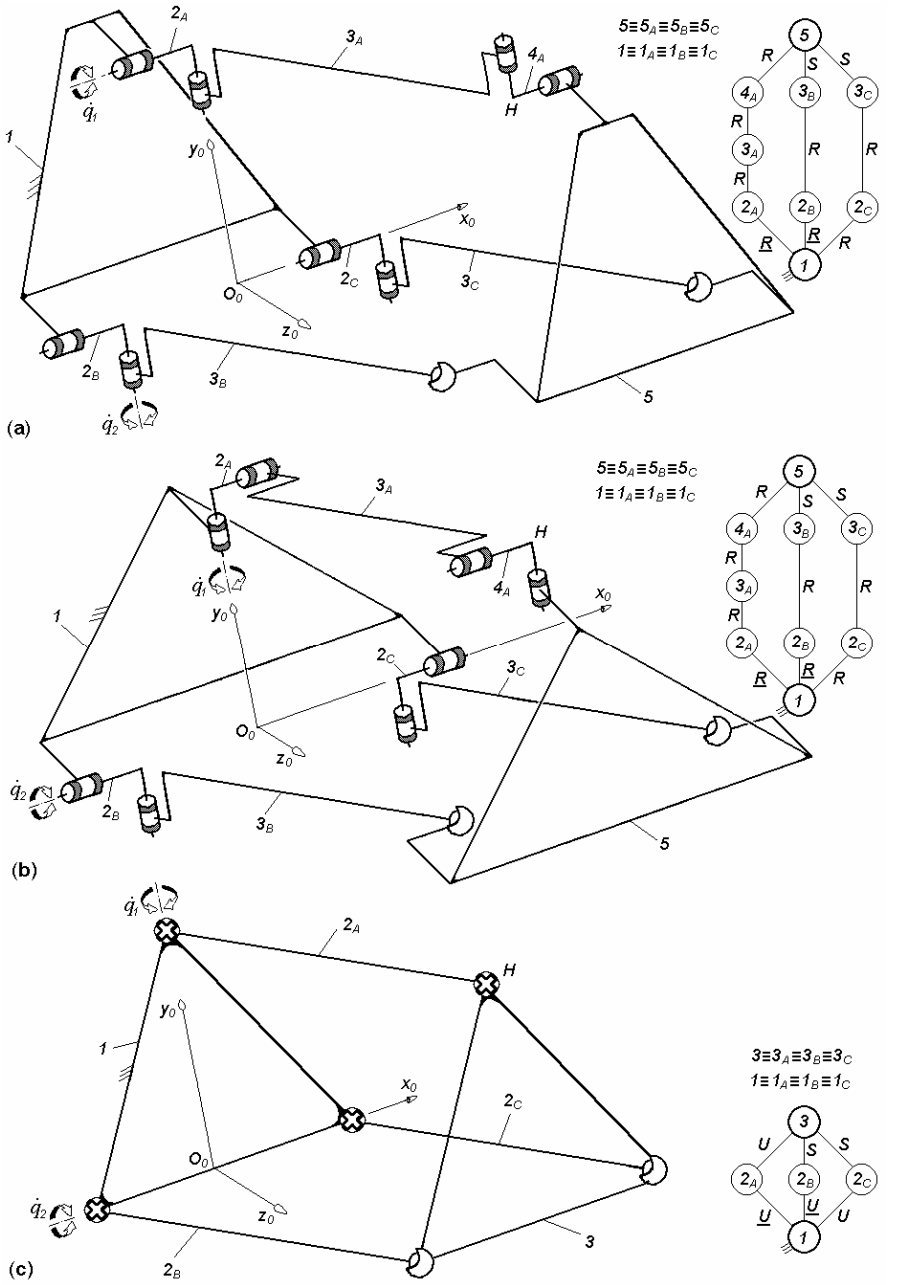

Fig. 2.61. Non overconstrained *T2* parallel mechanisms with an additional unactuated limb of types: *RRRR-RRS-RRS* (**a**), *RRRR-RRS-RRS* (**b**) and Pr^{ss} (**c**) – a simplified representation of the solution (**b**)